

Time-Resolved Photometry of Kuiper Belt Objects: Rotations, Shapes and Phase Functions

Scott S. Sheppard and David C. Jewitt
Institute for Astronomy, University of Hawaii,
2680 Woodlawn Drive, Honolulu, HI 96822
sheppard@ifa.hawaii.edu, jewitt@ifa.hawaii.edu

ABSTRACT

We present a systematic investigation of the rotational lightcurves of trans-Neptunian objects based on extensive optical data from Mauna Kea. Four of 13 objects (corresponding to 31%) in our sample ((33128) 1998 BU₄₈, 2000 GN₁₇₁, (20000) Varuna and 1999 KR₁₆) were found to exhibit lightcurves with peak-to-peak range ≥ 0.15 magnitude. In a larger sample obtained by combining our data with reliably determined lightcurves from the literature, 7 of 22 objects (32%) display significant (≥ 0.15 magnitude range) lightcurves. About 23% of the sampled objects have lightcurve ranges ≥ 0.4 magnitudes. Curiously, the objects are very large ($\gtrsim 250$ km diameter, assuming an albedo of 0.04) and, in the absence of rotation, should be near spherical due to self compression. We propose that the large amplitude, short period objects are rotationally distorted, low density rubble piles. Statistically, the trans-Neptunian objects are less spherical than their main-belt asteroid counterparts, indicating a higher specific angular momentum perhaps resulting from the formation epoch. In addition to the rotational lightcurves, we measured phase darkening for 7 Kuiper Belt objects in the 0 to 2 degree phase angle range. Unlike Pluto, the measured values show steep slopes and moderate opposition surge indicating backscatter from low albedo porous surface materials.

Subject headings: Kuiper Belt, Oort Cloud - minor planets, solar system: general

1. Introduction

More than 500 Trans-Neptunian Objects (TNOs) have been discovered in the decade since the discovery of 1992 QB₁ (Jewitt & Luu 1993). These objects comprise the Kuiper Belt (also known as the Edgeworth-Kuiper Belt) which is thought to contain about 70,000 objects with radii greater than 50 km (Jewitt, Luu and Chen 1996). The Kuiper Belt is thought to be a relic from the original protoplanetary disk, albeit one that has been dynamically disturbed and collisionally processed in ways that are not yet fully understood.

The Kuiper Belt is the most likely source of the Jupiter-family comets (Fernandez 1980, Duncan, Quinn and Tremaine 1988). It is by far the largest long-lived reservoir of small bodies in the planetary region, outnumbering the main-belt asteroids and Jovian Trojans by a factor of ~ 300 . The Kuiper Belt Objects (KBOs) are further thought to be chemically primitive, containing trapped volatiles and having experienced relatively little thermal evolution since formation. Thus we may be able to probe some aspects of the early history of the local solar nebula by studying the Kuiper Belt and related objects.

The determination of the physical characteristics of the KBOs has proceeded very slowly. This is because even the brightest known KBOs (other than Pluto and Charon) reach only apparent red magnitude $m_R \sim 19.5$ and thus are challenging with current spectroscopic technology. The surfaces of KBOs may have been altered over their lifetimes by collisions, cometary activity, and irradiation. The largest KBOs might even be partially differentiated from radiogenic heating. This could lead to the spinning up of objects to conserve angular momentum. Colors of the KBOs have been found to be diverse, ranging from neutral to very red ($V-R \sim 0.3$ to $V-R \sim 0.8$) (Luu & Jewitt 1996; Green et al. 1997; Tegler & Romanishin 2000; Jewitt & Luu 2001). While spectra of KBOs are mostly featureless, some show weak $2\mu\text{m}$ water ice absorptions (Brown, Cruikshank, & Pendleton 1999; Jewitt & Luu 2001). Most KBOs are too distant ($\gtrsim 30$ AU) and small to resolve with current technology. They are also very cold objects ($\sim 50\text{K}$) which emit most of their thermal radiation in the inaccessible far infrared wavelengths, requiring observations from above the Earth's atmosphere. Thus the most feasible way to determine KBOs shapes and surface features is through their photometric light variations.

The rotations and shapes of the KBOs may be a function of their size. Small KBOs (diameters $D < 100$ km) are thought to be collisionally produced (Farinella and Davis 1996). These objects retain no memory of the primordial angular momentum of their parent bodies. Instead, their spins are presumably set by the partitioning of kinetic energy delivered by the projectile responsible for break-up. Larger objects may be structurally damaged bodies held together by gravity (rubble piles). The spins of these objects should be much less influenced by recent impacts. A similar situation prevails in the main asteroid belt, where collisional modification of the rotations and shapes of the smaller objects is observationally well established (Catullo et al. 1984). The large objects in both the main-belt and the Kuiper Belt may provide a record of the primordial distribution of angular momenta imbued by the growth process. A key attribute of the Kuiper

Belt is that the population is very large compared to the main asteroid belt, allowing access to a substantial sample of objects that are too large to have been influenced by recent collisions.

We here use voluminous time resolved photometric observations to determine the rotational lightcurves, colors, and phase functions of KBOs. As our sample, we select the intrinsically brightest (presumably largest) KBOs. Specifically, we observed KBOs having absolute magnitude $H_R \leq 7.5$, corresponding to $D \geq 200$ km if a red geometric albedo of $p_R = 0.04$ is assumed. We use most of the known KBOs with $H_R \leq 6.0$ which corresponds to $D \geq 375$ km in our analysis. The objects observed were all bright in order to guarantee high signal-to-noise ratios in short exposures to adequately sample the KBO lightcurves.

2. Observations

The University of Hawaii 2.2 m diameter telescope atop Mauna Kea in Hawaii was used with a 2048×2048 pixel Tektronix CCD ($24 \mu\text{m}$ pixels) and a $0.''219 \text{ pixel}^{-1}$ scale at the f/10 Cassegrain focus. An antireflection coating provides very high average quantum efficiency (0.90) in the R-band. The field-of-view was $7'.5 \times 7'.5$. Exposures were taken using BVRI filters based on the Johnson-Kron-Cousins system, while the telescope was autoguided on bright nearby stars. The seeing ranged from $0.''6$ to $1.''5$ during the many nights of observation throughout 1999, 2000, and 2001. Objects moved relative to the fixed stars at a maximum of $4'' \text{ hr}^{-1}$ corresponding to trail lengths $\leq 0.''45$ in the longest (400 sec) exposures. Even for the fastest moving objects in the longest exposures the trailing motion is small compared to the seeing and so can be neglected as a source of error in the photometry.

The images were bias subtracted and then flat-fielded using the median of a set of dithered images of the twilight sky. Landolt (1992) standard stars were used for the absolute photometric calibration. Photometry of faint objects, such as the KBOs, must be done very carefully to achieve accurate results. To optimize the signal-to-noise ratio we performed aperture correction photometry by using a small aperture on the KBOs ($0.''65$ to $0.''88$ in radius) and both the same small aperture and a large aperture ($2.''40$ to $3.''29$ in radius) on (four or more) nearby bright field stars. We corrected the magnitude within the small aperture used for the KBOs by determining the correction from the small to the large aperture using the field stars (c.f. Tegler and Romanishin 2000; Jewitt & Luu 2001). Since the KBOs moved slowly we were able to use the same field stars from night to night within each observing run. Thus relative photometric calibration from night to night was very constant. The few observations that were taken in mildly non-photometric conditions were calibrated to observations of the same field stars on the photometric nights. The observational circumstances, geometry, and orbital characteristics of the 13 observed KBOs are shown in Tables 1 and 2 respectively.

3. Lightcurve Results

The photometric results for the 13 KBOs are listed in Table 3, where the columns include the start time of each integration, the corresponding Julian date, and the magnitude. No correction for light travel time has been made. Results of the lightcurve analysis for all the KBOs observed are summarized in Table 4 while the mean colors can be found in Table 5. We first discuss the lightcurves of (20000) Varuna, 2000 GN₁₇₁, (33128) 1998 BU₄₈, and 1999 KR₁₆ and give some details about the null results below.

We employed the phase dispersion minimization (PDM) method (Stellingwerf 1978) to search for periodicity in the data. In PDM, the metric is the so-called Θ parameter, which is essentially the variance of the unphased data divided by the variance of the data when phased by a given period. The best fit period should have a very small dispersion compared to the unphased data and thus $\Theta \ll 1$ indicates that a good fit has been found.

3.1. (20000) Varuna

Varuna shows a large, periodic photometric variation (Farnham 2001). We measured a range $\Delta m_R = 0.42 \pm 0.02$ mag. and best-fit, two-peaked lightcurve period $P = 6.3436 \pm 0.0002$ hrs (about twice the period reported by Farnham), with no evidence for a rotational modulation in the $B - V$, $V - R$ or $R - I$ color indices. These results, and their interpretation in terms of a rotating, elongated rubble pile of low bulk density, are described in detail in Jewitt and Sheppard (2002).

3.2. 2000 GN₁₇₁

PDM analysis shows that 2000 GN₁₇₁ has strong PDM minima near periods $P = 4.17$ hours and $P = 8.33$ hours, with weaker 24 hour alias periods flanking each of these (Figure 1). We phased the data to all the peaks with $\Theta < 0.4$ and found only the 4.17 and 8.33 hour periods to be consistent with all the data. The $P = 4.17$ hour period gives a lightcurve with a single maximum per period while the $P = 8.33$ hour lightcurve has two maxima per period as expected for rotational modulation caused by an aspherical shape. Through visual inspection of the phased lightcurves we find that the phase plot for $P = 4.17$ hour (Figure 2) is more scattered than that for the longer period of $P = 8.33$ hour (Figure 3). This is because the double-peaked phase plot shows a significant asymmetry of $\Delta \sim 0.08$ magnitudes between the two upper and lower peaks. A closer view of the PDM plot in Figure 4 around the double-peaked period allows us to obtain a rotation period of $P_{rot} = 8.329 \pm 0.005$ hours with a peak-to-peak variation of $\Delta m = 0.61 \pm 0.03$ magnitudes. We believe that the photometric variations in 2000 GN₁₇₁ are due to its elongated shape rather than to albedo variations on its surface.

Broadband BVRI colors of 2000 GN₁₇₁ show no variation throughout its rotation within the photometric uncertainties of a few % (Figures 5 and 6 and Table 6). This again suggests that the lightcurve is mostly caused by an elongated object with a nearly uniform surface. The colors $B - V = 0.92 \pm 0.04$, $V - R = 0.63 \pm 0.03$, and $R - I = 0.56 \pm 0.03$ (Table 5 and Table 6) show that 2000 GN₁₇₁ is red but unremarkably so as a KBO (Jewitt and Luu 2001).

3.3. (33128) 1998 BU₄₈

The KBO 1998 BU₄₈ showed substantial variability (> 0.4 magnitude with period > 4.0 hour) in R-band observations from 2 nights in 2001 February and April. However, a convincing lightcurve could not be found from just these 2 nights separated by 2 months. Additional observations were obtained in the period 2001 November 14 – 19. One minimum and one maximum in brightness within a single night was observed and put the full single-peaked lightcurve between about 4 and 6 hours. Through PDM analysis, 1998 BU₄₈ was found to have a peak-to-peak variation of $\Delta m = 0.68 \pm 0.04$ magnitudes with possible single-peaked periods near 4.1, 4.9, and 6.3 hours which are 24 hour aliases of each other (Figure 7). By examining the phased data using these three possible periods we find that the single-peaked periods of 4.9 ± 0.1 and 6.3 ± 0.1 hours are both plausible (Figure 8). The colors, $B - V = 0.77 \pm 0.05$, $V - R = 0.68 \pm 0.04$, and $R - I = 0.50 \pm 0.04$ (Table 5) show no sign of variation throughout the lightcurve, within the measurement uncertainties (Table 7 and Figure 8).

3.4. 1999 KR₁₆

This object was observed on four different observing runs during the course of 2000 and 2001. The data from 2001 are more numerous and of better quality than the data from 2000. We observed one brightness minimum and one maximum within a single night of data and from this estimated that the full single-peaked lightcurve should be near 6 hours. In a PDM plot constructed using only the inferior data from 2000 we found single-peaked minima at 4.66 and 5.82 hours. Phased lightcurves at these periods are acceptable for the year 2000 data, but the 4.66 hour period is inconsistent with the data from 2001. In the PDM plot using the R-band data from February, April, and May 2001 the best fit single-peaked period is shown to be around 5.9 hours with associated flanking peaks from 24 hours and 15 and 60 day sampling aliases (Figure 9). Closer examination of the PDM fit near 5.9 hours shows the 15 and 60 day aliasing much better and gives two best fit periods, one at 5.840 and the other at 5.929 hours (Figure 10). We phased the 2001 data to both single peaks and found neither to be significantly better than the other. The true single-peaked period for 1999 KR₁₆ is at one of these two values. The data phased to the 5.840 hour single-peaked period are shown in Figure 11. Neither of the possible double-peaked periods of 11.680 and 11.858 hours show differences between the peaks. The peak-to-peak amplitude of 1999 KR₁₆ is 0.18 ± 0.04 in the 2001 data consistent with that found in the 2000 data. Colors of

1999 KR₁₆, $B - V = 0.99 \pm 0.05$, $V - R = 0.75 \pm 0.04$, and $R - I = 0.70 \pm 0.04$, are on the red end of the KBO distribution (Table 5). The colors show no signs of variation through the rotation of the object to the accuracy of our measurements (Table 8 and Figure 11).

3.5. Null Lightcurves

Nine of the TNOs (2001 FZ₁₇₃, 2001 CZ₃₁, (38628) 2000 EB₁₇₃, (26375) 1999 DE₉, 1998 HK₁₅₁, (33340) 1998 VG₄₄, (19521) Chaos 1998 WH₂₄, 1997 CS₂₉, and (26181) 1996 GQ₂₁) show no measurable photometric variations. Practically, this means that their lightcurves have range ≤ 0.15 magnitudes and/or period ≥ 24 hours (Figures 12 and Table 4). A few objects show hints of variability that might, with better data, emerge as rotationally modulated lightcurves. Inspection of the 2001 CZ₃₁ data hints at a single-peaked lightcurve of period ~ 3 hours and amplitude ~ 0.15 magnitudes, but since the photometry has large error bars we can not be sure of this result. The TNO 1999 DE₉ may have a long period lightcurve of about 0.1 mag. range since the brightness on 2001 April 24 slowly increases towards the end of the night and the February data appear to have base magnitudes different by about 0.1 mag. The data from 2000 on 1999 DE₉ show the object to have a flat lightcurve. (33340) 1998 VG₄₄ may also have a long period lightcurve since its base magnitudes on 1999 November 11 and 12 are different by about 0.05 mag. The bright TNO (19521) 1998 WH₂₄ may have a possible lightcurve of about 4 hours single-peaked period and peak-to-peak range of 0.07 mag. Confirmation of these subtle lightcurves will require more accurate data, probably from larger telescopes than the one employed here.

4. Interpretation

The KBOs should be in principal axis rotation since the expected damping time of any other wobbles is much less than the age of the Solar System (Burns & Safronov 1973; Harris 1994). Orbital periods of KBOs are long (> 200 years) and thus the pole orientation to our line of sight should not change significantly between epochs. The apparent magnitude of a KBO depends on its physical characteristics and geometrical circumstances and can be represented as

$$m_R = m_\odot - 2.5 \log \left[p_R r^2 \phi(\alpha) / (2.25 \times 10^{16} R^2 \Delta^2) \right] \quad (1)$$

in which r [km] is the radius of the KBO, R [AU] is the heliocentric distance, Δ [AU] is the geocentric distance, m_\odot is the apparent red magnitude of the sun (-27.1), m_R is the apparent red magnitude, p_R is the red geometric albedo, and $\phi(\alpha)$ is the phase function in which the phase angle $\alpha = 0$ deg at opposition and $\phi(0) = 1$. The apparent brightness of an inert body viewed in reflected light may vary because of 1) changes in the observing geometry, including the effects of phase darkening as in Eq. (1) and 2) rotational modulation of the scattered light. These different effects are discussed below.

4.1. Non-uniform Surface Markings

Surface albedo markings or topographical shadowing can potentially influence the lightcurves. Judging by other planetary bodies, the resulting light variations are typically smaller than those caused by elongated shape, with fluctuations due to albedo being mostly less than about 10 to 20 percent (Degewij, Tedesco, Zellner 1979). A color variation at the maximum and minimum of a lightcurve may be seen if albedo is the primary cause for the lightcurve since materials with markedly different albedos often also have markedly different colors. For example, many pure ices and frosts have a very high albedo and are neutral to bluish in color. A lightcurve caused by an ice or frost patch should show a bluish color when at maximum brightness. Some of the most extreme albedo contrasts are found on Pluto and the Saturnian satellite Iapetus (Table 9). The latter is in synchronous rotation around Saturn with its leading hemisphere covered in a very low albedo material thought to be deposited from elsewhere in the Saturn system. Iapetus shows clear rotational color variations ($\Delta(B - V) \sim 0.1$ mag.) that are correlated with the rotational albedo variations. On the other hand, Pluto has large albedo differences across its surface but the hemispherically averaged color variations are only of order 0.01 mag. We feel that neither Iapetus nor Pluto constitutes a particularly good model for the KBOs. The large albedo contrast on Iapetus is a special consequence of its synchronous rotation and the impact of material trapped in orbit about Saturn. This process is without analog in the Kuiper Belt. Pluto is also not representative of the other KBOs. It is so large that it can sustain an atmosphere which may contribute to amplifying its lightcurve amplitude by allowing surface frosts to condense on brighter (cooler) spots. Thus brighter spots grow brighter while darker (hotter) spots grow darker through the sublimation of ices. This positive feedback mechanism requires an atmosphere and is unlikely to be relevant on the smaller KBOs studied here.

4.2. Aspherical Shape

The critical rotation period (T_{crit}) at which centripetal acceleration equals gravitational acceleration towards the center of a rotating spherical object is

$$T_{crit} = \left(\frac{3\pi}{G\rho} \right)^{1/2} \quad (2)$$

where G is the gravitational constant and ρ is the density of the object. With $\rho = 10^3$ kg m⁻³ the critical period is about 3.3 hours. Even at longer periods, real bodies will suffer centripetal deformation into aspherical shapes. For a given density and specific angular momentum (H), the nature of the deformation depends on the strength of the object. In the limiting case of a strengthless (fluid) body, the equilibrium shapes have been well studied (Chandrasekhar 1987). For $H \leq 0.304$ (in units of $(GM^3 a')^{1/2}$, where M [kg] is the mass of the object and a' [m] is the radius of an equal volume sphere) the equilibrium shapes are the oblate "MacLaurin" spheroids.

Oblate spheroids in rotation about their minor axis exhibit no rotational modulation of the cross-section and therefore are not candidate shapes for explaining the lightcurves of the KBOs. However, for $0.304 \leq H \leq 0.390$ the equilibrium figures are triaxial "Jacobi" ellipsoids which generate lightcurves of substantial amplitude when viewed equatorially. Strengthless objects with $H > 0.390$ are rotationally unstable to fission.

The KBOs, being composed of solid matter, clearly cannot be strengthless. However, it is likely that the interior structures of these bodies have been repeatedly fractured by impact, and that their mechanical response to applied rotational stress is approximately fluid-like. Such "rubble pile" structure has long been suspected in the main asteroid belt (Farinella et al. 1981) and has been specifically proposed to explain the short period and large amplitude of (20000) Varuna (Jewitt and Sheppard 2002). The rotational deformation of a rubble pile is uniquely related to its bulk density and specific angular momentum. Therefore, given that the shape and specific angular momentum can be estimated from the amplitude and period of the lightcurve, it is possible to use photometric data to estimate the density.

Elongated Objects exhibit rotational photometric variations caused by changes in the projected cross-section. The rotation period of an elongated object should be twice the single-peaked lightcurve variation due to its projection of both long axes (2 maxima) and short axes (2 minima) during one full rotation. From the ratio of maximum to minimum brightness we can determine the projection of the body shape into the plane of the sky. The rotational brightness range of a triaxial object with semiaxes $a \geq b \geq c$ in rotation about the c axis is given by (Binzel et al. 1989)

$$\Delta m = 2.5 \log \left(\frac{a}{b} \right) - 1.25 \log \left(\frac{a^2 \cos^2 \theta + c^2 \sin^2 \theta}{b^2 \cos^2 \theta + c^2 \sin^2 \theta} \right) \quad (3)$$

where Δm is expressed in magnitudes, and θ is the angle at which the rotation (c) axis is inclined to the line of sight (an object with $\theta = 90$ deg. is viewed equatorially).

It is to be expected that, through collisions, fragments would have random pole vector orientations. For example, the collisionally highly evolved asteroid belt shows a complete randomization of pole vector orientations, θ . Only the largest asteroids may show a preference for rotation vectors aligned perpendicular to the ecliptic ($\theta = 90^\circ$), though this is debatable (Binzel et al. 1989; Drummond et al. 1991; De Angelis 1995). In the absence of any pole orientation data for the KBOs, we will assume they have a random distribution of spin vectors. Given a random distribution, the probability of viewing an object within the angle range θ to $\theta + d\theta$ is proportional to $\sin(\theta)d\theta$. In such a distribution, the average viewing angle is $\theta = 60$ degrees. Therefore, on average, the sky-plane ratio of the axes of an elongated body is smaller than the actual ratio by a factor $\sin(60) \approx 0.87$.

In addition to rotational deformation, it is possible that some asteroids and KBOs consist of contact binaries (Jewitt & Sheppard 2002). For a contact binary consisting of equal spheres, the

axis ratio of 2:1 corresponds to a peak-to-peak lightcurve range $\Delta m = 0.75$ mag., as seen from the rotational equator. For such an object at the average viewing angle $\theta = 60$ degrees we expect $\Delta m = 0.45$ mag.

Collisionally produced fragments on average have axis ratios $2 : 2^{1/2} : 1$ (Fujiwara, Kamimoto, & Tsukamoto 1978; Capaccioni et al. 1984). When viewed equatorially, such fragments will have $\Delta m = 0.38$ mag. At the mean viewing angle $\theta = 60$ degrees we obtain $\Delta m = 0.20$ mag.

4.3. Lightcurve Model Results

The KBOs in our sample are very large ($D > 250$ km assuming a low albedo) and should, in the absence of rotational deformation, be spherical in shape from gravitational self compression. The large amplitudes and fast rotations of (20000) Varuna, 2000 GN₁₇₁, and (33128) 1998 BU₄₈ suggest that the lightcurves are caused by elongation and not surface albedo features. In support of this is the finding that (33128) 1998 BU₄₈ and (20000) Varuna have no color variations throughout their lightcurves and 2000 GN₁₇₁ has only a slight if any variation in color. Independently 2000 GN₁₇₁ shows two distinct lightcurve maxima and minima which is a strong reason to believe the object is elongated. The other lightcurve we found was for 1999 KR₁₆. Since its amplitude is much smaller and period longer, the lightcurve of 1999 KR₁₆ may be more dominated by nonuniform albedo features on its surface, though we found no measurable color variation over the rotation.

Table 10 lists the parameters of albedo, Jacobi ellipsoid and binary models that fit the axis ratios estimated from the lightcurve data (Table 4). For each object and model, we list the minimum bulk density, ρ , required to maintain a stable configuration, as described in Jewitt and Sheppard (2002). We briefly describe the procedure below for 2000 GN₁₇₁. Results for the rest of the significant light variation objects in our sample ((20000) Varuna, (33128) 1998 BU₄₈, and 1999 KR₁₆) can be seen in Table 10 using the data from Table 4.

We use Equation 3 to estimate the axis ratio a/b . If we assume that the rotation axis is perpendicular to our line of sight ($\theta = 90$) we obtain

$$\frac{a}{b} = 10^{0.4\Delta m_R} \quad (4)$$

Using $\Delta m_R = 0.61$ magnitudes we obtain from Equation 4 $a/b = 1.75 : 1$ for 2000 GN₁₇₁. This is a lower limit to the intrinsic axis ratio because of the effects of projection into the plane of the sky. If 2000 GN₁₇₁ is a Jacobi triaxial ellipsoid with $P = 8.329$ hours then its $a : b : c$ axis ratio would be $1.75 : 1 : 0.735$ and the lower limit on the density would be $\rho = 635$ kg m⁻³ (Chandrasekhar 1987; see Jewitt & Sheppard 2002 for a KBO context discussion of Jacobi ellipsoids). Finally if 2000 GN₁₇₁ were a contact binary the ratio of the two radii, $a_1 : a_2$, would be $1.15 : 1$ with a lower limit to the density of $\rho = 585$ kg m⁻³ (see Jewitt & Sheppard 2002 for a discussion of contact binaries in the KBO context). Finally, though it is unlikely, if 2000 GN₁₇₁

is spherical and the lightcurve is due to a 1.75 : 1 contrast in albedo then the lower limit to the density of the KBO would be $\rho = 157 \text{ kg m}^{-3}$ from Equation 2 and using $P = 8.329$ hours.

5. Discussion

In Table 9 we show objects in the Solar System which have one axis of at least 200 km and which show large amplitude lightcurves. Interestingly there is a group of asteroids that are large ($D = 200$ to 300 km) and which have substantial lightcurve amplitudes. They also possess fast rotations. These objects are probably rotationally deformed “rubble piles” which may be similar to a Jacobi ellipsoid type object (Farinella et al. 1981). Such rubble pile structures may form in the main asteroid belt because all objects have been effected by the high-velocity ($\sim 5 \text{ km/s}$) collisions that occur there (Farinella, Paolicchi, Zappala 1982). The effect of collisions is highly dependent on the object size. Objects with $D > 300$ km are large enough not to be completely turned into rubble piles or have their momentum greatly altered. Objects with diameters 200 to 300 km are large enough to be gravitationally bound but impacts over the age of the Solar System will transform them into rubble piles and may significantly change their angular momentum. Most asteroids with $D < 200$ km are thought to be fragments from catastrophic collisions and are not massive enough to be gravitationally spherical.

How does the collisional outcome scale with velocity and density differences in the asteroid belt versus the Kuiper Belt? We assume the target body has catastrophic break up when the projectile kinetic energy equals the gravitational binding energy of the target

$$\frac{1}{2}M_p\Delta v^2 = \frac{3GM_t^2}{5r_t} \quad (5)$$

where Δv is the mean collisional speed, M is mass, r is radius, and subscripts p and t refer to projectile and target, respectively. For collisions with a target of given radius, the ratio of the sizes of the projectiles needed to cause disruption in the main-belt and in the Kuiper Belt is

$$\frac{r_{p,KB}}{r_{p,MB}} = \left[\left(\frac{\rho_{t,MB}}{\rho_{t,KB}} \right) \left(\frac{\Delta v_{KB}}{\Delta v_{MB}} \right)^2 \right]^{-1/3} \quad (6)$$

where we have assumed all Kuiper Belt objects have density ρ_{KB} , all main belt asteroids have density ρ_{MB} . Here $r_{p,MB}$ and $r_{p,KB}$ are the radii of the projectile in the main belt and Kuiper Belt which are needed to fracture the target in their respective belts, $\rho_{t,MB}$ and $\rho_{t,KB}$ are the densities of the target body in the main belt and Kuiper Belt respectively, and Δv_{MB} and Δv_{KB} are the respective collision velocities. If we put in nominal values of $\rho_{t,MB} = 3000 \text{ kg m}^3$, $v_{MB} = 5 \text{ km s}^{-1}$ and $\rho_{t,KB} = 1000 \text{ kg m}^3$, $v_{KB} = 1.5 \text{ km s}^{-1}$ for the main belt asteroids and Kuiper Belt

respectively we find

$$r_{p,KB} \approx 1.5r_{p,MB}. \quad (7)$$

Thus for targets of equal size, a projectile has to be about 50% larger in the Kuiper Belt than in the main belt to be able to cause catastrophic break up of the target body. This difference is not large and since the current collisional timescales for the asteroids and Kuiper Belt objects are similar (Davis & Farinella 1997; Durda & Stern 2000), other factors such as material strength and the number density of objects during early formation of each belt will be important in determining collisional differences.

The current Kuiper Belt has been found to be erosive for KBOs with $D < 100$ km while many of the larger objects are probably rubble piles (Davis & Farinella 1997). Laboratory and computer simulations show that self-gravitating targets are more easily fractured than dispersed (Asphaug et al. 1998). Once formed, rubble pile structures can insulate the rest of the body from the energy of impact, further inhibiting disruption. Collision experiments by Ryan, Davis, and GIBLIN (1999) also show that porous ices dissipate energy efficiently. The outcome of impact into a rubble pile depends heavily on the angle of impact. We note that glancing low velocity collisions substantially alter the spin of the target body and can create elongated objects and contact binaries (Leinhardt, Richardson, & Quinn 2000). These simulations all hint that rubble pile structures are able to remain gravitationally bound after an impact, but that their angular momentum may be altered in the process which could produce elongated shapes.

To date eight binary Kuiper Belt objects have been reported. It seems that there may be a large fraction of binary KBOs. It also appears that about 32% of KBOs are highly elongated. Both the binaries and the highly elongated shapes indicate large specific angular momentum, most likely delivered by glancing collisions. The current rate of collisions is too small however for any substantial modifications of the spins or shapes of KBOs (Jewitt and Sheppard 2002). Instead, we prefer the hypothesis that the binaries and elongated shapes are products of an early, denser phase in the Kuiper Belt, perhaps associated with its formation.

5.1. Other Lightcurve Observations

We now consider lightcurve observations of KBOs published by others in order to make a larger sample. Unfortunately, few KBOs to date have been shown through independent observations to have repeatable lightcurves. Hainaut et al. (2000) reported that (19308) 1996 TO₆₆ has a lightcurve which varies in amplitude over the course of one year and interpreted this as a result of possible on-going cometary activity. Object 1996 TO₆₆ may show a color difference throughout its rotation (Sekiguchi et al. 2002). In contrast, 1996 TO₆₆ was reported to have a flat lightcurve by Romanishin & Tegler (1999) during the same year in which Hainaut et al. (2000) detected variation. Our own observations show that 1996 TO₆₆ does have a significant lightcurve, basically confirming the variation originally observed by Hainaut et al. (2000) and contradicting

the null detection by Romanishin & Tegler (Sheppard 2002). Conversely, an object reported to have a lightcurve by Romanishin & Tegler (1999), (15820) 1994 TB, was found by us to display no significant variation (Sheppard 2002). Because of these conflicts of unrepeatability, and since many of the Romanishin & Tegler targets were very sparsely sampled with raw data that remains unpublished, we use their work with caution in the following analysis.

Our combined sample of 22 KBOs comprises only well observed objects with numerous observations that could constrain any significant photometric variation from this (Table 4) and other (Table 11) works. Among the objects newly observed in this survey (Table 4), the fraction with significant lightcurve variation is $f(\Delta m_R \geq 0.15) = \frac{4}{13}$ (31%) and $f(\Delta m_R \geq 0.40) = \frac{3}{13}$ (23%). Including the objects reliably observed by others (Table 11) yields $f(\Delta m_R \geq 0.15) = \frac{7}{22}$ (32%) and $f(\Delta m_R \geq 0.40) = \frac{5}{22}$ (23%). Although we have evidence that some of their lightcurves are unrepeatable, we note that Romanishin & Tegler (1999) found a comparable $f(\Delta m_R \geq 0.10) = \frac{3}{11}$ (27%). We consider that these results all point to a similar fraction $f(\Delta m_R \geq 0.15) \sim 32\%$ and $f(\Delta m_R \geq 0.40) \sim 23\%$.

The samples of objects with significant lightcurves and flat lightcurves were tested for correlations with orbital parameters and colors. No significant correlations were found. From the sample of 22 objects, 2 of the 9 (22%) resonant objects, 4 of the 8 (50%) classical objects, and 1 of the 5 (20%) scattered objects had measurable lightcurves ($\Delta m_R \geq 0.15$). Many of the objects shown in Table 11 are detailed elsewhere by us (Sheppard 2002) because they were objects particularly targeted by us to confirm their reported lightcurves and determine amplitudes and periods if a lightcurve was seen. The 13 objects reported in this paper (Table 4) were selected because of their size and brightness and not because of previous reports of their variability.

In comparison to the percentages of KBOs with large amplitude lightcurves (> 0.40 or about 1.5 difference in brightness), the four main belt asteroids with $D > 400$ km have $f(\Delta m_R \geq 0.40) = \frac{0}{4}$ (0%), the largest being only about 0.15 magnitudes (Lagerkvist, Harris, & Zappala 1989; Tedesco 1989). For main-belt asteroids with $D > 200$ km $f(\Delta m_R \geq 0.40) = \frac{5}{27}$ (19%) when their poles orientations are $\theta = 90$ degrees to our line of site. With the average pole orientation of $\theta = 60$ degrees only (11%) ($f(\Delta m_R \geq 0.40) = \frac{3}{27}$) have large amplitude lightcurves. These large amplitude lightcurve objects are thought to be the Jacobi ellipsoid type objects. Asteroids with $D < 200$ km have $f(\Delta m_R \geq 0.40) = \frac{111}{482}$ (23%) while the Centaurs (Chiron, Asbolus, Pholus, Chariklo, Hylonome, (31824) 1999 UG5, and (32532) 2001 PT13) have $f(\Delta m_R \geq 0.40) = \frac{0}{7}$ (0%). These objects are small and thus thought to be collisional fragments.

Figure 13 shows how the largest ($D > 200$ km) main belt asteroids compare with the Kuiper Belt objects. Many of the Kuiper Belt objects fall in the upper and upper left parts of this figure, where the Jacobi ellipsoids are encountered in the asteroid belt. There is a bias in the KBO sample since light variations of less than about 0.1 magnitudes are very hard to detect, as are long single-peak periods > 24 hours.

The Student’s t-test was used to measure the significance of the differences between the means

of the asteroid and KBO periods and amplitudes. In order to reduce the effects of observational bias we used only periods less than 10 hours and amplitudes greater than 0.2 magnitudes from Figure 13. We found that the period distributions of the asteroids are significantly shorter than for the KBOs. The mean periods are 5.56 ± 0.89 and 7.80 ± 1.20 hours for the asteroids and KBOs respectively, giving a t-statistic of -3.84 (12 degrees of freedom) which is significant at the 99.7% confidence level. This difference is formally significant at the 3σ level by the Student’s t-test, but it would be highly desirable to obtain more data from another large unbiased survey in order to be sure of the effect. The KBOs have a larger mean amplitude, but the significance between the difference of means, 0.36 ± 0.11 vs. 0.50 ± 0.16 magnitudes for the asteroids and KBOs respectively, is only 95% (2σ) with a t-statistic of -1.83 . This may be because the KBOs are less dense and more elongated, on average, than asteroids. Below we discuss in more detail the shape distribution of the Kuiper Belt.

5.2. Shape Distribution Models

What constraints can be placed on the intrinsic distribution of KBO shapes from the apparent (sky-plane projected) distribution? We used a Monte-Carlo model to project several assumed intrinsic distributions into the plane of the sky and then compared them with the observations. This was done by using a pole orientation distribution proportional to $\sin\theta$. The apparent axis ratio for each object was then calculated from this pole orientation distribution and the intrinsic axis ratio selected from one of several assumed distributions.

Firstly, as an extreme case, we ask whether the data are consistent with selection from intrinsic distributions in which all the objects have a single axis ratio $x = b/a$, with $x = 0.80, 0.66, 0.57$ or 0.50 (Figure 14). The Figure shows that the form of the resulting amplitude distribution differs dramatically from what is observed. We conclude that the distribution KBO lightcurve amplitudes cannot be modeled as the result of projection on any single axis ratio. A range of shapes must be present. While not surprising, this result does serve to demonstrate that the KBO lightcurve sample is of sufficient size to be diagnostic.

Secondly, we explored the effect of the width of the distribution using

$$\Psi(x)dx = \exp\left[\frac{-(x - x_0)^2}{2\sigma^2}\right] dx \quad (8)$$

where $\Psi(x)dx$ is the number of KBOs with axis ratios in the range x to $x + dx$, σ is the standard deviation or width parameter and x_0 is the mean axis ratio. Examples for $x_0 = 0.66$ and $\sigma = 0, 0.35, 0.75,$ and 1.0 are plotted in Figure 15. We assumed that all objects had axis ratios $0.5 \leq x \leq 1.0$. The Figure shows that the data require an intrinsically broad distribution of body shapes, specifically with a dispersion comparable to the mean axis ratio.

Thirdly, we assumed that the axis ratios of the KBOs followed a differential power-law

distribution of the form

$$\Psi(x)dx = x^{-q}dx \tag{9}$$

where q is a constant, and $\Psi(x)dx$ is again the number of KBOs with axis ratios in the range x to $x + dx$. We assumed $0.5 \leq x \leq 1.0$. A positive q favors objects with small axis ratios while negative q favors objects that are near spherical. The results can be seen in Figure 16. The $q = -5$ distribution is very similar to an exponential distribution with its peak at an axis ratio of $x = 1$. Again we see that the models fit the data better with a broader distribution of axis ratios.

Fourthly, we ask whether the data are consistent with selection from an intrinsic distribution of shapes caused by collisional fragmentation. The fragment shape distribution is taken from Catullo et al. (1984). Figure 17 shows that the KBO Δm distribution is inconsistent with the collisional fragment distribution in the sense that more highly elongated KBOs are found than would be expected from the impact fragments. This finding is consistent with collisional models (Farinella and Davis 1996, Kenyon and Luu 1999) in the sense that only KBOs smaller than a critical diameter ~ 100 km are likely to be impact fragments, while the observed KBOs are all larger than this.

Finally, we ask whether the data are consistent with selection from an intrinsic distribution of shapes like that measured in the large ($D > 200$ km) main-belt asteroid population. We take this distribution from the published lightcurve data base of Lagerkvist, Harris, & Zappala (1989) which has been updated by A. Harris on the world wide web at <http://cfa-www.harvard.edu/iau/lists/LightcurveDat.html>. The results are shown in Figure 17, where we see that the KBOs contain a larger fraction of highly elongated objects than are found amongst the main-belt asteroids. A plausible explanation for such a large fraction of the highly elongated Kuiper Belt objects is that the objects are very large yet structurally weak and of low density. This would allow many of the Kuiper Belt objects to be gravitationally bound rubble piles easily distorted by centripetal forces due to their rotation.

5.3. KBO Density Comparisons in the Solar System

The Kuiper Belt objects are thought to consist of water ice with some rocky material mixed in, similar to the comets. How do the densities of the outer satellites compare to what we have found for our sample of Kuiper Belt objects? In Figure 18 we plot all the outer icy bodies in the Solar System that have well known densities and are less than 3000 km in diameter. There is a clear trend, with larger objects being denser. The KBOs seem to follow this trend. We also note there appears to be an object size vs. lightcurve amplitude and size vs. period trend for the KBOs in our data. Objects that have densities less than that of water ice (1000 kg m^{-3}) must have significant internal porosity or be composed of ices less dense than water (see Jewitt and Sheppard 2002).

To date only about 10 main belt asteroids have reliably measured bulk densities. Most of

these are from perturbation calculations between asteroids though two have been measured by passing spacecraft and a few others found from the orbital motions of known companions. Most asteroid densities are consistent with that of rock, $2000 \leq \rho \leq 3000 \text{ kg m}^{-3}$. Some of the asteroids densities have been found to be lower than expected and attributed to internal porosity possibly from rubble pile structure (Yeomans et al. 1997).

In Table 9 we present new densities for five main belt asteroids calculated under the assumption that they are equilibrium rotational (Jacobi ellipsoid) figures. We used their lightcurves as seen at maximum amplitude, to eliminate the effects of projection. The densities are higher than those of the Kuiper Belt objects obtained using the same method (Figure 19) but lower than expected for solid rock objects. This provides another hint that these objects may be internally porous. The densities of 15 Eunomia ($790 \pm 210 \text{ kg m}^{-3}$) and 16 Psyche ($1800 \pm 600 \text{ kg m}^{-3}$) were reported separately from measurements of gravitational perturbations (Hilton 1997; Viateau 2000). The higher density for 16 Psyche is particularly interesting because this object is an M-type asteroid and thus expected to have a high density. The main belt asteroid 45 Eugenia was found to have a companion which was used by Merline et al. (1999) to find a density of $1200_{-200}^{+600} \text{ kg m}^{-3}$. Asteroid densities found by others are probably underestimated since they assumed that the objects were spheres. A sphere has the highest volume to projected area ratio and thus any deviation from a sphere will cause the object to appear to have a lower density. We calculated the density for these objects using the assumption they are Jacobi ellipsoids and thus the parameters used are the well known period and amplitude from the lightcurves. Interestingly the five best examples of main belt rotationally deformed asteroids (Table 9) are found in all the main classes, 2 C-type, 1 each of S, P, and M-types.

6. Phase Functions of KBOs

At large phase angles, the phase function in Equation 1 may be approximated as

$$\phi(\alpha) = 10^{-\beta\alpha} \tag{10}$$

where α is the phase angle in degrees, and β is the "linear" phase coefficient. Empirically, the magnitude of β is inversely correlated with the surface albedo (Gehrels 1970; Bowell et al. 1989; Belskaya and Shevchenko 2000), suggesting that we might be able to indirectly assess the albedos of KBOs from their phase functions. Unfortunately, this is not possible. The maximum phase angle attained by an object at distance R [AU] is roughly α_{max} [degrees] = $\frac{180}{\pi R}$. At $R = 30$ AU, for instance, $\alpha_{max} = 1.9$ degrees. This is exactly the phase angle range in which the opposition surge is potentially important (Scaltriti and Zappala 1980; Belskaya and Shevchenko 2000). The opposition surge is a complex, multiple scattering phenomenon which occurs in the grains of a porous regolith. The magnitude of the opposition surge, which causes an increase in scattered intensity over and above that predicted by Equation 10 at small α , is determined by coherent-backscattering and is a complex function of regolith physical and optical properties. It is

not simply related to the albedo and Equation 10 must be modified to take account of this surge. Nevertheless, the phase functions provide a new basis for comparison of the KBOs, and should be measured if we are to accurately assess the sizes of KBOs from their optical data.

Seven of the KBOs were observed over a range of phase angles sufficient for us to measure the phase darkening. We plot the quantity $m_R(1, 1, \alpha) = m_R - 5\log(R\Delta)$ against α for these 7 KBOs in Figures 20 and Figure 21. When observations from consecutive nights were available we averaged the phase angle and apparent magnitude over those nights to create a single point with small uncertainty. If an object showed a lightcurve, its time-averaged mean apparent magnitude was used. The linear least squares fits to the KBO data are listed in Table 12 and shown in Figure 20. Within the uncertainties, we find that photometry of the 7 KBOs is compatible with $\beta(\alpha < 2^\circ) = 0.15 \pm 0.01 \text{ mag deg}^{-1}$. In contrast the phase function for Pluto was found to be linear throughout the 0 to 2 degrees phase angle range with $\beta(\alpha < 2^\circ) = 0.0372 \pm 0.0016 \text{ mag deg}^{-1}$, indicating a very shallow if any opposition surge and consistent with a high albedo surface (Tholen and Tedesco 1994).

Since the small phase angle observations are affected by the "opposition surge", caused by multiple scattering within the porous regolith, we also fit the data using the Bowell et al. (1989) $H - G$ scattering parametrization. This technique gives a curved relation at small phase angles that becomes asymptotically like the linear β relation at large phase angles and thus attempts to account for the opposition surge. In the Bowell et al. formalism H is the absolute magnitude of the object, analogous to $m_R(1, 1, 0)$. The parameter G provides a measure of the slope of the phase function at large angles, analogous to β . It is scaled so that $G = 0$ corresponds to the darkest surfaces found on the asteroids while $G = 1$ corresponds to the brightest (Bowell et al. 1989). The results of the $H - G$ fits are presented in Table 12 and Figures 21 and 22. The KBOs show steep slopes with a possible moderate opposition surge. The best-fit values of the G parameter are very low with an average of -0.21 . This small G value more closely resembles that of dark, C-type asteroids ($G \sim 0.15$) than the brighter, S-types ($G \sim 0.25$) in the main-belt. This is consistent with, though does not prove, the assumption that the majority of KBOs are of very low albedo. The similarity of the slopes of the phase functions of all KBOs in our sample suggests comparative uniformity of the surface compositions, physical states, and albedos. As a comparison, Pluto was found to have a best fit $G = 0.88 \pm 0.02$ using data from Tholen & Tedesco (1994). The dramatic difference between the backscattering phase functions of Pluto and the smaller KBOs studied here is shown in Figure 22. This difference is again consistent with the smaller KBOs having low albedo (0.04?) surfaces qualitatively different from the high albedo (0.6), ice-covered surface of Pluto.

7. Summary

We have conducted a systematic program to assess the rotations and sky-plane shapes of Kuiper Belt Objects from their optical lightcurves.

1. Four of 13 (31%) bright Kuiper Belt objects in our sample ((33128) 1998 BU₄₈, 2000 GN₁₇₁, (20000) Varuna, and 1999 KR₁₆) show lightcurves with range $\Delta m \geq 0.15$ mag. In an enlarged sample combining objects from the present work with objects from the literature, 7 of 22 (32%) objects have $\Delta m \geq 0.15$ mag.

2. The fraction of KBOs with $\Delta m \geq 0.4$ mag (23%) exceeds the corresponding fraction in the main-belt asteroids (11%) by a factor of two. The KBO Δm distribution is inconsistent with the distribution of impact fragment shapes reported by Catullo et al. (1984).

3. The large Kuiper Belt Objects (33128) 1998 BU₄₈, 2000 GN₁₇₁ and (20000) Varuna show large periodic variability with photometric ranges 0.68 ± 0.04 , 0.61 ± 0.03 and 0.45 ± 0.03 magnitudes, respectively, and short double-peaked periods of 9.8 ± 0.1 , 8.329 ± 0.005 and 6.3565 ± 0.0002 hours, respectively. Their BVRI colors are invariant with respect to rotational phase at the few percent level of accuracy.

4. If these objects are equilibrium rubble piles distorted by centripetal forces due to their own rotation, the implied densities must be comparable to or less than that of water. Such low densities may be naturally explained if the KBOs are internally porous.

5. In the phase angle range $0 \leq \alpha \leq 2$ deg the average slope of the phase function of 7 KBOs is $\beta(\alpha < 2^\circ) = 0.15 \pm 0.01$ mag deg⁻¹ (equivalently, $G = -0.2$). The corresponding slope for ice-covered Pluto is $\beta(\alpha < 2^\circ) \approx 0.04$ mag/deg (equivalently, $G = 0.88$). The large difference is caused by pronounced opposition brightening of the KBOs, strongly suggesting that they possess porous, low albedo surfaces unlike that of ice-covered Pluto.

Acknowledgments

We thank John Dvorak, Paul deGroot, Ian Renaud-Kim, and Susan Parker for their operation of the UH telescope, Alan Harris for a quick and thoughtful review. This work was supported by a grant to D.J. from NASA.

REFERENCES

- Asphaug, E, Ostro, S., Hudson, R., Scheeres, D., & Benz, W. 1998, *Nature*, 393, 437
- Belskaya, I. & Shevchenko, V. 2000, *Icarus*, 147, 94
- Binzel, R., Farinella, P., Zappala V., & Cellino, A. 1989, in *Asteroids II*, ed. R. Binzel, T. Gehrels, and M. Matthews (Tucson: Univ. of Arizona Press), 416
- Boehnhardt, H., Tozzi G., Birkle, K. et al. 2001, *AA*, 378, 653
- Bowell, E., Hapke, B., Domingue, D., Lumme, K., Peltoniemi, J., & Harris, A. 1989, in *Asteroids II*, ed. R. Binzel, T. Gehrels, and M. Matthews (Tucson: Univ. of Arizona Press), 524

- Brown, R., Cruikshank, D., & Pendleton, Y. 1999, *ApJ Lett*, 519, L101
- Burns, J., & Safronov, V. 1973, *MNRAS*, 165, 403
- Capaccioni, F., Cerroni, P., Coradini, M., Farinella, P., Flamini, E., Martelli, G., Paolicchi, P., Smith, P., & Zappala, V. 1984, *Nature*, 308, 832
- Catullo, V., Zappala, V., Farinella, P., & Paolicchi, P. 1984, *AA*, 138, 464
- Chandrasekhar, S. 1987, *Ellipsoidal Figures of Equilibrium*. Dover, New York.
- Collander-Brown, S., Fitzsimmons, A., Fletcher, E., Irwin, M., & Williams, I. 1999, *MNRAS*, 308, 588
- Davies, J., McBride, N. & Green, S. 1997, *Icarus*, 125, 61
- De Angelis, G. 1995, *PSS*, 43, 649
- Degewij, J., Tedesco, E., & Zellner, B. 1979, *Icarus*, 40, 364
- Drummond, J., Weidenschilling, S., Chapman, C., & Davis, D. 1991, *Icarus*, 89, 44
- Durda, D. & Stern, A. 2000, *Icarus*, 145, 220
- Farnham, T. 2001, *IAU Circular 7583* (February 16)
- Farinella, P., Paolicchi, P., Tedesco, E., & Zappala, V. 1981, *Icarus*, 46, 114
- Farinella, P., Paolicchi, P., & Zappala, V. 1982, *Icarus*, 52, 409
- Farinella, P. & Davis, D. 1996, *Sci*, 273, 938
- Fujiwara, A., Kamimoto, G., & Tsukamoto, A. 1978, *Nature*, 272, 602
- Gehrels, T. 1970, in *Surfaces and Interiors of Planets and Satellites*, ed. A. Dollfus (London: Academic Press), pg. 355
- Green, S., McBride, N., O’Ceallaigh, D. Fitzsimmons, A., Williams, I., & Irwin, M. 1997, *MNRAS*, 290, 186
- Hainaut, O., Delahodde, C., Boehnhardt, H., Dotto, E., Barucci, M., Meech, K., Bauer, J., West, R., & Doressoundiram, A. 2000, *AA*, 356, 1076
- Harris, A. 1994, *Icarus*, 107, 209
- Hilton, J. 1997, *AJ*, 114, 402
- Jewitt, D. & Luu, J. 1993, *Nature*, 362, 730
- Jewitt, D., Luu, J., and Chen, J. 1996. *AJ*, 112, 1225
- Jewitt, D., Aussel, H., & Evans, A. 2001, *Nature*, 411, 446
- Jewitt, D. & Luu, J. 2001, *AJ*, 122, 2099
- Jewitt, D. & Sheppard, S. 2002, *AJ*, 123, 2110
- Kenyon, S. & Luu, J. 1999, *AJ*, 118, 1101
- Landolt, A. 1992, *AJ*, 104, 340

- Lagerkvist, C., Harris, A., & Zappala, V. 1989, in Asteroids II, ed. R. Binzel, T. Gehrels, and M. Matthews (Tucson: Univ. of Arizona Press), 1162
- Leinhardt, Z., Richardson, D., & Quinn, T. 2000, *Icarus*, 146, 133
- Lupo, M. & Lewis, J. 1979, *Icarus*, 40, 157
- Luu, J. & Jewitt, D. 1996, *AJ*, 112, 2310
- Luu, J. & Jewitt, D. 1998, *AJ*, 494, L117
- Merline, B., Close, L., Dumas, C., Chapman, C., Roddier, F., Menard, F., Slater, D., Duvert, G., Shelton, C., & Morgan, T. 1999, *Nature*, 401, 565
- Ortiz, J., Lopez-Moreno, J., Gutierrez, P., & Baumont, S. 2001, *BAAS*, 33, 1047
- Romanishin, W. & Tegler, S. 1999, *Nature*, 398, 129
- Romanishin, W., Tegler, S., Rettig, T., Consolmagno, G., & Botthof, B. 2001, *Proc. Nat. Academy Sci.*, 98, 11863
- Ryan, E., Davis, D., & Giblin, I. 1999, *Icarus*, 142, 56
- Scaltriti, F. & Zappala, V. 1980, *AA*, 83, 249
- Sekiguchi, T., Boehnhardt, H., Hainaut, O., & Delahodde, C. 2002, *AA*, 385, 281
- Sheppard, S. 2002, in preparation
- Stellingwerf, R. 1978, *ApJ*, 224, 953
- Tedesco, E. 1989, in Asteroids II, ed. R. Binzel, T. Gehrels, and M. Matthews (Tucson: Univ. of Arizona Press), pg. 1090
- Tegler, S. & Romanishin, W. 2000, *Nature*, 407, 979
- Tholen, D. & Tedesco E. 1994, *Icarus*, 108, 200
- Viateau, B. 2000, *AA*, 354, 725
- Yeomans, D., Barriot, J., Dunham, D. et al. 1997, *Science*, 278, 2106

Fig. 1.— The phase dispersion minimization (PDM) plot for 2000 GN₁₇₁. A smaller theta corresponds to a better fit. Best fits from this plot are the 4.12 hour single-peaked fit and the 8.32 hour double-peaked fit. Both are flanked by 24 hour alias periods.

Fig. 2.— Phased R-band data from the UT April 20 – 25 and May 11 – 13, 2001 observations of 2000 GN₁₇₁. The period has been phased to 4.17 hours which is the best fit single-peaked period. The May data have been corrected for geometry and phase angle differences relative to the April data (see Table 1). The points are much more scattered here than for the better fit double-peaked period (Figure 3).

Fig. 3.— Phased R-band data from the UT April 20 – 25 and May 11 – 13, 2001 observations for 2000 GN₁₇₁. The period has been phased to 8.329 hours which is the best fit double-peaked period. The May data have been corrected for geometry and phase angle differences relative to the April data (see Table 1).

Fig. 4.— Closer view of the phase dispersion minimization (PDM) plot for 2000 GN₁₇₁ around the double-peaked period near 8.33 hours. The best fit at 8.329 hours is flanked by aliases from the ~ 15 day separation of the 2 data sets obtained for this object.

Fig. 5.— The phased BVRI data from the UT April 20 – 25 and May 11 – 13, 2001 observations of 2000 GN₁₇₁. The period has been phased to 8.329 hours which is the best fit double-peaked period. The May data have been corrected for geometry and phase angle differences relative to the April data (Table 1). The BVI data have been shifted by the amount indicated on the graph in order to correspond to the R data. No color variation is seen within our uncertainties. A Fourier fit shows the two pronounced maximum and minimum.

Fig. 6.— The colors of 2000 GN₁₇₁ plotted against rotational phase.

Fig. 7.— Phase dispersion minimization (PDM) plot for (33128) 1998 BU₄₈ from the November 2001 data. Best fits from this plot are the 4.9 and 6.3 hour single-peaked fits and the 9.8 and 12.6 hour double-peaked fits.

Fig. 8.— BVRI phased data from the UT November 14 – 19 observations of (33128) 1998 BU₄₈. The period has been phased to 6.29 hours which is one of the best fit single-peaked periods for (33128) 1998 BU₄₈, the other being around 4.9 hours.

Fig. 9.— Phase dispersion minimization (PDM) plot for 1999 KR₁₆ using all the R-band data from February, April and May 2001. Best fits from this plot are near the 5.9 hour single-peak period and the 11.8 hour double-peaked period. Both are flanked by aliases of the 24 hr and ~ 15 and ~ 60 day sampling periodicities.

Fig. 10.— A closer view of the phase dispersion minimization (PDM) plot for 1999 KR₁₆ around the best fit single-peaked periods near 5.9 hours.

Fig. 11.— The phased BVRI data from the UT April 24 – 25 and May 11 – 13, 2001 observations of 1999 KR₁₆. The period has been phased to 5.840 hours which is one of the best fit single-peaked period for 1999 KR₁₆, the other being at 5.929 hours.

Fig. 12.— The null lightcurves of KBOs found to have no significant variation: a) 2001 FZ₁₇₃ b) 2001 CZ₃₁ c) (38628) 2000 EB₁₇₃ d) (26375) 1999 DE₉ e) 1998 HK₁₅₁ f) (33340) 1998 VG₄₄ g) (19521) Chaos 1998 WH₂₄ h) 1997 CS₂₉ i) (26181) 1996 GQ₂₁.

Fig. 13.— Rotational variability and periods of all the asteroids with diameters > 200 km and of Kuiper Belt objects in our sample. Objects in the upper and upper left portions of the graph are possibly rotationally deformed rubble piles. The asteroid amplitudes which were taken from pole orientations of 90 degrees have been corrected to a mean pole orientation at 60 degrees to better compare them with the KBOs of unknown orientation. KBOs with amplitudes ≤ 0.1 magnitudes and periods ≥ 12 hours are subject to observational bias against detection.

Fig. 14.— Monte Carlo simulations using a constant axis ratio for all KBOs. Error bars for the KBO points are based on a Poisson distribution.

Fig. 15.— Monte Carlo simulations using Gaussians centered on the axis ratio of 1:1.5 with different standard deviations (Equation 8). Error bars for the KBO points are based on a Poisson distribution.

Fig. 16.— Monte Carlo simulations using power laws of different slopes (Equation 9). Error bars for the KBO points are based on a Poisson distribution.

Fig. 17.— Monte Carlo simulations using all large asteroids ($D > 200$ km) and a collisional distribution from Catullo et al. (1984). Error bars for the KBO points are based on a Poisson distribution.

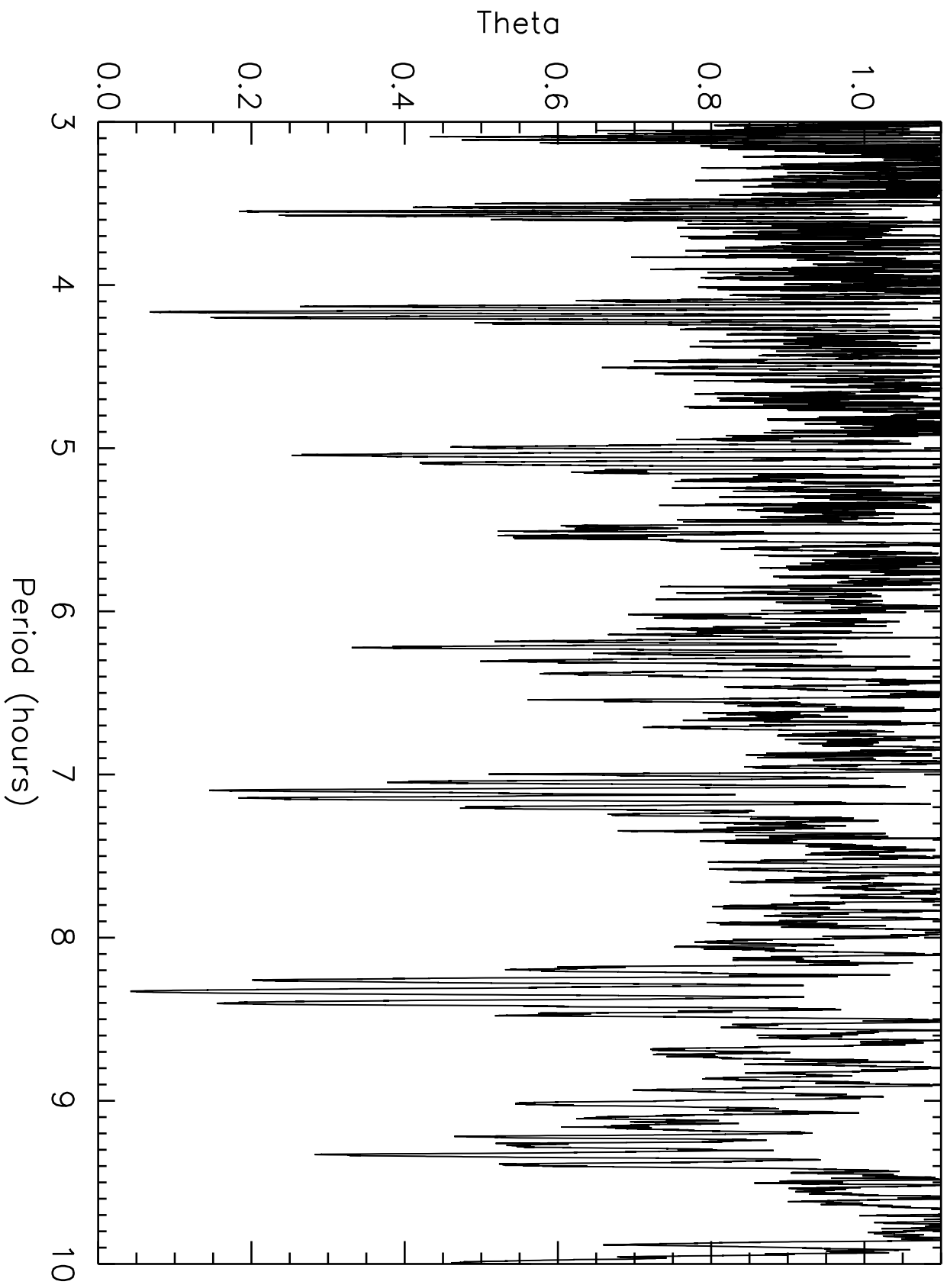
Fig. 18.— Sizes and densities of icy bodies. A trend is observed in which the larger the object the higher the density. The solid line is over plotted to show the expected bulk density of a pure water ice sphere with size (Lupo and Lewis 1979). Other lines indicate how the density would behave with added porosity and rock. Data points for satellite densities are from the JPL Solar System Dynamics web page.

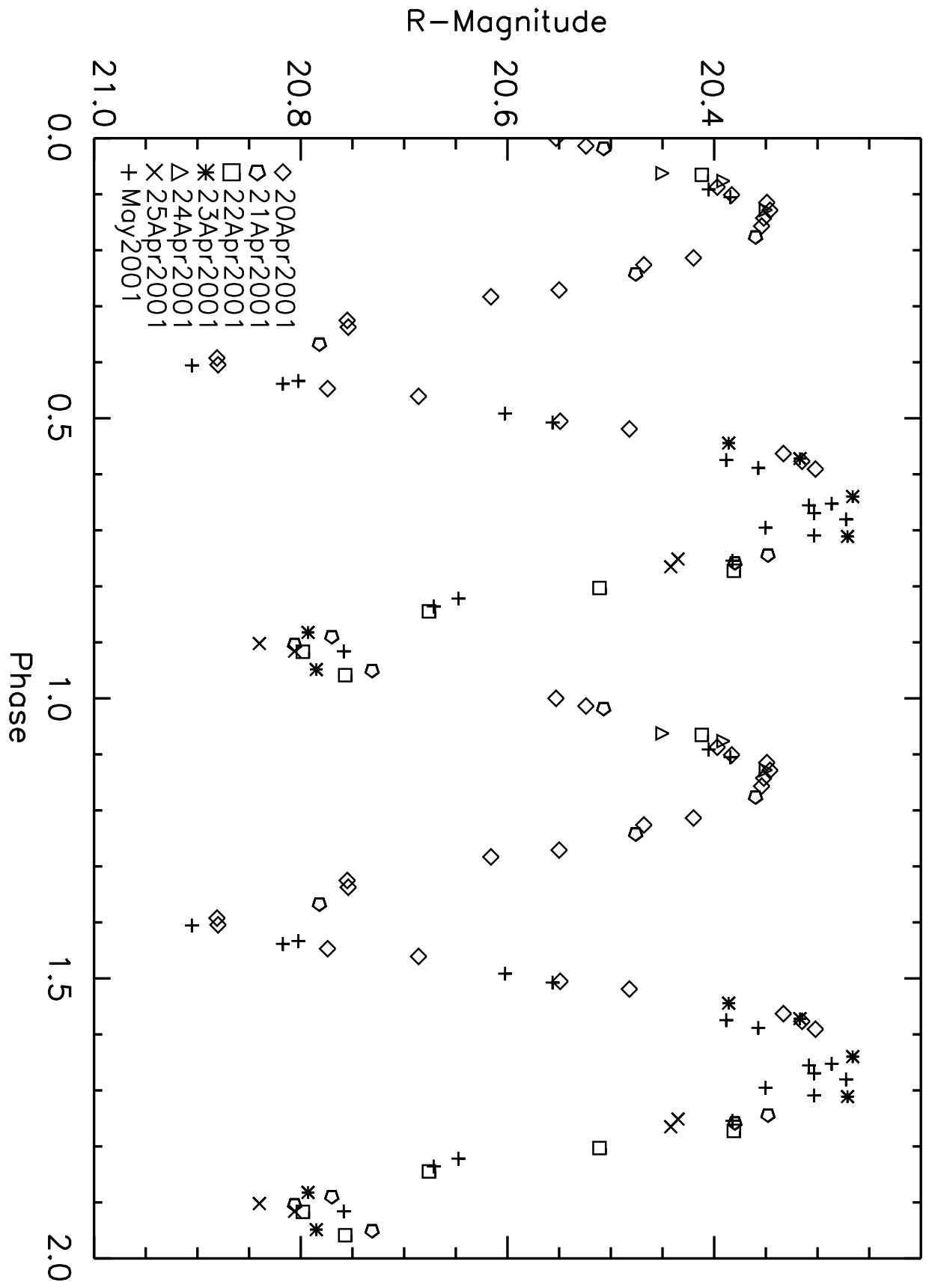
Fig. 19.— Size and densities of possible rotationally deformed KBOs and main belt asteroids. The asteroids have lower densities than expected for solid rock, but are still denser than the KBOs.

Fig. 20.— Phase functions for Kuiper Belt objects observed at several phase angles. The best linear fit gives a phase coefficient of $\beta(\alpha < 2^\circ) = 0.15$ magnitudes per degree. Objects with more than two data points show evidence of the nonlinear opposition surge.

Fig. 21.— Phase functions of all 7 KBOs observed at multiple phase angles. The reduced magnitudes have been normalized to show all objects relative slopes. Over plotted are fits of the slope parameter $G = 0.05$, 0.15 (C-type), and 0.25 (S-type). The best fit slope parameters of all KBOs are below $G = 0.05$ which is consistent with scattering from low albedo surfaces.

Fig. 22.— Comparison of phase functions for the typical KBO 1999 KR₁₆ and Pluto. The Solid line is the best fit HG phase function for 1999 KR₁₆ with $G = -0.08$. Data points for Pluto are from Tholen & Tedesco (1994) and are offset in the vertical direction from -1.0. Pluto has a best fit $G = 0.88$ shown with the dashed line.





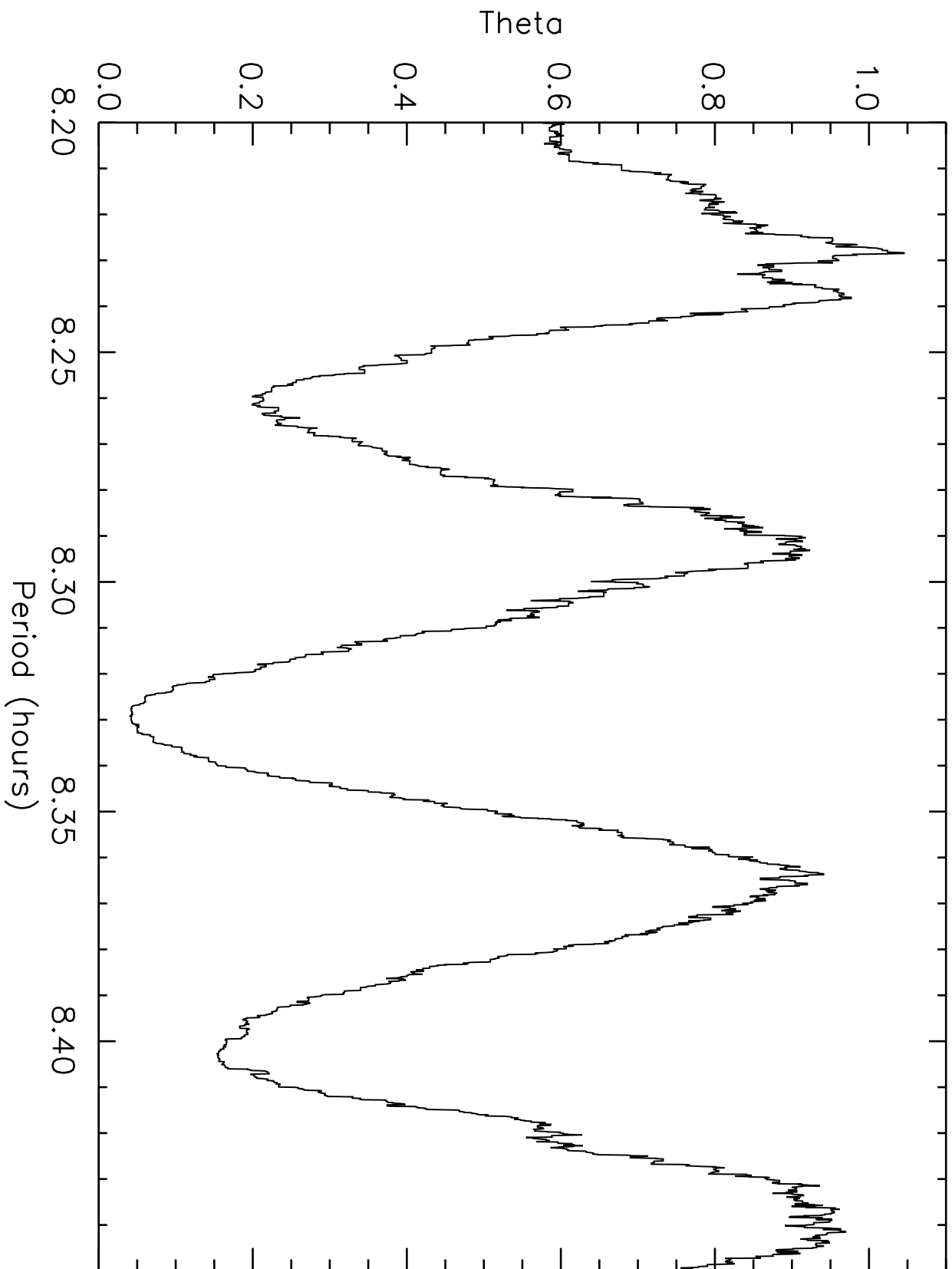
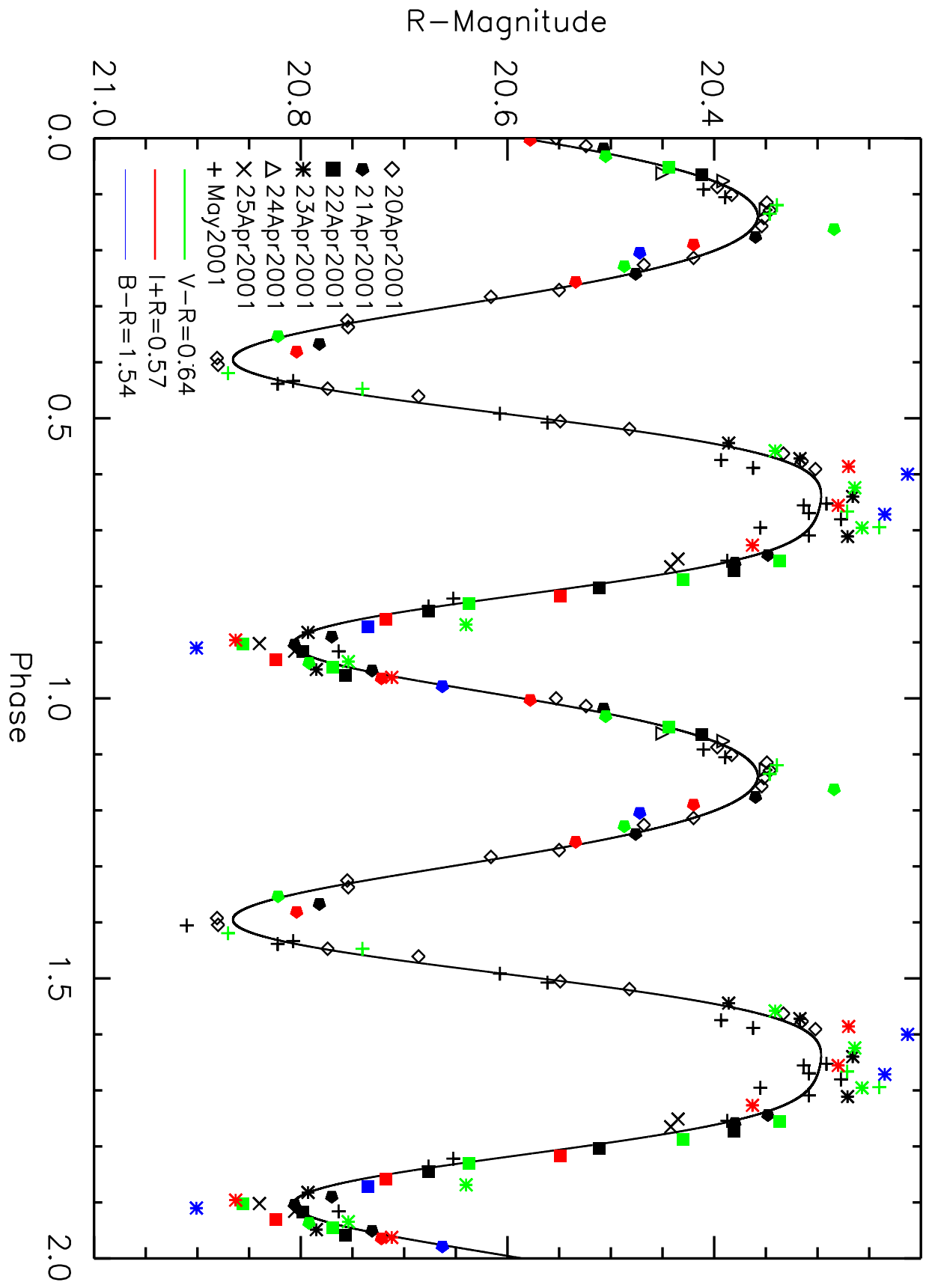


TABLE 1. Geometrical Circumstances of the Observations

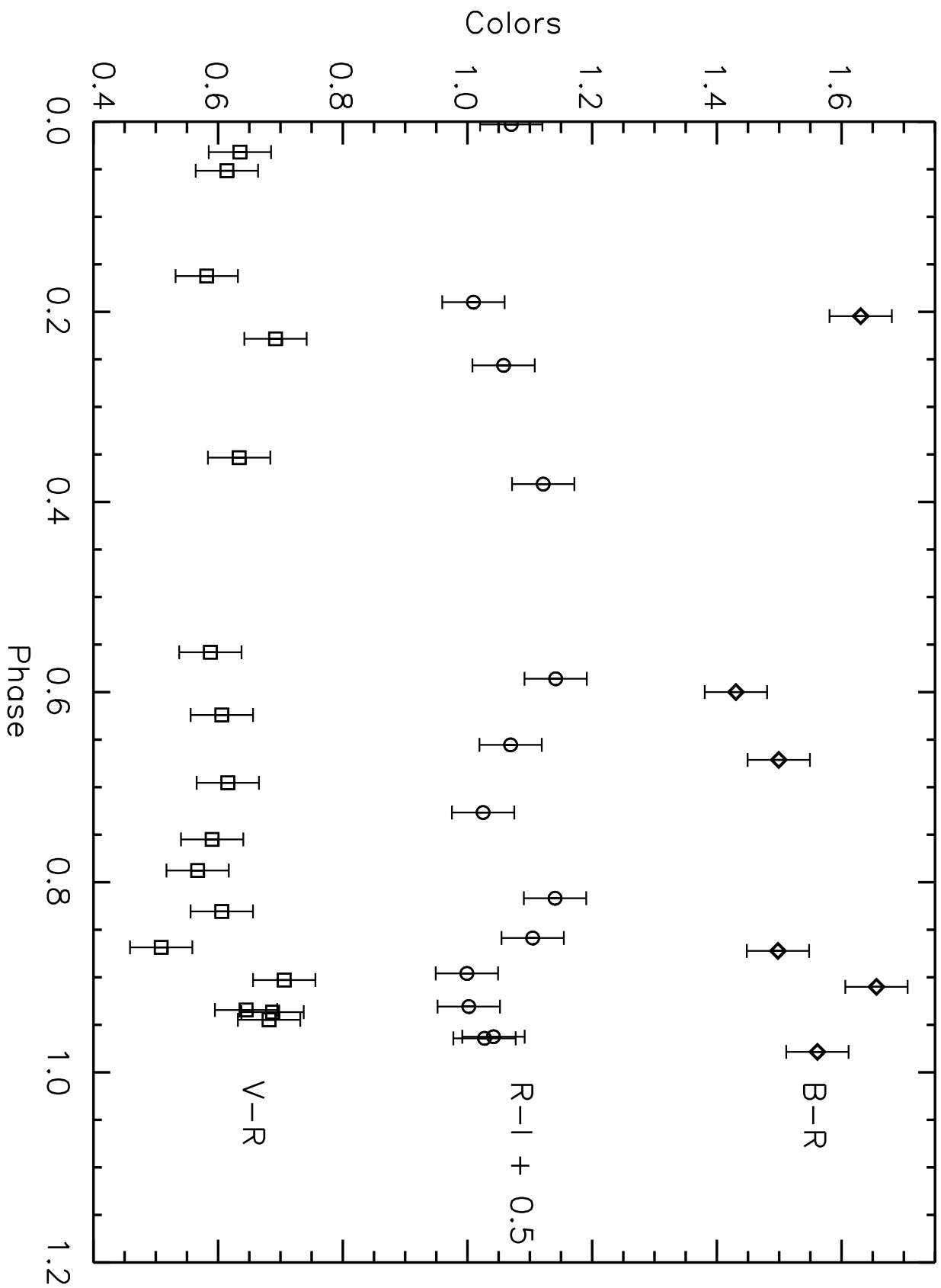
Name	UT Date	R (AU)	Δ (AU)	α (deg)	
(38628)	2000 EB ₁₇₃	2001 Feb 21	29.77	29.12	1.45
(38628)	2000 EB ₁₇₃	2001 Apr 21	29.75	28.77	0.47
(38628)	2000 EB ₁₇₃	2001 Apr 22	29.74	28.77	0.49
(38628)	2000 EB ₁₇₃	2001 Jun 30	29.71	29.52	1.93
(26375)	1999 DE ₉	2000 Apr 28	33.79	33.36	1.55
(26375)	1999 DE ₉	2000 Apr 30	33.79	33.39	1.58
(26375)	1999 DE ₉	2000 May 1	33.79	33.40	1.59
(26375)	1999 DE ₉	2001 Feb 19	33.96	32.98	0.18
(26375)	1999 DE ₉	2001 Feb 21	33.96	32.97	0.12
(26375)	1999 DE ₉	2001 Apr 24	34.00	33.47	1.45
(26375)	1999 DE ₉	2001 Apr 25	34.00	33.49	1.47
(26181)	1996 GQ ₂₁	2001 Feb 21	39.25	38.75	1.26
(26181)	1996 GQ ₂₁	2001 Apr 20	39.28	38.27	0.12
(26181)	1996 GQ ₂₁	2001 Apr 21	39.28	38.27	0.11
(26181)	1996 GQ ₂₁	2001 Apr 22	39.28	38.27	0.11
(26181)	1996 GQ ₂₁	2001 Apr 23	39.28	38.28	0.11
(26181)	1996 GQ ₂₁	2001 Apr 25	39.28	38.28	0.14
	2000 GN ₁₇₁	2001 Apr 20	28.80	27.82	0.44
	2000 GN ₁₇₁	2001 Apr 21	28.80	27.82	0.48
	2000 GN ₁₇₁	2001 Apr 22	28.80	27.83	0.51
	2000 GN ₁₇₁	2001 Apr 23	28.80	27.83	0.54
	2000 GN ₁₇₁	2001 Apr 24	28.80	27.84	0.58
	2000 GN ₁₇₁	2001 Apr 25	28.80	27.84	0.61
	2000 GN ₁₇₁	2001 May 11	28.79	27.95	1.11
	2000 GN ₁₇₁	2001 May 12	28.79	27.96	1.14
	2000 GN ₁₇₁	2001 May 13	28.79	27.97	1.17
(19521) Chaos	1998 WH ₂₄	1999 Nov 09	42.39	41.42	0.28
(19521) Chaos	1998 WH ₂₄	1999 Nov 10	42.39	41.42	0.26
(33340)	1998 VG ₄₄	1999 Nov 11	30.46	29.49	0.32
(33340)	1998 VG ₄₄	1999 Nov 12	30.46	29.48	0.29
	2001 FZ ₁₇₃	2001 Apr 24	33.23	32.42	1.04
	2001 FZ ₁₇₃	2001 Apr 25	33.23	32.43	1.06
(33128)	1998 BU ₄₈	2001 Feb 21	27.60	26.64	0.45
(33128)	1998 BU ₄₈	2001 Apr 25	27.68	27.42	2.02
(33128)	1998 BU ₄₈	2001 Nov 14	27.93	27.96	2.03
(33128)	1998 BU ₄₈	2001 Nov 16	27.94	27.92	2.03
(33128)	1998 BU ₄₈	2001 Nov 17	27.94	27.91	2.03
(33128)	1998 BU ₄₈	2001 Nov 18	27.94	27.89	2.03
(33128)	1998 BU ₄₈	2001 Nov 19	27.94	27.88	2.03
	1999 KR ₁₆	2000 Apr 28	38.04	37.05	0.31
	1999 KR ₁₆	2000 Apr 30	38.03	37.05	0.36
	1999 KR ₁₆	2000 May 01	38.03	37.06	0.38
	1999 KR ₁₆	2001 Feb 18	37.84	37.33	1.30
	1999 KR ₁₆	2001 Feb 19	37.84	37.32	1.28
	1999 KR ₁₆	2001 Apr 24	37.80	36.80	0.16
	1999 KR ₁₆	2001 Apr 25	37.80	36.80	0.18
	1999 KR ₁₆	2001 May 11	37.80	36.86	0.59
	1999 KR ₁₆	2001 May 12	37.79	36.86	0.62

TABLE 1. (continued)

Name	UT Date	R (AU)	Δ (AU)	α (deg)
1999 KR ₁₆	2001 May 13	37.79	36.87	0.64
1997 CS ₂₉	2001 Feb 21	43.59	42.77	0.73
2001 CZ ₃₁	2001 Feb 20	41.41	40.47	0.44
2001 CZ ₃₁	2001 Feb 21	41.41	40.48	0.46
2001 CZ ₃₁	2001 Apr 20	41.41	41.19	1.36
1998 HK ₁₅₁	2001 May 01	30.38	29.40	0.46
1998 HK ₁₅₁	2001 May 02	30.38	29.40	0.43



Colors 2000 GN171 (8.329 hours)



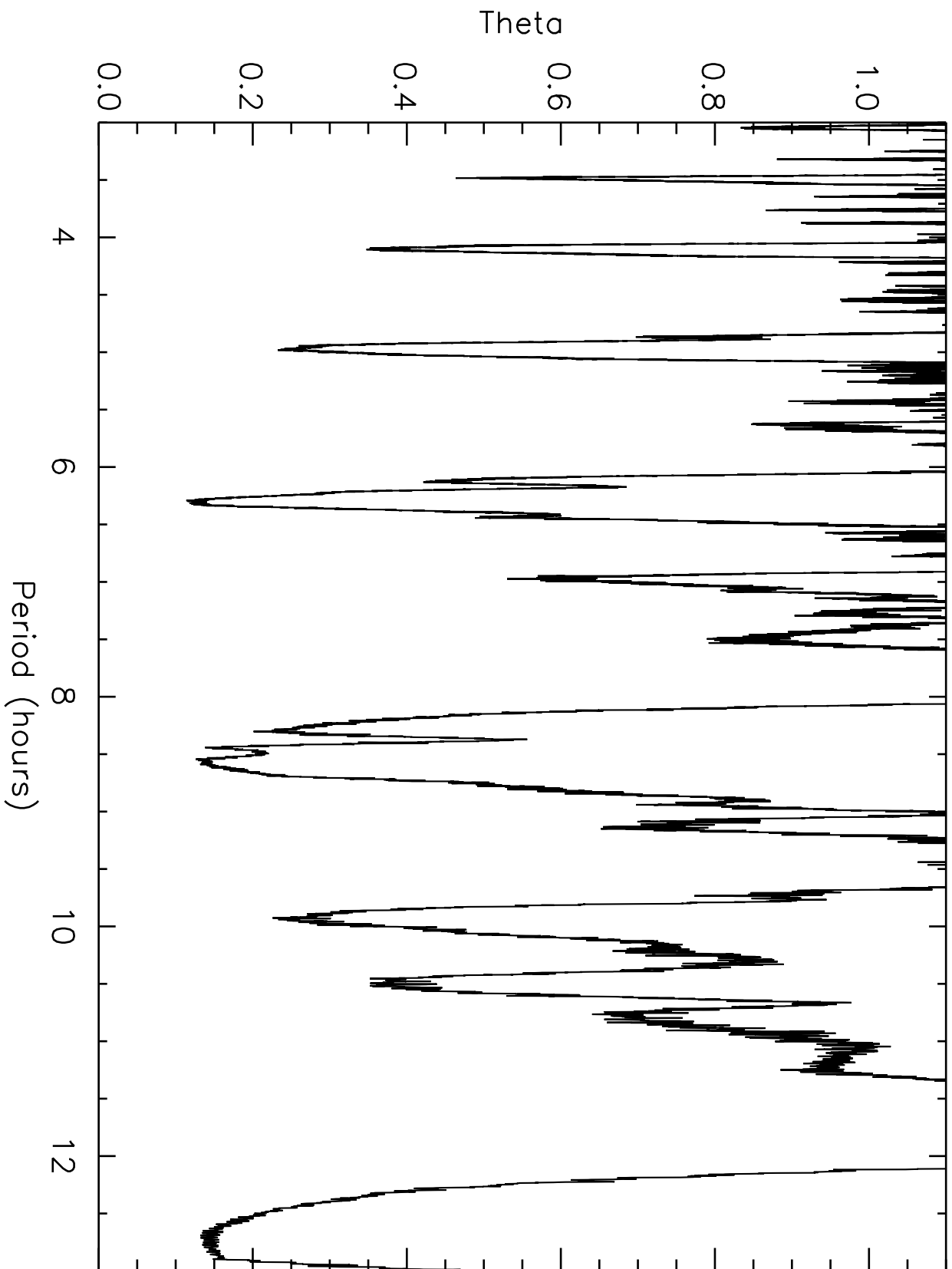


TABLE 2. Parameters of Observed Objects^a

Name	Class ^b	H (mag)	i (°)	e	a (AU)	
(38628) 2000 EB ₁₇₃	R	4.7	15.5	0.273	39.3	
(20000) Varuna 2000 WR ₁₀₆	C	3.7	17.1	0.055	43.2	
(26375) 1999 DE ₉	S	4.7	7.6	0.423	55.9	
(26181) 1996 GQ ₂₁	S	5.2	13.4	0.588	92.8	
	2000 GN ₁₇₁	R	5.8	10.8	0.279	39.3
(19521) Chaos 1998 WH ₂₄	C	4.9	12.0	0.110	46.1	
(33340) 1998 VG ₄₄	R	6.5	3.0	0.260	39.6	
	2001 FZ ₁₇₃	S	6.2	12.2	0.622	88.0
(33128) 1998 BU ₄₈	S	7.2	14.2	0.387	33.5	
	1999 KR ₁₆	C	5.8	24.9	0.298	48.5
	1997 CS ₂₉	C	5.2	2.2	0.015	44.2
	2001 CZ ₃₁	C	5.5	10.2	0.097	45.3
	1998 HK ₁₅₁	R	7.6	6.0	0.224	39.1

^aParameters from the Minor Planet Center. H is the absolute magnitude which is its brightness if the object were at 1 AU from the Sun and Earth and the phase angle is zero, i is the inclination, e is the eccentricity, and a is the semimajor axis.

^bS is a Scattered type object, C is a Classical type object, and R is a Resonance type object.

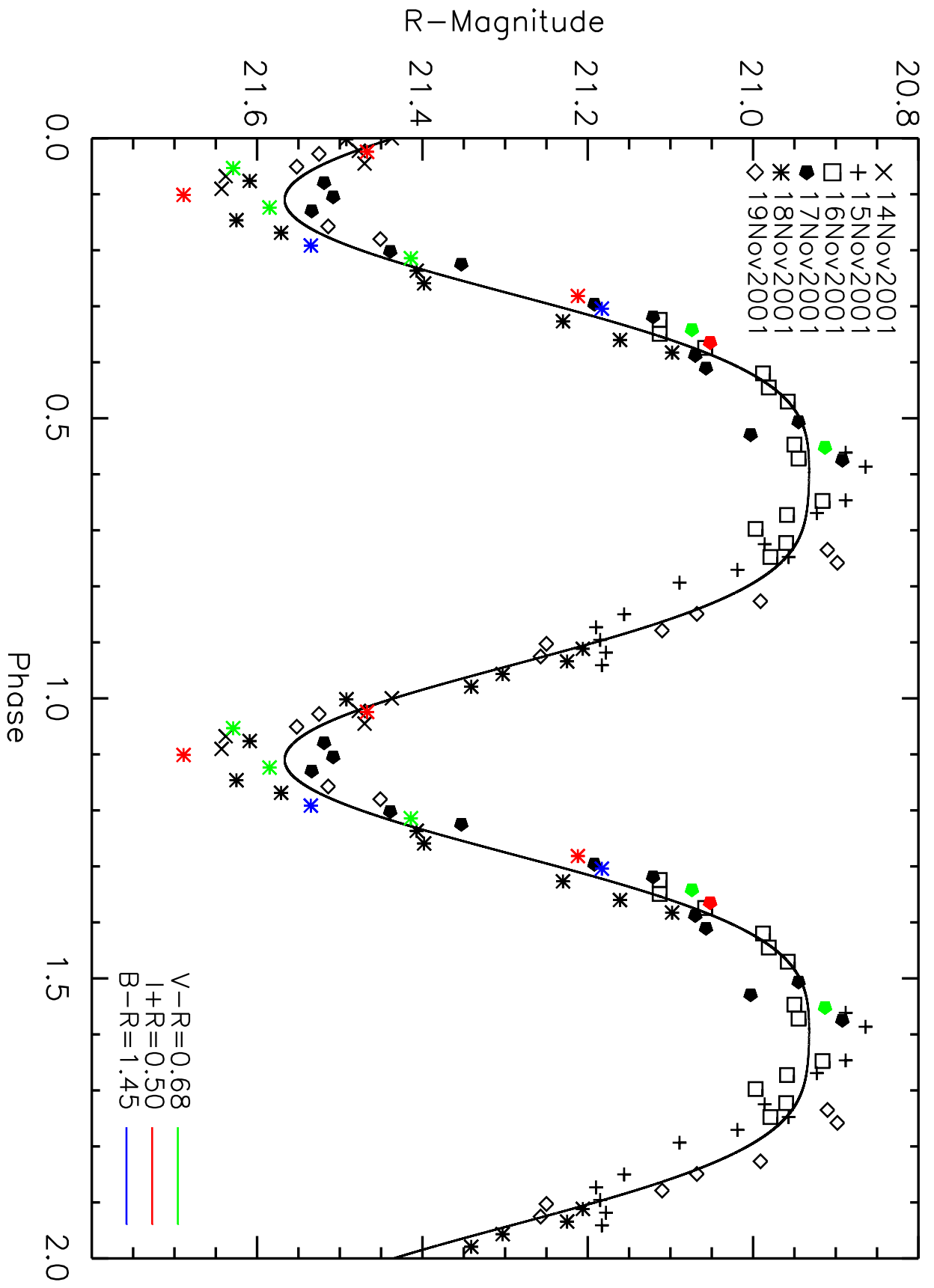


TABLE 3. Observations of Kuiper Belt Objects

Object	Image ^a	UT Date ^b	Julian Date ^c	Exp ^d (sec)	Mag. ^e (m_R)
(38628)	2000 EB ₁₇₃				
	6066	2001 Feb 21.4853	2451961.9853	200	19.318
	6067	2001 Feb 21.4889	2451961.9889	200	19.323
	6072	2001 Feb 21.5195	2451962.0195	200	19.360
	6073	2001 Feb 21.5231	2451962.0231	200	19.363
	6081	2001 Feb 21.5658	2451962.0658	200	19.364
	6082	2001 Feb 21.5695	2451962.0695	200	19.362
	6087	2001 Feb 21.5939	2451962.0939	200	19.352
	6088	2001 Feb 21.5975	2451962.0975	200	19.364
	6094	2001 Feb 21.6273	2451962.1273	200	19.347
	6095	2001 Feb 21.6310	2451962.1310	200	19.355
	6096	2001 Feb 21.6347	2451962.1347	200	19.343
	6097	2001 Feb 21.6384	2451962.1384	200	19.377
	6101	2001 Feb 21.6573	2451962.1573	200	19.352
	6102	2001 Feb 21.6610	2451962.1610	200	19.356
	2039	2001 Apr 21.3006	2452020.8006	200	19.178
	2040	2001 Apr 21.3043	2452020.8043	200	19.184
	2044	2001 Apr 21.3270	2452020.8270	200	19.215
	2045	2001 Apr 21.3308	2452020.8308	200	19.183
	2048	2001 Apr 21.3474	2452020.8474	200	19.207
	2056	2001 Apr 21.3914	2452020.8914	200	19.189
	2057	2001 Apr 21.3951	2452020.8951	200	19.201
	2064	2001 Apr 21.4159	2452020.9158	200	19.193
	2074	2001 Apr 21.4702	2452020.9702	200	19.166
	2075	2001 Apr 21.4739	2452020.9739	200	19.199
	2078	2001 Apr 21.4891	2452020.9891	200	19.196
	2079	2001 Apr 21.4928	2452020.9928	200	19.184
	2083	2001 Apr 21.5117	2452021.0117	200	19.165
	2084	2001 Apr 21.5154	2452021.0154	200	19.185
	2087	2001 Apr 21.5298	2452021.0297	200	19.174
	2088	2001 Apr 21.5334	2452021.0334	200	19.164
	2092	2001 Apr 21.5536	2452021.0536	300	19.234
	2093	2001 Apr 21.5585	2452021.0585	300	19.180
	2094	2001 Apr 21.5634	2452021.0634	300	19.147
	2095	2001 Apr 21.5682	2452021.0682	300	19.188
	3076	2001 Apr 22.4437	2452021.9437	200	19.195
	3078	2001 Apr 22.4510	2452021.9507	200	19.198
	3024	2001 Jun 30.2807	2452090.7807	300	19.394
	3025	2001 Jun 30.2857	2452090.7857	300	19.384
	3039	2001 Jun 30.3349	2452090.8349	300	19.345
(26375)	1999 DE ₉				
	2026	2000 Apr 28.2686	2451662.7686	300	20.073
	2027	2000 Apr 28.2739	2451662.7739	300	20.081
	2028	2000 Apr 28.2788	2451662.7788	300	20.025
	2029	2000 Apr 28.2837	2451662.7836	300	20.053
	2030	2000 Apr 28.2885	2451662.7885	300	20.040
	2034	2000 Apr 28.3111	2451662.8111	300	20.032
	2035	2000 Apr 28.3163	2451662.8163	300	20.026

TABLE 3. (continued)

Object	Image ^a	UT Date ^b	Julian Date ^c	Exp ^d (sec)	Mag. ^e (m_R)
	2036	2000 Apr 28.3212	2451662.8212	300	20.051
	2038	2000 Apr 28.3359	2451662.8358	300	20.098
	2039	2000 Apr 28.3408	2451662.8408	300	20.028
	2040	2000 Apr 28.3457	2451662.8457	300	20.038
	2041	2000 Apr 28.3506	2451662.8505	300	20.039
	2043	2000 Apr 28.3611	2451662.8611	300	20.014
	2044	2000 Apr 28.3659	2451662.8659	300	20.008
	2045	2000 Apr 28.3707	2451662.8706	300	20.025
	2046	2000 Apr 28.3754	2451662.8754	300	20.025
	2047	2000 Apr 28.3802	2451662.8802	300	20.040
	2048	2000 Apr 28.3850	2451662.8849	300	19.985
	2052	2000 Apr 28.4085	2451662.9085	300	20.028
	2053	2000 Apr 28.4133	2451662.9133	300	20.014
	2054	2000 Apr 28.4183	2451662.9182	300	20.012
	2055	2000 Apr 28.4232	2451662.9231	300	20.038
	4021	2000 Apr 30.2664	2451664.7664	300	20.096
	4022	2000 Apr 30.2714	2451664.7714	300	20.067
	4023	2000 Apr 30.2762	2451664.7762	300	20.055
	4024	2000 Apr 30.2811	2451664.7811	300	20.075
	4026	2000 Apr 30.2967	2451664.7967	300	20.095
	4027	2000 Apr 30.3015	2451664.8015	300	20.080
	4028	2000 Apr 30.3062	2451664.8062	300	20.072
	4029	2000 Apr 30.3110	2451664.8110	300	20.068
	4030	2000 Apr 30.3158	2451664.8158	300	20.082
	4033	2000 Apr 30.3307	2451664.8308	300	20.099
	4034	2000 Apr 30.3356	2451664.8356	300	20.074
	4035	2000 Apr 30.3405	2451664.8405	300	20.089
	4036	2000 Apr 30.3455	2451664.8455	300	20.051
	4040	2000 Apr 30.3713	2451664.8713	300	20.061
	4041	2000 Apr 30.3762	2451664.8762	300	20.042
	4044	2000 Apr 30.3908	2451664.8908	300	20.015
	5028	2000 May 1.28693	2451665.7869	300	20.079
	5035	2000 May 1.33803	2451665.8380	300	20.082
	5041	2000 May 1.37821	2451665.8782	300	20.060
	4068	2001 Feb 19.4342	2451959.9342	200	19.850
	4072	2001 Feb 19.4486	2451959.9486	200	19.836
	6039	2001 Feb 21.3302	2451961.8302	200	19.738
	6040	2001 Feb 21.3339	2451961.8339	200	19.749
	6045	2001 Feb 21.3640	2451961.8640	200	19.753
	6046	2001 Feb 21.3677	2451961.8677	200	19.801
	6052	2001 Feb 21.4045	2451961.9045	200	19.759
	6053	2001 Feb 21.4082	2451961.9082	200	19.772
	6060	2001 Feb 21.4505	2451961.9505	200	19.780
	6061	2001 Feb 21.4541	2451961.9541	200	19.817
	5017	2001 Apr 24.2621	2452023.7621	250	20.133
	5018	2001 Apr 24.2663	2452023.7663	250	20.159
	5023	2001 Apr 24.2949	2452023.7949	250	20.120
	5024	2001 Apr 24.2991	2452023.7991	250	20.146

TABLE 3. (continued)

Object	Image ^a	UT Date ^b	Julian Date ^c	Exp ^d (sec)	Mag. ^e (m_R)
	5027	2001 Apr 24.3173	2452023.8173	250	20.139
	5028	2001 Apr 24.3215	2452023.8215	250	20.129
	5031	2001 Apr 24.3393	2452023.8393	250	20.122
	5032	2001 Apr 24.3435	2452023.8435	250	20.133
	5035	2001 Apr 24.3617	2452023.8617	250	20.126
	5036	2001 Apr 24.3659	2452023.8659	250	20.099
	5039	2001 Apr 24.3835	2452023.8835	250	20.106
	5040	2001 Apr 24.3877	2452023.8877	250	20.077
	5043	2001 Apr 24.4056	2452023.9056	250	20.067
	5044	2001 Apr 24.4098	2452023.9098	250	20.081
	5048	2001 Apr 24.4333	2452023.9333	250	20.008
	5049	2001 Apr 24.4375	2452023.9375	250	20.040
	6034	2001 Apr 25.3339	2452024.8339	250	20.137
	6035	2001 Apr 25.3383	2452024.8383	200	20.117
(26181)	1996 GQ ₂₁				
	6076	2001 Feb 21.5371	2451962.0371	300	20.545
	6077	2001 Feb 21.5419	2451962.0419	300	20.603
	6085	2001 Feb 21.5838	2451962.0838	300	20.556
	6086	2001 Feb 21.5887	2451962.0887	300	20.587
	6090	2001 Feb 21.6074	2451962.1074	300	20.563
	6091	2001 Feb 21.6122	2451962.1122	300	20.581
	6092	2001 Feb 21.6170	2451962.1170	300	20.562
	6093	2001 Feb 21.6219	2451962.1219	300	20.555
	6098	2001 Feb 21.6425	2451962.1425	300	20.535
	6099	2001 Feb 21.6473	2451962.1473	300	20.555
	6100	2001 Feb 21.6522	2451962.1522	300	20.556
	1053	2001 Apr 20.3924	2452019.8924	300	20.374
	1054	2001 Apr 20.3974	2452019.8974	300	20.380
	1058	2001 Apr 20.4167	2452019.9167	300	20.377
	1059	2001 Apr 20.4214	2452019.9214	300	20.387
	1062	2001 Apr 20.4360	2452019.9360	300	20.376
	1063	2001 Apr 20.4408	2452019.9408	300	20.367
	1067	2001 Apr 20.4586	2452019.9586	300	20.359
	1068	2001 Apr 20.4633	2452019.9633	300	20.404
	1071	2001 Apr 20.4782	2452019.9782	300	20.369
	1072	2001 Apr 20.4830	2452019.9830	300	20.379
	1075	2001 Apr 20.4983	2452019.9983	300	20.358
	1076	2001 Apr 20.5031	2452020.0031	300	20.343
	1079	2001 Apr 20.5185	2452020.0185	300	20.349
	1080	2001 Apr 20.5233	2452020.0233	300	20.378
	1084	2001 Apr 20.5435	2452020.0435	300	20.410
	1086	2001 Apr 20.5540	2452020.0540	300	20.367
	1087	2001 Apr 20.5588	2452020.0588	300	20.367
	1088	2001 Apr 20.5636	2452020.0636	300	20.410
	1089	2001 Apr 20.5684	2452020.0684	300	20.383
	1090	2001 Apr 20.5732	2452020.0732	300	20.361
	1091	2001 Apr 20.5782	2452020.0782	300	20.356
	1092	2001 Apr 20.5830	2452020.0830	300	20.304

TABLE 3. (continued)

Object	Image ^a	UT Date ^b	Julian Date ^c	Exp ^d (sec)	Mag. ^e (m_R)
	2042	2001 Apr 21.3169	2452020.8169	300	20.336
	2043	2001 Apr 21.3217	2452020.8217	300	20.374
	2058	2001 Apr 21.3996	2452020.8996	300	20.365
	2059	2001 Apr 21.4045	2452020.9045	300	20.370
	2065	2001 Apr 21.4200	2452020.9200	300	20.382
	3066	2001 Apr 22.4071	2452021.9070	300	20.369
	3068	2001 Apr 22.4168	2452021.9168	300	20.367
	3084	2001 Apr 22.4767	2452021.9767	300	20.347
	3085	2001 Apr 22.4815	2452021.9814	300	20.328
	3086	2001 Apr 22.4862	2452021.9862	300	20.343
	3088	2001 Apr 22.4966	2452021.9966	300	20.367
	3089	2001 Apr 22.5014	2452022.0014	300	20.331
	3090	2001 Apr 22.5062	2452022.0062	300	20.366
	3092	2001 Apr 22.5271	2452022.0271	300	20.389
	3093	2001 Apr 22.5319	2452022.0319	300	20.372
	3095	2001 Apr 22.5469	2452022.0469	350	20.339
	3096	2001 Apr 22.5522	2452022.0522	350	20.305
	3098	2001 Apr 22.5633	2452022.0633	350	20.345
	3099	2001 Apr 22.5686	2452022.0686	350	20.357
	3100	2001 Apr 22.5740	2452022.0740	350	20.388
	4071	2001 Apr 23.4500	2452022.9500	300	20.347
	4072	2001 Apr 23.4548	2452022.9548	300	20.325
	4077	2001 Apr 23.4667	2452022.9667	300	20.341
	4078	2001 Apr 23.4716	2452022.9716	300	20.386
	4080	2001 Apr 23.4814	2452022.9814	300	20.356
	4082	2001 Apr 23.4912	2452022.9912	300	20.312
	4083	2001 Apr 23.4960	2452022.9960	300	20.339
	4084	2001 Apr 23.5008	2452023.0008	300	20.329
	4085	2001 Apr 23.5056	2452023.0056	300	20.369
	4086	2001 Apr 23.5103	2452023.0103	300	20.388
	4087	2001 Apr 23.5151	2452023.0151	300	20.300
	4088	2001 Apr 23.5198	2452023.0198	300	20.357
	4090	2001 Apr 23.5296	2452023.0296	300	20.379
	4091	2001 Apr 23.5345	2452023.0345	300	20.300
	4092	2001 Apr 23.5392	2452023.0392	300	20.356
	4093	2001 Apr 23.5440	2452023.0440	300	20.346
	4094	2001 Apr 23.5488	2452023.0488	300	20.336
	4095	2001 Apr 23.5535	2452023.0535	300	20.359
	4096	2001 Apr 23.5583	2452023.0583	300	20.340
	4098	2001 Apr 23.5684	2452023.0684	300	20.321
	4099	2001 Apr 23.5732	2452023.0732	300	20.322
	6060	2001 Apr 25.4942	2452024.9942	300	20.350
	6061	2001 Apr 25.4990	2452024.9990	300	20.382
	6064	2001 Apr 25.5154	2452025.0154	300	20.349
	6065	2001 Apr 25.5201	2452025.0201	300	20.323
	6066	2001 Apr 25.5251	2452025.0250	300	20.338
	6067	2001 Apr 25.5299	2452025.0299	300	20.372
	6072	2001 Apr 25.5618	2452025.0617	300	20.310

TABLE 3. (continued)

Object	Image ^a	UT Date ^b	Julian Date ^c	Exp ^d (sec)	Mag. ^e (m_R)
2000 GN ₁₇₁	6073	2001 Apr 25.5665	2452025.0665	300	20.323
	6074	2001 Apr 25.5713	2452025.0713	300	20.282
	1042	2001 Apr 20.3331	2452019.8331	300	20.553
	1043	2001 Apr 20.3379	2452019.8379	300	20.524
	1047	2001 Apr 20.3634	2452019.8634	300	20.397
	1048	2001 Apr 20.3682	2452019.8682	300	20.383
	1049	2001 Apr 20.3730	2452019.8740	300	20.349
	1050	2001 Apr 20.3778	2452019.8778	300	20.346
	1051	2001 Apr 20.3826	2452019.8825	300	20.352
	1052	2001 Apr 20.3876	2452019.8875	250	20.354
	1056	2001 Apr 20.4073	2452019.9073	250	20.420
	1057	2001 Apr 20.4116	2452019.9116	250	20.468
	1060	2001 Apr 20.4272	2452019.9272	250	20.550
	1061	2001 Apr 20.4314	2452019.9314	250	20.616
	1064	2001 Apr 20.4460	2452019.9460	250	20.755
	1065	2001 Apr 20.4502	2452019.9502	250	20.754
	1069	2001 Apr 20.4693	2452019.9693	250	20.881
	1070	2001 Apr 20.4735	2452019.9735	250	20.880
	1073	2001 Apr 20.4883	2452019.9883	300	20.774
	1074	2001 Apr 20.4931	2452019.9931	300	20.686
	1077	2001 Apr 20.5085	2452020.0085	300	20.549
	1078	2001 Apr 20.5133	2452020.0133	300	20.482
	1081	2001 Apr 20.5285	2452020.0285	300	20.333
	1082	2001 Apr 20.5333	2452020.0333	300	20.315
	1083	2001 Apr 20.5381	2452020.0381	300	20.302
	2036	2001 Apr 21.2854	2452020.7854	300	20.348
	2037	2001 Apr 21.2903	2452020.7903	300	20.380
	2046	2001 Apr 21.3360	2452020.8360	300	20.770
	2047	2001 Apr 21.3409	2452020.8409	300	20.806
	2050	2001 Apr 21.3571	2452020.8571	300	20.731
	2054	2001 Apr 21.3805	2452020.8805	300	20.507
	2068	2001 Apr 21.4354	2452020.9354	300	20.360
	2072	2001 Apr 21.4583	2452020.9583	300	20.476
	2081	2001 Apr 21.5017	2452021.0017	300	20.782
	3053	2001 Apr 22.3364	2452021.8364	350	20.381
	3055	2001 Apr 22.3470	2452021.8470	300	20.511
	3058	2001 Apr 22.3615	2452021.8615	300	20.676
	3062	2001 Apr 22.3865	2452021.8865	300	20.798
	3065	2001 Apr 22.4010	2452021.9010	300	20.757
	3075	2001 Apr 22.4380	2452021.9380	300	20.412
4039	2001 Apr 23.2983	2452022.7983	300	20.386	
4041	2001 Apr 23.3080	2452022.8080	300	20.317	
4045	2001 Apr 23.3315	2452022.8315	350	20.266	
4049	2001 Apr 23.3562	2452022.8562	350	20.271	
4065	2001 Apr 23.4156	2452022.9156	300	20.793	
4069	2001 Apr 23.4387	2452022.9387	300	20.785	
5060	2001 Apr 24.5193	2452024.0193	300	20.450	

TABLE 3. (continued)

Object	Image ^a	UT Date ^b	Julian Date ^c	Exp ^d (sec)	Mag. ^e (m_R)
	5061	2001 Apr 24.5242	2452024.0241	300	20.391
	5064	2001 Apr 24.5421	2452024.0421	300	20.350
	6053	2001 Apr 25.4524	2452024.9524	300	20.435
	6054	2001 Apr 25.4572	2452024.9572	300	20.442
	6062	2001 Apr 25.5048	2452025.0048	300	20.840
	6063	2001 Apr 25.5096	2452025.0096	300	20.806
	1029	2001 May 11.3078	2452040.8078	350	20.893
	1032	2001 May 11.3262	2452040.8262	350	20.678
	1033	2001 May 11.3318	2452040.8318	300	20.632
	1037	2001 May 11.3550	2452040.8550	300	20.464
	1038	2001 May 11.3598	2452040.8598	300	20.433
	1042	2001 May 11.3831	2452040.8831	300	20.384
	1043	2001 May 11.3880	2452040.8880	300	20.379
	1048	2001 May 11.4174	2452040.9174	300	20.458
	1052	2001 May 11.4409	2452040.9409	300	20.723
	1053	2001 May 11.4457	2452040.9457	300	20.747
	1058	2001 May 11.4735	2452040.9735	300	20.834
	2070	2001 May 12.4380	2452041.9380	300	20.426
	2071	2001 May 12.4428	2452041.9428	300	20.379
	3027	2001 May 13.2696	2452042.7695	300	20.481
	3028	2001 May 13.2744	2452042.7744	300	20.460
	3052	2001 May 13.3786	2452042.8786	300	20.981
	3054	2001 May 13.3882	2452042.8882	300	20.878
	3067	2001 May 13.4643	2452042.9643	300	20.362
	3069	2001 May 13.4740	2452042.9740	300	20.348
(19521) Chaos					
1998 WH ₂₄					
	1036	1999 Nov 9.5220	2451492.0220	300	20.631
	1037	1999 Nov 9.5266	2451492.0267	300	20.637
	1038	1999 Nov 9.5313	2451492.0314	300	20.651
	1040	1999 Nov 9.5515	2451492.0516	300	20.641
	1041	1999 Nov 9.5562	2451492.0562	300	20.632
	1042	1999 Nov 9.5608	2451492.0609	300	20.684
	1043	1999 Nov 9.5655	2451492.0656	300	20.669
	1046	1999 Nov 9.5910	2451492.0910	300	20.724
	1047	1999 Nov 9.5956	2451492.0957	300	20.724
	1048	1999 Nov 9.6003	2451492.1003	300	20.700
	1049	1999 Nov 9.6049	2451492.1050	300	20.705
	2041	1999 Nov 10.443	2451492.9430	300	20.625
	2042	1999 Nov 10.447	2451492.9477	300	20.665
	2045	1999 Nov 10.477	2451492.9773	300	20.667
	2046	1999 Nov 10.482	2451492.9820	300	20.677
	2050	1999 Nov 10.493	2451492.9939	300	20.665
	2051	1999 Nov 10.498	2451492.9986	300	20.685
	2052	1999 Nov 10.503	2451493.0033	300	20.645
	2056	1999 Nov 10.533	2451493.0337	300	20.630
	2057	1999 Nov 10.538	2451493.0383	300	20.662
	2058	1999 Nov 10.543	2451493.0430	300	20.644
	2060	1999 Nov 10.561	2451493.0618	300	20.610

TABLE 3. (continued)

Object	Image ^a	UT Date ^b	Julian Date ^c	Exp ^d (sec)	Mag. ^e (m_R)	
(33340)	1998 VG ₄₄	2061	1999 Nov 10.566	2451493.0665	300	20.613
		2062	1999 Nov 10.571	2451493.0711	300	20.617
		2065	1999 Nov 10.585	2451493.0853	300	20.616
		2066	1999 Nov 10.590	2451493.0900	300	20.626
		2068	1999 Nov 10.599	2451493.0993	300	20.639
	3044	1999 Nov 11.4635	2451493.9635	400	20.936	
	3046	1999 Nov 11.4775	2451493.9775	400	20.933	
	3050	1999 Nov 11.4941	2451493.9941	400	20.922	
	3052	1999 Nov 11.5089	2451494.0089	400	20.946	
	3054	1999 Nov 11.5229	2451494.0229	400	20.930	
	3056	1999 Nov 11.5368	2451494.0368	400	20.921	
	3057	1999 Nov 11.5438	2451494.0438	400	20.921	
	3060	1999 Nov 11.5648	2451494.0648	400	20.933	
	3061	1999 Nov 11.5717	2451494.0717	400	20.950	
	3064	1999 Nov 11.5883	2451494.0883	400	20.974	
	3066	1999 Nov 11.6023	2451494.1023	400	20.947	
	3067	1999 Nov 11.6093	2451494.1093	400	20.923	
	4058	1999 Nov 12.4784	2451494.9784	400	20.952	
	4059	1999 Nov 12.4854	2451494.9854	400	20.980	
	4060	1999 Nov 12.4924	2451494.9924	400	21.034	
	4062	1999 Nov 12.5124	2451495.0124	400	20.979	
	4063	1999 Nov 12.5194	2451495.0194	400	21.015	
	4066	1999 Nov 12.5403	2451495.0403	400	20.967	
	4067	1999 Nov 12.5474	2451495.0474	400	20.977	
	4069	1999 Nov 12.5614	2451495.0614	400	21.002	
	4073	1999 Nov 12.5830	2451495.0830	400	20.959	
	4074	1999 Nov 12.5877	2451495.0877	400	20.954	
	2001 FZ ₁₇₃	5019	2001 Apr 24.2717	2452023.7717	400	21.083
		5020	2001 Apr 24.2778	2452023.7777	400	21.031
5025		2001 Apr 24.3042	2452023.8042	400	21.053	
5026		2001 Apr 24.3102	2452023.8102	400	21.073	
5029		2001 Apr 24.3265	2452023.8265	400	21.087	
5030		2001 Apr 24.3324	2452023.8324	400	21.111	
5037		2001 Apr 24.3709	2452023.8709	400	21.129	
5038		2001 Apr 24.3768	2452023.8768	400	21.103	
5041		2001 Apr 24.3930	2452023.8930	400	21.087	
5042		2001 Apr 24.3989	2452023.8989	400	21.110	
5046		2001 Apr 24.4207	2452023.9207	400	21.103	
5047		2001 Apr 24.4267	2452023.9266	400	21.070	
5050		2001 Apr 24.4534	2452023.9533	400	21.066	
5054		2001 Apr 24.4810	2452023.9810	400	20.994	
5055		2001 Apr 24.4870	2452023.9869	400	21.025	
6022		2001 Apr 25.2610	2452024.7610	400	21.066	
6023		2001 Apr 25.2669	2452024.7669	400	21.059	
6030	2001 Apr 25.3088	2452024.8088	400	21.041		
6031	2001 Apr 25.3147	2452024.8147	400	21.067		

TABLE 3. (continued)

Object	Image ^a	UT Date ^b	Julian Date ^c	Exp ^d (sec)	Mag. ^e (m_R)
	6040	2001 Apr 25.3697	2452024.8697	400	21.026
	6041	2001 Apr 25.3756	2452024.8755	400	21.069
	6046	2001 Apr 25.4079	2452024.9079	400	21.087
	6047	2001 Apr 25.4157	2452024.9157	400	21.073
	6058	2001 Apr 25.4814	2452024.9814	400	21.025
	6059	2001 Apr 25.4873	2452024.9873	400	21.076
(33128)	1998 BU ₄₈				
	6064	2001 Feb 21.4720	2451961.9720	400	20.648
	6065	2001 Feb 21.4780	2451961.9780	400	20.652
	6070	2001 Feb 21.5064	2451962.0064	400	20.653
	6071	2001 Feb 21.5123	2451962.0123	400	20.626
	6079	2001 Feb 21.5525	2451962.0525	400	20.763
	6080	2001 Feb 21.5585	2451962.0585	400	20.809
	6020	2001 Apr 25.2478	2452024.7477	400	21.296
	6021	2001 Apr 25.2537	2452024.7537	400	21.242
	6024	2001 Apr 25.2738	2452024.7738	400	21.086
	6025	2001 Apr 25.2797	2452024.7797	400	21.060
	6028	2001 Apr 25.2955	2452024.7955	400	20.985
	6029	2001 Apr 25.3014	2452024.8014	400	20.962
	6032	2001 Apr 25.3216	2452024.8216	400	20.884
	6033	2001 Apr 25.3275	2452024.8275	400	20.866
	6036	2001 Apr 25.3432	2452024.8432	400	20.886
	6037	2001 Apr 25.3491	2452024.8491	400	20.859
	6042	2001 Apr 25.3823	2452024.8823	400	20.926
	6043	2001 Apr 25.3882	2452024.8882	400	20.961
	1080	2001 Nov 14.6182	2452228.1182	400	21.437
	1081	2001 Nov 14.6242	2452228.1241	400	21.477
	1082	2001 Nov 14.6301	2452228.1301	400	21.470
	1083	2001 Nov 14.6360	2452228.1360	400	21.638
	1084	2001 Nov 14.6419	2452228.1419	400	21.643
	2063	2001 Nov 15.5516	2452229.0516	400	20.888
	2064	2001 Nov 15.5582	2452229.0582	400	20.864
	2066	2001 Nov 15.5739	2452229.0739	400	20.888
	2067	2001 Nov 15.5799	2452229.0799	400	20.923
	2069	2001 Nov 15.5944	2452229.0944	400	20.986
	2070	2001 Nov 15.6004	2452229.1004	400	20.957
	2071	2001 Nov 15.6064	2452229.1064	400	21.019
	2072	2001 Nov 15.6124	2452229.1124	400	21.089
	2074	2001 Nov 15.6272	2452229.1272	400	21.156
	2075	2001 Nov 15.6333	2452229.1333	400	21.190
	2076	2001 Nov 15.6392	2452229.1392	400	21.185
	2077	2001 Nov 15.6452	2452229.1452	400	21.178
	2078	2001 Nov 15.6511	2452229.1511	400	21.183
	3115	2001 Nov 16.5378	2452230.0378	400	21.113
	3116	2001 Nov 16.5444	2452230.0444	400	21.113
	3117	2001 Nov 16.5509	2452230.0509	400	21.058
	3119	2001 Nov 16.5628	2452230.0628	400	20.988
	3120	2001 Nov 16.5695	2452230.0694	400	20.981

TABLE 3. (continued)

Object	Image ^a	UT Date ^b	Julian Date ^c	Exp ^d (sec)	Mag. ^e (m_R)
	3121	2001 Nov 16.5761	2452230.0761	400	20.958
	3124	2001 Nov 16.5962	2452230.0962	400	20.950
	3125	2001 Nov 16.6027	2452230.1027	400	20.945
	3128	2001 Nov 16.6225	2452230.1225	400	20.916
	3129	2001 Nov 16.6291	2452230.1291	400	20.959
	3130	2001 Nov 16.6356	2452230.1356	400	20.997
	3131	2001 Nov 16.6422	2452230.1422	400	20.960
	3132	2001 Nov 16.6488	2452230.1488	400	20.979
	4087	2001 Nov 17.5219	2452231.0219	400	21.519
	4088	2001 Nov 17.5285	2452231.0285	400	21.508
	4089	2001 Nov 17.5351	2452231.0351	400	21.534
	4092	2001 Nov 17.5541	2452231.0541	400	21.439
	4093	2001 Nov 17.5601	2452231.0601	400	21.353
	4096	2001 Nov 17.5788	2452231.0788	400	21.192
	4097	2001 Nov 17.5847	2452231.0847	400	21.121
	4100	2001 Nov 17.6028	2452231.1027	400	21.070
	4101	2001 Nov 17.6087	2452231.1087	400	21.057
	4105	2001 Nov 17.6339	2452231.1339	400	20.945
	4106	2001 Nov 17.6398	2452231.1398	400	21.003
	4108	2001 Nov 17.6518	2452231.1518	400	20.892
	5082	2001 Nov 18.5263	2452231.9294	400	21.206
	5083	2001 Nov 18.5322	2452231.9353	400	21.225
	5084	2001 Nov 18.5381	2452231.9412	400	21.303
	5085	2001 Nov 18.5440	2452231.9471	400	21.341
	5086	2001 Nov 18.5499	2452231.9530	400	21.492
	5089	2001 Nov 18.5695	2452231.9726	400	21.609
	5092	2001 Nov 18.5878	2452231.9909	400	21.625
	5093	2001 Nov 18.5937	2452231.9968	400	21.571
	5096	2001 Nov 18.6115	2452232.0146	400	21.407
	5097	2001 Nov 18.6174	2452232.0205	400	21.398
	5100	2001 Nov 18.6351	2452232.0382	400	21.230
	5101	2001 Nov 18.6439	2452232.0470	400	21.161
	5102	2001 Nov 18.6498	2452232.0529	400	21.098
	6076	2001 Nov 19.5284	2452232.9298	400	20.910
	6077	2001 Nov 19.5344	2452232.9358	400	20.898
	6080	2001 Nov 19.5524	2452232.9538	400	20.991
	6081	2001 Nov 19.5583	2452232.9597	400	21.068
	6082	2001 Nov 19.5661	2452232.9675	400	21.110
	6083	2001 Nov 19.5723	2452232.9738	400	21.250
	6084	2001 Nov 19.5782	2452232.9797	400	21.257
	6089	2001 Nov 19.6051	2452233.0066	400	21.525
	6090	2001 Nov 19.6111	2452233.0125	400	21.552
	6095	2001 Nov 19.6391	2452233.0405	400	21.514
	6096	2001 Nov 19.6450	2452233.0464	400	21.451
1999 KR ₁₆	2061	2000 Apr 28.4409	2451662.9409	400	21.253
	2062	2000 Apr 28.4468	2451662.9468	400	21.262
	2063	2000 Apr 28.4528	2451662.9527	400	21.320

TABLE 3. (continued)

Object	Image ^a	UT Date ^b	Julian Date ^c	Exp ^d (sec)	Mag. ^e (m_R)
	2064	2000 Apr 28.4587	2451662.9587	400	21.317
	2065	2000 Apr 28.4647	2451662.9646	400	21.281
	2070	2000 Apr 28.4959	2451662.9959	400	21.295
	2071	2000 Apr 28.5019	2451663.0019	400	21.181
	2072	2000 Apr 28.5078	2451663.0078	400	21.211
	2073	2000 Apr 28.5138	2451663.0137	400	21.135
	2076	2000 Apr 28.5317	2451663.0317	400	21.133
	2077	2000 Apr 28.5376	2451663.0376	400	21.325
	2078	2000 Apr 28.5436	2451663.0435	400	21.200
	4037	2000 Apr 30.3519	2451664.8519	400	21.085
	4038	2000 Apr 30.3579	2451664.8579	400	21.114
	4039	2000 Apr 30.3639	2451664.8639	400	21.111
	4045	2000 Apr 30.3968	2451664.8968	400	21.257
	4046	2000 Apr 30.4028	2451664.9028	400	21.279
	4047	2000 Apr 30.4087	2451664.9087	400	21.292
	4052	2000 Apr 30.4252	2451664.9252	400	21.247
	4053	2000 Apr 30.4312	2451664.9312	400	21.226
	4054	2000 Apr 30.4372	2451664.9372	400	21.203
	4055	2000 Apr 30.4431	2451664.9431	400	21.207
	4056	2000 Apr 30.4490	2451664.9490	400	21.204
	4059	2000 Apr 30.4671	2451664.9671	400	21.148
	4060	2000 Apr 30.4731	2451664.9731	400	21.149
	4061	2000 Apr 30.4790	2451664.9790	400	21.181
	4062	2000 Apr 30.4850	2451664.9850	400	21.129
	4065	2000 Apr 30.5028	2451665.0028	400	21.154
	4066	2000 Apr 30.5088	2451665.0088	400	21.132
	4067	2000 Apr 30.5147	2451665.0147	400	21.085
	4068	2000 Apr 30.5206	2451665.0206	400	21.130
	4069	2000 Apr 30.5266	2451665.0266	400	21.136
	4070	2000 Apr 30.5328	2451665.0328	400	21.058
	5036	2000 May 1.3443	2451665.8443	400	21.227
	5038	2000 May 1.3567	2451665.8567	400	21.182
	5039	2000 May 1.3627	2451665.8627	400	21.228
	5042	2000 May 1.3847	2451665.8847	400	21.264
	5043	2000 May 1.3908	2451665.8908	400	21.219
	5044	2000 May 1.3968	2451665.8968	400	21.204
	5048	2000 May 1.4224	2451665.9224	400	21.157
	5049	2000 May 1.4285	2451665.9285	400	21.160
	5050	2000 May 1.4346	2451665.9346	400	21.118
	5054	2000 May 1.4583	2451665.9583	400	21.162
	5055	2000 May 1.4644	2451665.9644	400	21.121
	5056	2000 May 1.4704	2451665.9704	400	21.178
	5059	2000 May 1.4905	2451665.9905	400	21.147
	5060	2000 May 1.4965	2451665.9965	400	21.075
	5061	2000 May 1.5025	2451666.0025	400	21.153
	5064	2000 May 1.5221	2451666.0221	400	21.068
	5065	2000 May 1.5282	2451666.0282	400	21.070
	5066	2000 May 1.5342	2451666.0342	400	21.174

TABLE 3. (continued)

Object	Image ^a	UT Date ^b	Julian Date ^c	Exp ^d (sec)	Mag. ^e (m_R)
	3091	2001 Feb 18.4971	2451958.9971	400	21.215
	3092	2001 Feb 18.5030	2451959.0030	400	21.214
	3093	2001 Feb 18.5089	2451959.0089	400	21.202
	3094	2001 Feb 18.5147	2451959.0147	400	21.262
	3099	2001 Feb 18.5667	2451959.0667	400	21.406
	3100	2001 Feb 18.5725	2451959.0725	400	21.356
	3107	2001 Feb 18.6320	2451959.1320	400	21.345
	3108	2001 Feb 18.6379	2451959.1379	400	21.308
	4076	2001 Feb 19.4657	2451959.9657	400	21.189
	4077	2001 Feb 19.4719	2451959.9719	400	21.192
	4083	2001 Feb 19.4889	2451959.9889	400	21.305
	4085	2001 Feb 19.5007	2451960.0007	400	21.317
	4087	2001 Feb 19.5138	2451960.0138	400	21.298
	4089	2001 Feb 19.5257	2451960.0257	400	21.313
	4090	2001 Feb 19.5317	2451960.0317	400	21.313
	4091	2001 Feb 19.5377	2451960.0377	400	21.413
	4092	2001 Feb 19.5437	2451960.0437	400	21.300
	4093	2001 Feb 19.5498	2451960.0498	400	21.436
	4097	2001 Feb 19.5874	2451960.0874	400	21.403
	4098	2001 Feb 19.5933	2451960.0933	400	21.369
	4099	2001 Feb 19.5992	2451960.0992	400	21.331
	4100	2001 Feb 19.6051	2451960.1051	400	21.342
	4101	2001 Feb 19.6110	2451960.1110	400	21.309
	4102	2001 Feb 19.6169	2451960.1169	400	21.327
	4103	2001 Feb 19.6228	2451960.1228	400	21.285
	4104	2001 Feb 19.6287	2451960.1287	400	21.266
	4105	2001 Feb 19.6346	2451960.1346	400	21.319
	4106	2001 Feb 19.6467	2451960.1467	400	21.262
	4107	2001 Feb 19.6526	2451960.1526	400	21.268
	4108	2001 Feb 19.6585	2451960.1585	400	21.248
	4109	2001 Feb 19.6644	2451960.1644	400	21.243
	5052	2001 Apr 24.4673	2452023.9673	400	20.975
	5053	2001 Apr 24.4735	2452023.9734	400	21.013
	5056	2001 Apr 24.4948	2452023.9948	400	21.100
	5057	2001 Apr 24.5008	2452024.0008	400	21.085
	5058	2001 Apr 24.5067	2452024.0067	400	21.143
	5059	2001 Apr 24.5126	2452024.0126	400	21.196
	5062	2001 Apr 24.5296	2452024.0296	400	21.214
	5063	2001 Apr 24.5357	2452024.0356	400	21.220
	5065	2001 Apr 24.5476	2452024.0476	400	21.184
	5066	2001 Apr 24.5536	2452024.0536	400	21.201
	5067	2001 Apr 24.5595	2452024.0595	400	21.183
	5068	2001 Apr 24.5654	2452024.0654	400	21.164
	6038	2001 Apr 25.3570	2452024.8570	400	21.113
	6039	2001 Apr 25.3629	2452024.8629	400	21.107
	6044	2001 Apr 25.3954	2452024.8954	400	21.012
	6045	2001 Apr 25.4013	2452024.9013	400	21.012
	6048	2001 Apr 25.4223	2452024.9223	400	20.992

TABLE 3. (continued)

Object	Image ^a	UT Date ^b	Julian Date ^c	Exp ^d (sec)	Mag. ^e (m_R)
	6049	2001 Apr 25.4283	2452024.9282	400	20.987
	6050	2001 Apr 25.4343	2452024.9343	400	21.004
	6051	2001 Apr 25.4402	2452024.9402	400	20.999
	6052	2001 Apr 25.4462	2452024.9462	400	21.053
	6055	2001 Apr 25.4626	2452024.9626	400	21.033
	6056	2001 Apr 25.4685	2452024.9685	400	21.071
	6057	2001 Apr 25.4745	2452024.9745	400	21.050
	6068	2001 Apr 25.5358	2452025.0358	400	21.134
	6069	2001 Apr 25.5418	2452025.0418	400	21.193
	6070	2001 Apr 25.5478	2452025.0478	400	21.185
	6071	2001 Apr 25.5538	2452025.0538	400	21.195
	1021	2001 May 11.2553	2452040.7552	400	21.122
	1022	2001 May 11.2613	2452040.7613	400	21.139
	1023	2001 May 11.2673	2452040.7673	400	21.166
	1026	2001 May 11.2879	2452040.7879	400	21.145
	1027	2001 May 11.2939	2452040.7939	400	21.161
	1030	2001 May 11.3140	2452040.8140	400	21.250
	1031	2001 May 11.3200	2452040.8200	400	21.262
	1034	2001 May 11.3368	2452040.8368	400	21.253
	1035	2001 May 11.3428	2452040.8428	400	21.286
	1036	2001 May 11.3488	2452040.8488	400	21.258
	2030	2001 May 12.2574	2452041.7574	400	21.153
	2032	2001 May 12.2694	2452041.7694	400	21.200
	2036	2001 May 12.2959	2452041.7959	400	21.267
	2039	2001 May 12.3149	2452041.8149	400	21.271
	2040	2001 May 12.3209	2452041.8209	400	21.267
	2050	2001 May 12.3418	2452041.8418	400	21.258
	2052	2001 May 12.3539	2452041.8539	400	21.269
	2056	2001 May 12.3803	2452041.8803	400	21.240
	2058	2001 May 12.3922	2452041.8922	400	21.217
	2059	2001 May 12.3982	2452041.8982	400	21.215
	2067	2001 May 12.4194	2452041.9194	400	21.155
	2068	2001 May 12.4254	2452041.9254	400	21.137
	2072	2001 May 12.4478	2452041.9478	400	21.130
	2074	2001 May 12.4598	2452041.9598	400	21.107
	2078	2001 May 12.4862	2452041.9862	400	21.102
	2079	2001 May 12.4922	2452041.9922	400	21.146
	3025	2001 May 13.2574	2452042.7574	400	21.209
	3026	2001 May 13.2634	2452042.7634	400	21.224
	3032	2001 May 13.2963	2452042.7963	400	21.222
	3034	2001 May 13.3085	2452042.8085	400	21.242
	3036	2001 May 13.3205	2452042.8205	400	21.262
	3039	2001 May 13.3384	2452042.8384	400	21.263
	3049	2001 May 13.3623	2452042.8623	400	21.159
	3050	2001 May 13.3683	2452042.8683	400	21.219
	3056	2001 May 13.3980	2452042.8980	400	21.094
	3058	2001 May 13.4102	2452042.9102	400	21.125
	3060	2001 May 13.4222	2452042.9222	400	21.108

TABLE 3. (continued)

Object	Image ^a	UT Date ^b	Julian Date ^c	Exp ^d (sec)	Mag. ^e (m_R)	
1997 CS ₂₉	3063	2001 May 13.4403	2452042.9403	400	21.122	
	3065	2001 May 13.4523	2452042.9523	400	21.071	
	3066	2001 May 13.4583	2452042.9583	400	21.127	
1997 CS ₂₉	6023	2001 Feb 21.2469	2451961.7469	400	21.361	
	6024	2001 Feb 21.2529	2451961.7529	400	21.364	
	6031	2001 Feb 21.2818	2451961.7818	400	21.354	
	6032	2001 Feb 21.2877	2451961.7877	400	21.368	
	6033	2001 Feb 21.2936	2451961.7936	400	21.370	
	6037	2001 Feb 21.3172	2451961.8172	400	21.375	
	6038	2001 Feb 21.3231	2451961.8231	400	21.386	
	6043	2001 Feb 21.3505	2451961.8505	400	21.372	
	6044	2001 Feb 21.3565	2451961.8564	400	21.365	
	6049	2001 Feb 21.3846	2451961.8846	400	21.367	
	6050	2001 Feb 21.3906	2451961.8906	400	21.367	
	6051	2001 Feb 21.3966	2451961.8966	400	21.368	
	6054	2001 Feb 21.4129	2451961.9129	400	21.354	
	6055	2001 Feb 21.4190	2451961.9190	400	21.323	
	6058	2001 Feb 21.4372	2451961.9372	400	21.333	
	6059	2001 Feb 21.4432	2451961.9432	400	21.361	
	6062	2001 Feb 21.4590	2451961.9590	400	21.311	
	6063	2001 Feb 21.4650	2451961.9650	400	21.335	
	6068	2001 Feb 21.4938	2451961.9938	400	21.346	
	6069	2001 Feb 21.4998	2451961.9998	400	21.329	
	2001 CZ ₃₁	5037	2001 Feb 20.2983	2451960.7982	300	21.639
		5038	2001 Feb 20.3117	2451960.8117	300	21.651
		5039	2001 Feb 20.3164	2451960.8164	300	21.671
5040		2001 Feb 20.3211	2451960.8211	300	21.676	
5049		2001 Feb 20.3643	2451960.8643	300	21.780	
5050		2001 Feb 20.3691	2451960.8691	300	21.780	
5051		2001 Feb 20.3738	2451960.8738	300	21.732	
5052		2001 Feb 20.3785	2451960.8785	300	21.854	
5053		2001 Feb 20.3833	2451960.8833	300	21.747	
5054		2001 Feb 20.3880	2451960.8880	300	21.681	
5055		2001 Feb 20.3927	2451960.8927	300	21.705	
5056		2001 Feb 20.3975	2451960.8975	300	21.577	
5057		2001 Feb 20.4022	2451960.9022	300	21.669	
5058		2001 Feb 20.4070	2451960.9070	300	21.662	
5059		2001 Feb 20.4117	2451960.9117	300	21.632	
5060		2001 Feb 20.4165	2451960.9165	300	21.652	
5061		2001 Feb 20.4212	2451960.9212	300	21.635	
5062		2001 Feb 20.4260	2451960.9260	300	21.660	
5063		2001 Feb 20.4307	2451960.9307	300	21.725	
5064		2001 Feb 20.4354	2451960.9354	300	21.791	
5065		2001 Feb 20.4402	2451960.9402	300	21.794	
5066		2001 Feb 20.4449	2451960.9449	300	21.799	
5067		2001 Feb 20.4498	2451960.9498	300	21.752	

TABLE 3. (continued)

Object	Image ^a	UT Date ^b	Julian Date ^c	Exp ^d (sec)	Mag. ^e (m_R)
	5068	2001 Feb 20.4545	2451960.9545	300	21.775
	5069	2001 Feb 20.4593	2451960.9593	300	21.789
	5075	2001 Feb 20.4991	2451960.9991	300	21.611
	5076	2001 Feb 20.5039	2451961.0039	300	21.739
	5077	2001 Feb 20.5086	2451961.0086	300	21.582
	5078	2001 Feb 20.5133	2451961.0133	300	21.628
	5079	2001 Feb 20.5181	2451961.0181	300	21.716
	6034	2001 Feb 21.3003	2451961.8003	350	21.729
	6035	2001 Feb 21.3058	2451961.8058	350	21.796
	6036	2001 Feb 21.3113	2451961.8113	350	21.679
	6041	2001 Feb 21.3387	2451961.8387	350	21.686
	6042	2001 Feb 21.3442	2451961.8442	350	21.663
	6047	2001 Feb 21.3722	2451961.8722	350	21.864
	6048	2001 Feb 21.3776	2451961.8776	350	21.796
	6056	2001 Feb 21.4258	2451961.9258	350	21.668
	6057	2001 Feb 21.4312	2451961.9312	350	21.610
	1029	2001 Apr 20.2553	2452019.7553	400	21.869
	1030	2001 Apr 20.2613	2452019.7613	400	21.939
	1034	2001 Apr 20.2850	2452019.7850	400	21.940
	1036	2001 Apr 20.2968	2452019.7968	400	21.816
	1037	2001 Apr 20.3028	2452019.8028	400	21.839
	1038	2001 Apr 20.3089	2452019.8089	400	21.779
	1039	2001 Apr 20.3150	2452019.8150	400	21.811
	1040	2001 Apr 20.3213	2452019.8213	400	21.775
	1044	2001 Apr 20.3458	2452019.8458	400	21.829
	1045	2001 Apr 20.3518	2452019.8518	400	21.907
1998 HK ₁₅₁	4080	2000 Apr 30.5807	2451665.0807	400	21.813
	4081	2000 Apr 30.5866	2451665.0866	400	21.687
	4082	2000 Apr 30.5926	2451665.0926	400	21.827
	4083	2000 Apr 30.5985	2451665.0985	400	21.608
	5045	2000 May 1.4036	2451665.9036	400	21.771
	5046	2000 May 1.4098	2451665.9098	400	21.711
	5047	2000 May 1.4158	2451665.9158	400	21.770
	5052	2000 May 1.4457	2451665.9456	400	21.760
	5053	2000 May 1.4517	2451665.9517	400	21.716
	5057	2000 May 1.4780	2451665.9780	400	21.788
	5058	2000 May 1.4840	2451665.9840	400	21.778
	5062	2000 May 1.5093	2451666.0093	400	21.782
	5063	2000 May 1.5154	2451666.0153	400	21.747
	5067	2000 May 1.5411	2451666.0411	400	21.588
	5068	2000 May 1.5471	2451666.0471	400	21.806
	5069	2000 May 1.5530	2451666.0530	400	21.766
	5070	2000 May 1.5589	2451666.0589	400	21.722
	5071	2000 May 1.5648	2451666.0649	400	21.678
	5072	2000 May 1.5708	2451666.0708	400	21.804
	5073	2000 May 1.5767	2451666.0767	400	21.663
	5074	2000 May 1.5827	2451666.0827	400	21.688

TABLE 3. (continued)

Object	Image ^a	UT Date ^b	Julian Date ^c	Exp ^d (sec)	Mag. ^e (m_R)
	5075	2000 May 1.5889	2451666.0889	400	21.656
	5076	2000 May 1.5949	2451666.0949	400	21.658

^aImage number.

^bDecimal Universal Date at the start of the integration.

^cJulian Date at the start of the integration.

^dExposure time for the image.

^eApparent red magnitude, uncertainties are ± 0.02 to 0.03 for the brighter objects (< 21.0 mags.) and ± 0.04 to 0.05 for fainter objects.

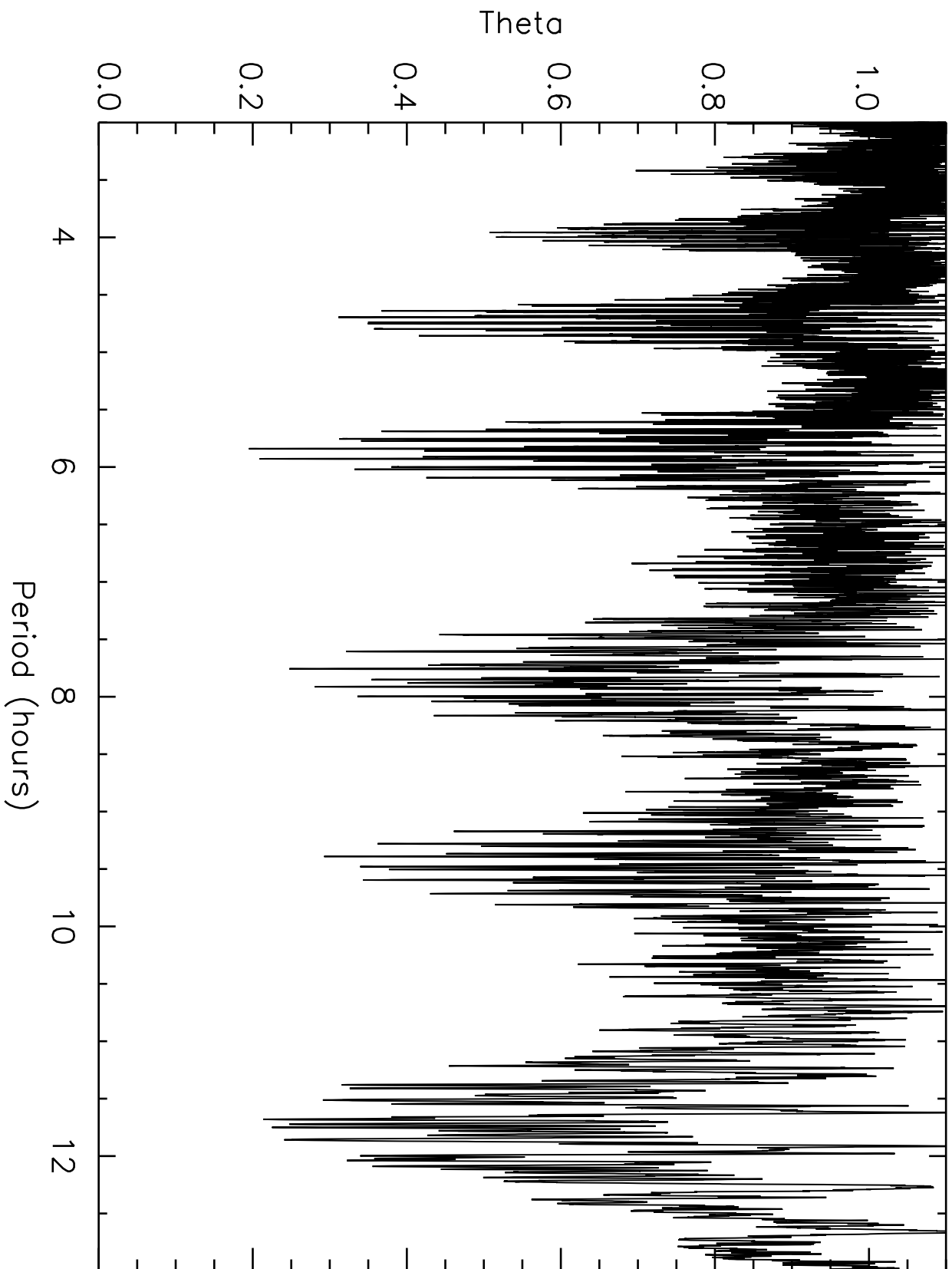


TABLE 4. Properties of Observed KBOs

Name	m_R^a (mag)	Nights ^b (#)	Δm_R^c (mag)	Single ^d (hrs)	Double ^e (hrs)
(38628)	2000 EB ₁₇₃	3	< 0.06	-	-
(20000) Varuna	2000 WR ₁₀₆ ^f	8	0.42 ± 0.03	-	6.34 ± 0.01
(26375)	1999 DE ₉	3	< 0.10	> 12?	-
(26181)	1996 GQ ₂₁	6	< 0.10	-	-
	2000 GN ₁₇₁	9	0.61 ± 0.03	-	8.329 ± 0.005
(19521) Chaos	1998 WH ₂₄	2	< 0.10	?	?
(33340)	1998 VG ₄₄	3	< 0.10	-	-
	2001 FZ ₁₇₃	2	< 0.06	-	-
(33128)	1998 BU ₄₈	7	0.68 ± 0.04	4.9 ± 0.1 6.3 ± 0.1	9.8 ± 0.1 12.6 ± 0.1
	1999 KR ₁₆	10	0.18 ± 0.04	5.929 ± 0.001 5.840 ± 0.001	11.858 ± 0.002 11.680 ± 0.002
	1997 CS ₂₉	1	< 0.08	-	-
	2001 CZ ₃₁	5	< 0.20	?	?
	1998 HK ₁₅₁	2	< 0.15	-	-

^aMean red magnitude on the date having the majority of observations.

^bNumber of nights used to determine the lightcurve.

^cThe peak to peak range of the lightcurve.

^dThe lightcurve period if there is one maximum per period.

^eThe lightcurve period if there is two maximum per period.

^fSee Jewitt and Sheppard (2002) for details.

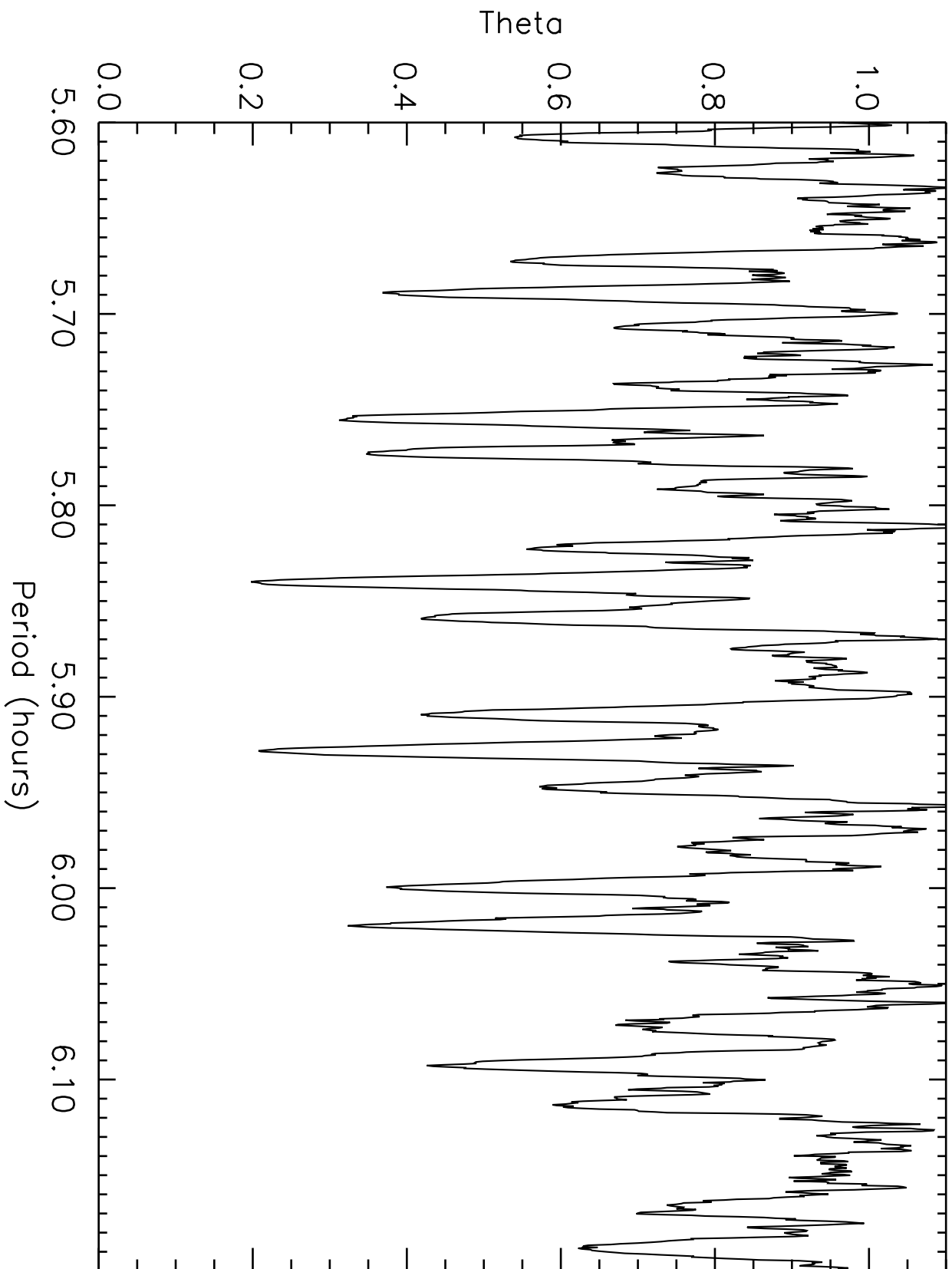


TABLE 5. Colors of Observed Kuiper Belt Objects

Name		B-V (mag)	V-R (mag)	R-I (mag)
(38628)	2000 EB ₁₇₃ ^a	0.93 ± 0.04	0.65 ± 0.03	0.59 ± 0.03
(20000) Varuna	2000 WR ₁₀₆ ^b	0.85 ± 0.01	0.64 ± 0.01	0.62 ± 0.01
(26375)	1999 DE ₉ ^a	0.94 ± 0.03	0.57 ± 0.03	0.56 ± 0.03
(26181)	1996 GQ ₂₁	-	0.69 ± 0.03	-
	2000 GN ₁₇₁	0.92 ± 0.04	0.63 ± 0.03	0.56 ± 0.03
(19521) Chaos	1998 WH ₂₄ ^c	0.94 ± 0.03	0.62 ± 0.03	-
(33340)	1998 VG ₄₄ ^d	0.93 ± 0.05	0.61 ± 0.04	0.77 ± 0.04
	2001 FZ ₁₇₃	-	-	-
(33128)	1998 BU ₄₈	0.77 ± 0.05	0.68 ± 0.04	0.50 ± 0.04
	1999 KR ₁₆	0.99 ± 0.05	0.75 ± 0.04	0.70 ± 0.04
	1997 CS ₂₉ ^a	1.16 ± 0.06	0.61 ± 0.05	0.66 ± 0.05
	2001 CZ ₃₁	0.60 ± 0.15	0.5 ± 0.1	0.3 ± 0.1
	1998 HK ₁₅₁ ^d	-	0.45 ± 0.04	0.42 ± 0.04

^aFrom Jewitt & Luu 2001.

^bSee Jewitt & Sheppard 2002.

^cFrom Tegler & Romanishin 2000.

^dFrom Boehnhardt et al. 2001.

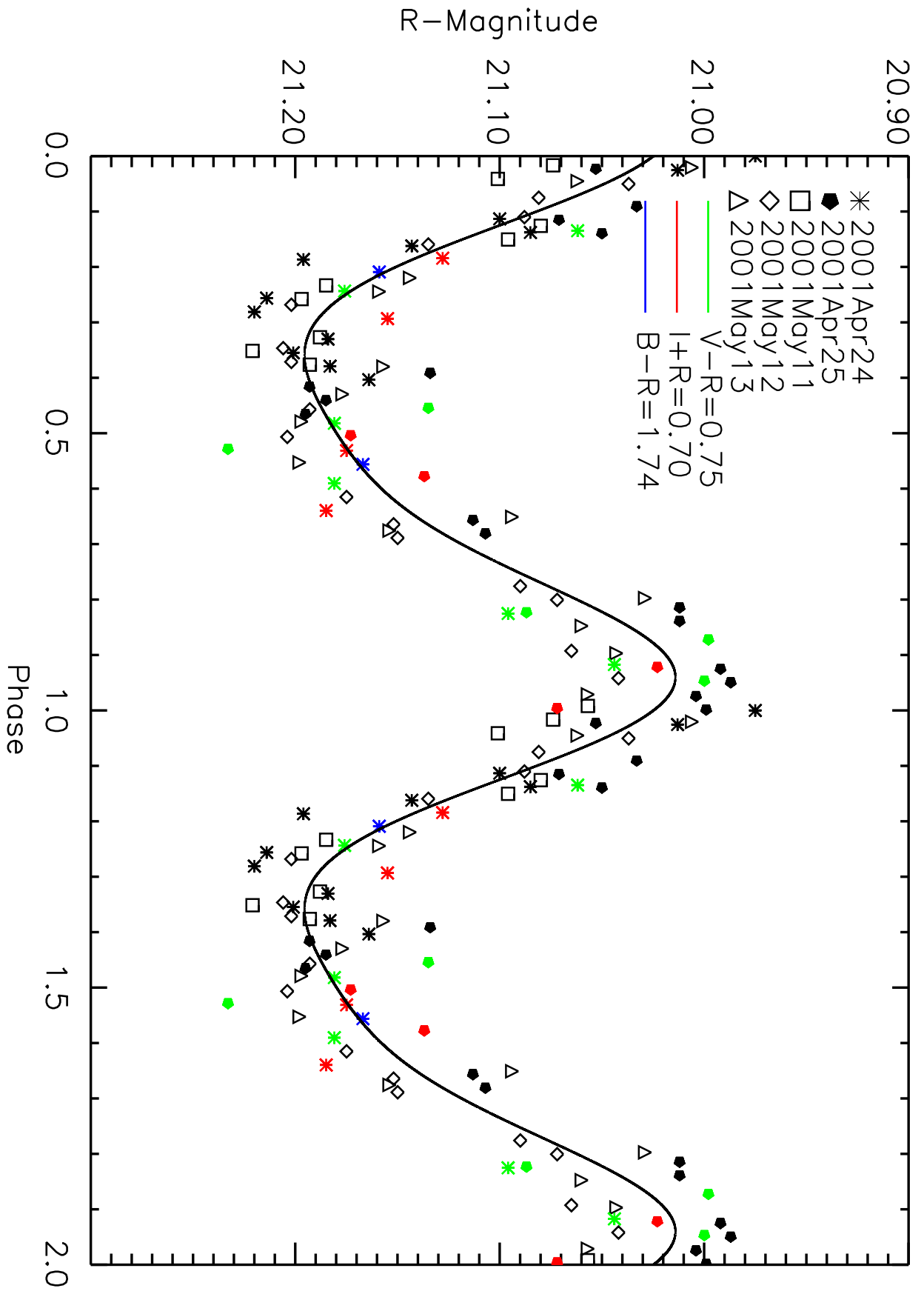


TABLE 6. Color Measurements of 2000 GN₁₇₁

Image	UT Date	JD _c ^a	Phase ^b	R ^c	B-R	V-R	R-I
2049	2001 Apr 21.3523	2452020.8523	0.937	20.745	-	0.687	-
2055	2001 Apr 21.3853	2452020.8853	0.032	20.510	-	0.635	-
2067	2001 Apr 21.4306	2452020.9306	0.162	20.342	-	0.582	-
2071	2001 Apr 21.4535	2452020.9535	0.228	20.435	-	0.692	-
2080	2001 Apr 21.4969	2452020.9969	0.353	20.828	-	0.634	-
2051	2001 Apr 21.3619	2452020.8619	0.964	20.679	-	-	0.527
2053	2001 Apr 21.3753	2452020.8752	0.003	20.578	-	-	0.570
2069	2001 Apr 21.4401	2452020.9401	0.190	20.360	-	-	0.510
2073	2001 Apr 21.4632	2452020.9632	0.256	20.522	-	-	0.558
2082	2001 Apr 21.5066	2452021.0066	0.381	20.856	-	-	0.621
2052	2001 Apr 21.3668	2452020.8668	0.979	20.642	1.561	-	-
2070	2001 Apr 21.4452	2452020.9452	0.205	20.381	1.631	-	-
3052	2001 Apr 22.3304	2452021.8303	0.755	20.387	-	0.590	-
3054	2001 Apr 22.3417	2452021.8417	0.788	20.503	-	0.567	-
3057	2001 Apr 22.3566	2452021.8566	0.831	20.671	-	0.606	-
3061	2001 Apr 22.3817	2452021.8817	0.903	20.790	-	0.706	-
3064	2001 Apr 22.3962	2452021.8962	0.945	20.727	-	0.682	-
3074	2001 Apr 22.4333	2452021.9333	0.052	20.470	-	0.614	-
3056	2001 Apr 22.3518	2452021.8518	0.817	20.620	-	-	0.640
3059	2001 Apr 22.3663	2452021.8663	0.859	20.753	-	-	0.605
3063	2001 Apr 22.3914	2452021.8914	0.931	20.756	-	-	0.502
3060	2001 Apr 22.3711	2452021.8711	0.872	20.777	1.498	-	-
4040	2001 Apr 23.3032	2452022.8031	0.558	20.393	-	0.588	-
4044	2001 Apr 23.3261	2452022.8261	0.624	20.298	-	0.606	-
4048	2001 Apr 23.3508	2452022.8508	0.695	20.281	-	0.616	-
4064	2001 Apr 23.4109	2452022.9109	0.869	20.771	-	0.509	-
4068	2001 Apr 23.4338	2452022.9338	0.934	20.749	-	0.645	-
4042	2001 Apr 23.3128	2452022.8128	0.586	20.341	-	-	0.641
4046	2001 Apr 23.3370	2452022.8370	0.656	20.279	-	-	0.569
4050	2001 Apr 23.3617	2452022.8616	0.727	20.318	-	-	0.525
4066	2001 Apr 23.4204	2452022.9204	0.896	20.792	-	-	0.499
4070	2001 Apr 23.4435	2452022.9435	0.963	20.684	-	-	0.542
4043	2001 Apr 23.3177	2452022.8177	0.600	20.322	1.431	-	-
4047	2001 Apr 23.3424	2452022.8424	0.671	20.276	1.499	-	-
4067	2001 Apr 23.4253	2452022.9253	0.910	20.785	1.656	-	-
3029 ^d	2001 May 13.2793	2452042.7793	0.119	20.366	-	0.614	-
3030 ^d	2001 May 13.2847	2452042.7847	0.135	20.352	-	0.635	-
3053 ^d	2001 May 13.3834	2452042.8834	0.419	20.823	-	0.688	-
3055 ^d	2001 May 13.3931	2452042.8931	0.447	20.753	-	0.627	-
3068 ^d	2001 May 13.4691	2452042.9691	0.666	20.276	-	0.635	-
3070 ^d	2001 May 13.4788	2452042.9788	0.694	20.281	-	0.600	-
MEAN					1.55 ± 0.03	0.63 ± 0.03	0.56 ± 0.03

^aJulian day at start of exposure.

^bPhase of 2000 GN₁₇₁ corresponding to color measurement. Phases of 0.2 and 0.7 correspond to maximum brightness (~ 20.3) and 0.4 and 0.9 correspond to minimum brightness (~ 20.9).

^cR magnitude interpolated to the time of the corresponding BVI data.

^dR and V magnitudes are corrected for phase and distance difference from April data.

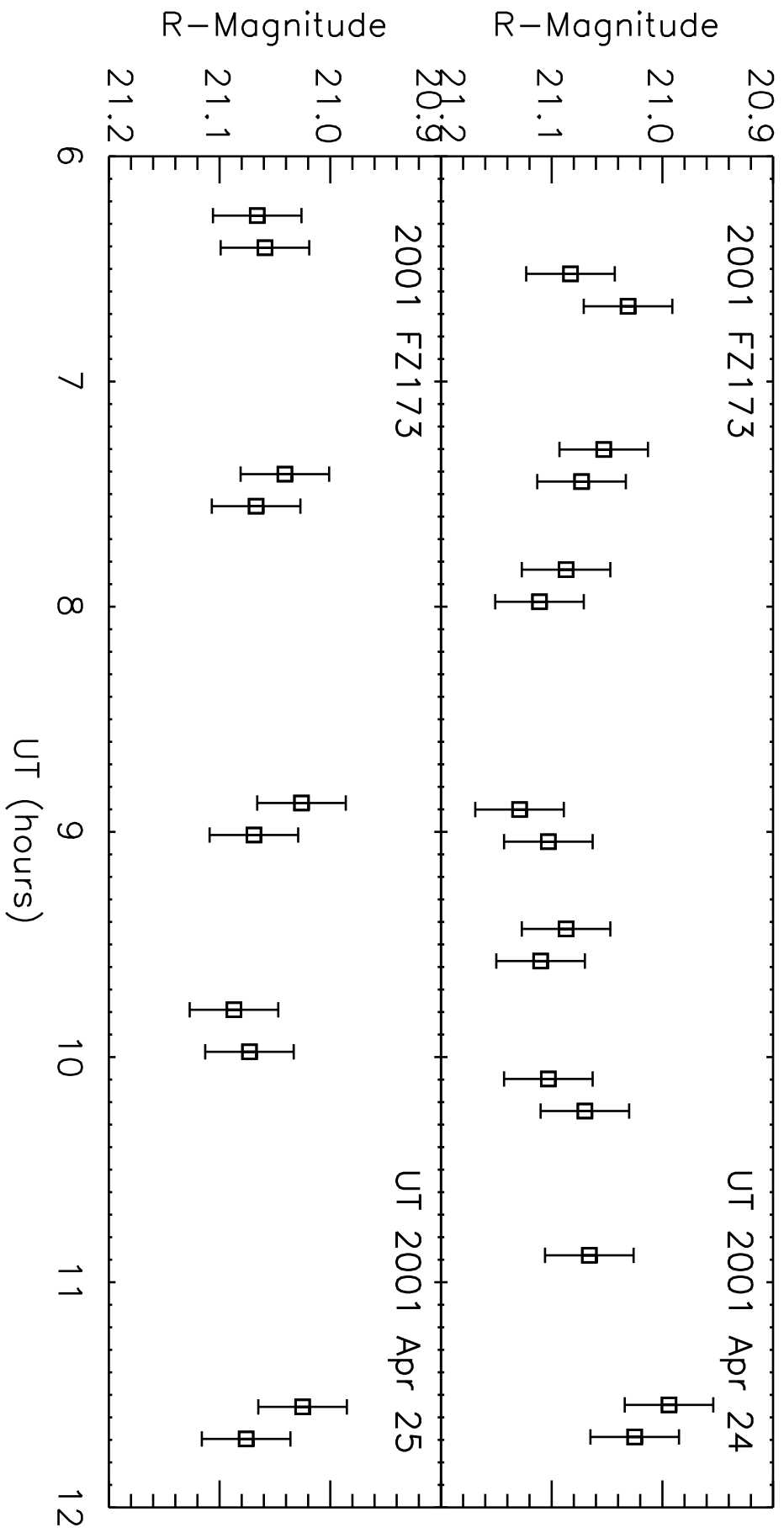


TABLE 7. Color Measurements of (33128) 1998 BU₄₈

Image	UT Date	JD _c ^a	Phase ^b	R ^c	B-R	V-R	R-I
4098	2001 Nov 17.5907	2452231.0907	0.3418	21.138	-	0.613	-
4107	2001 Nov 17.6458	2452231.1458	0.5519	20.934	-	0.656	-
4099	2001 Nov 17.5968	2452231.0967	0.3647	21.091	-	-	0.542
5088	2001 Nov 18.5635	2452231.9666	0.1916	21.490	1.497	-	-
5091	2001 Nov 18.5819	2452231.9850	0.3042	21.227	1.408	-	-
5095	2001 Nov 18.6056	2452232.0087	0.0533	21.529	-	0.777	-
5087	2001 Nov 18.5558	2452231.9589	0.1237	21.564	-	0.698	-
5090	2001 Nov 18.5760	2452231.9791	0.2141	21.446	-	0.645	-
5098	2001 Nov 18.6233	2452232.0264	0.0242	21.483	-	-	0.519
5094	2001 Nov 18.5997	2452232.0028	0.1011	21.566	-	-	0.380
5099	2001 Nov 18.6292	2452232.0323	0.2817	21.283	-	-	0.574
MEAN					1.45 ± 0.05	0.68 ± 0.04	0.50 ± 0.04

^aJulian day at start of exposure.

^bPhase of (33128) 1998 BU₄₈ corresponding to color measurement of the single-peaked 6.29 hour lightcurve. The phase of 0.6 corresponds to maximum brightness (~ 20.9) and 0.1 corresponds to minimum brightness (~ 21.6).

^cR magnitude interpolated to the time of the corresponding BVI data.

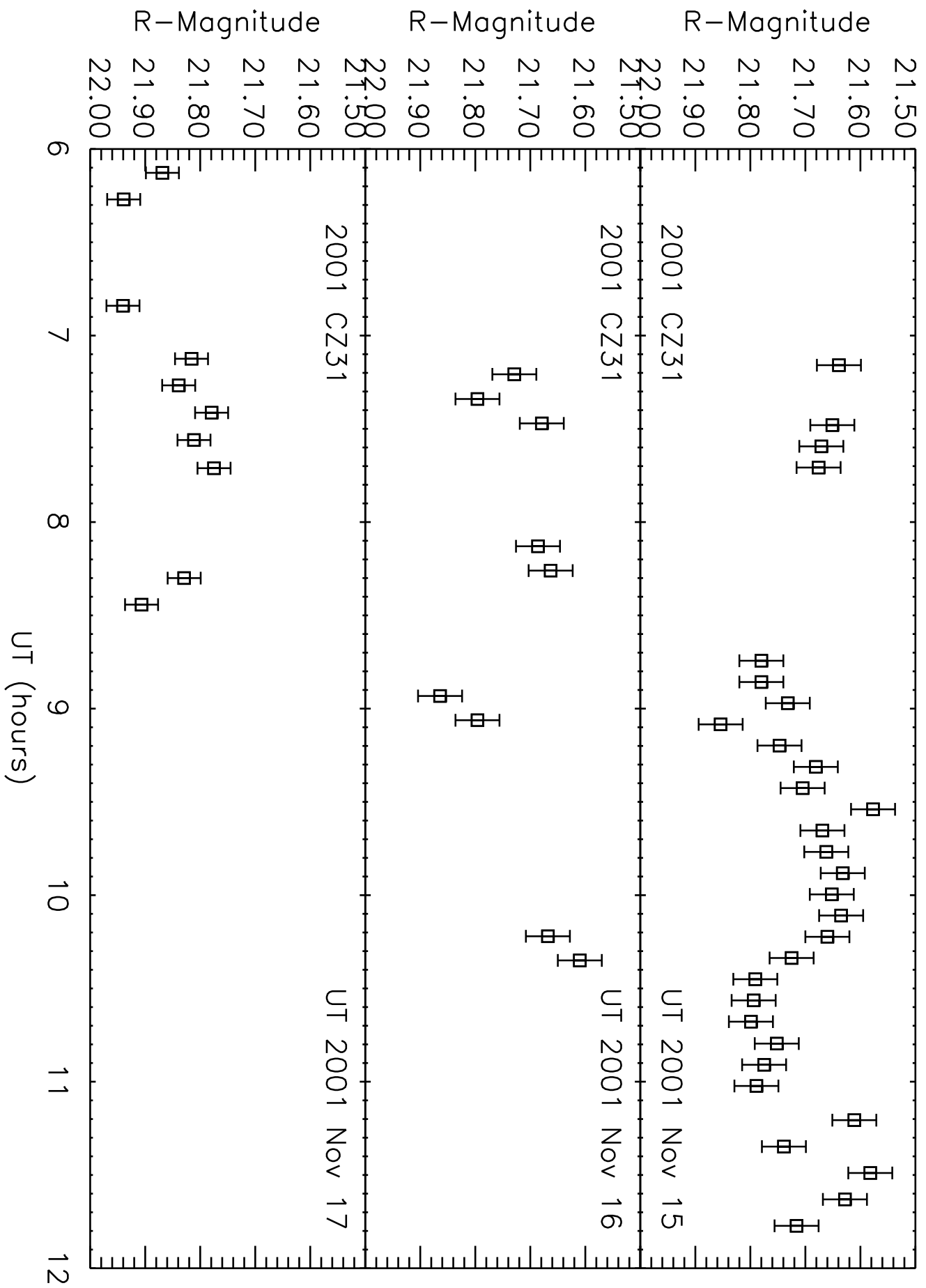


TABLE 8. Color Measurements of 1999 KR₁₆

Image	UT Date	JD _c ^a	Phase ^b	R ^c	B-R	V-R	R-I
2031	2001 May 12.2634	2452041.7634	0.135	21.107	-	0.705	-
2035	2001 May 12.2899	2452041.7899	0.244	21.173	-	0.753	-
2051	2001 May 12.3479	2452041.8479	0.482	21.183	-	0.748	-
2055	2001 May 12.3743	2452041.8743	0.590	21.161	-	0.770	-
2069	2001 May 12.4314	2452041.9314	0.825	21.048	-	0.798	-
2073	2001 May 12.4538	2452041.9538	0.917	21.016	-	0.778	-
2033	2001 May 12.2754	2452041.7754	0.184	21.141	-	-	0.713
2037	2001 May 12.3020	2452041.8019	0.293	21.189	-	-	0.734
2053	2001 May 12.3599	2452041.8599	0.531	21.174	-	-	0.699
2057	2001 May 12.3862	2452041.8862	0.640	21.145	-	-	0.660
2034	2001 May 12.2815	2452041.7814	0.209	21.156	1.743	-	-
2054	2001 May 12.3659	2452041.8659	0.556	21.169	1.738	-	-
3035	2001 May 13.3145	2452042.8144	0.454	21.187	-	0.698	-
3038	2001 May 13.3325	2452042.8325	0.528	21.175	-	0.808	-
3057	2001 May 13.4042	2452042.9042	0.823	21.050	-	0.787	-
3059	2001 May 13.4162	2452042.9161	0.872	21.027	-	0.721	-
3062	2001 May 13.4342	2452042.9342	0.947	21.014	-	0.736	-
3037	2001 May 13.3265	2452042.8265	0.504	21.179	-	-	0.706
3040	2001 May 13.3444	2452042.8444	0.577	21.164	-	-	0.727
3061	2001 May 13.4282	2452042.9282	0.922	21.015	-	-	0.692
3064	2001 May 13.4463	2452042.9463	0.996	21.023	-	-	0.652
MEAN					1.74 ± 0.04	0.75 ± 0.03	0.70 ± 0.03

^aJulian day at start of exposure.

^bPhase of 1999 KR₁₆ corresponding to color measurement of the single-peaked 5.84 hour light curve. The phase of 0.9 corresponds to maximum brightness (~ 21.0) and 0.4 corresponds to minimum brightness (~ 21.2).

^cR magnitude interpolated to the time of the corresponding BVI data. R magnitudes are corrected for phase and distance difference from April data so they can be compared to the plots directly.

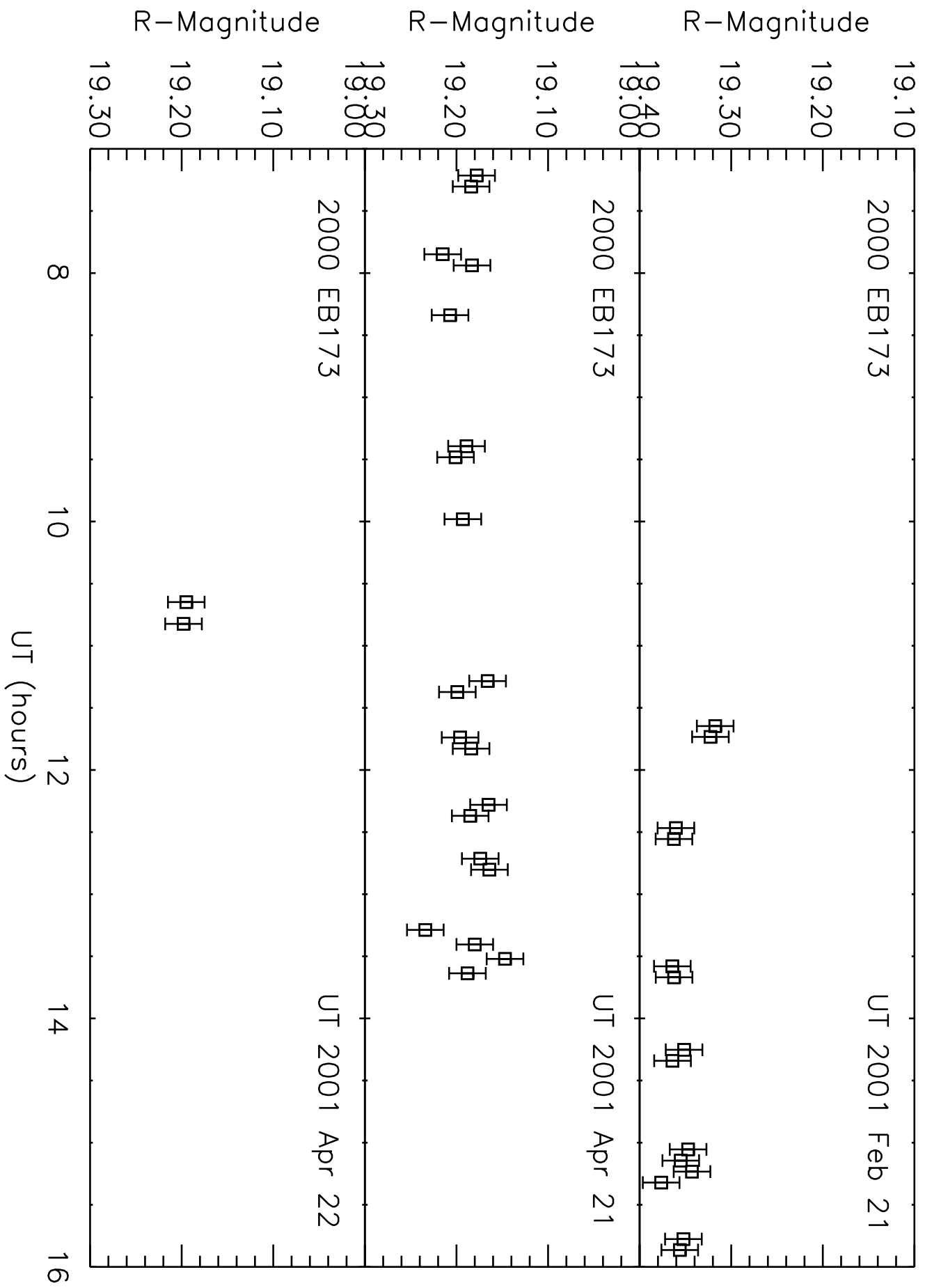


TABLE 9. List of Large Objects with Large Amplitude Lightcurves.^a

Name	Type	$a \times b \times c$ (km)	ρ (kg m ³)	Δ mag (mag)	Period (hrs)	comment
Pluto	planet	2300	2061	0.33	6.4d	albedo
Iapetus	satellite	1430	1025	2	79.3d	albedo
Hyperion	satellite	350 × 240 × 200	~ 1250	0.5	chaos	fragment?
624 Hektor	Trojan	300 × 150	~ 2500	1.2	6.9	contact binary?
Amalthea	satellite	270 × 166 × 150	~ 3000	-	-	frag?/albedo
15 Eunomia	asteroid	~ 270 × 160 × 115	1160	0.56	6.1	Jacobi?
87 Sylvia	asteroid	~ 270 × 150 × 115	1640	0.62	5.2	Jacobi?
16 Psyche	asteroid	~ 260 × 175 × 120	2340	0.42	4.2	Jacobi?
107 Camilla	asteroid	~ 240 × 150 × 105	1850	0.52	4.8	Jacobi?
Janus	satellite	220 × 190 × 160	656	-	-	fragment?
45 Eugenia	asteroid	~ 210 × 145 × 100	1270	0.41	5.7	Jacobi?

^aObjects that have diameters > 200 km and lightcurves with peak-to-peak amplitudes > 0.40 magnitudes. Pluto is the only exception since its lightcurve is slightly less than 0.40 magnitudes.

Notes to Table 9.

The Jacobi type main belt asteroids had their axis ratios and densities calculated from their amplitudes and periods as described for the KBOs in the text. Data for the other objects were culled from the best measurements in the literature.

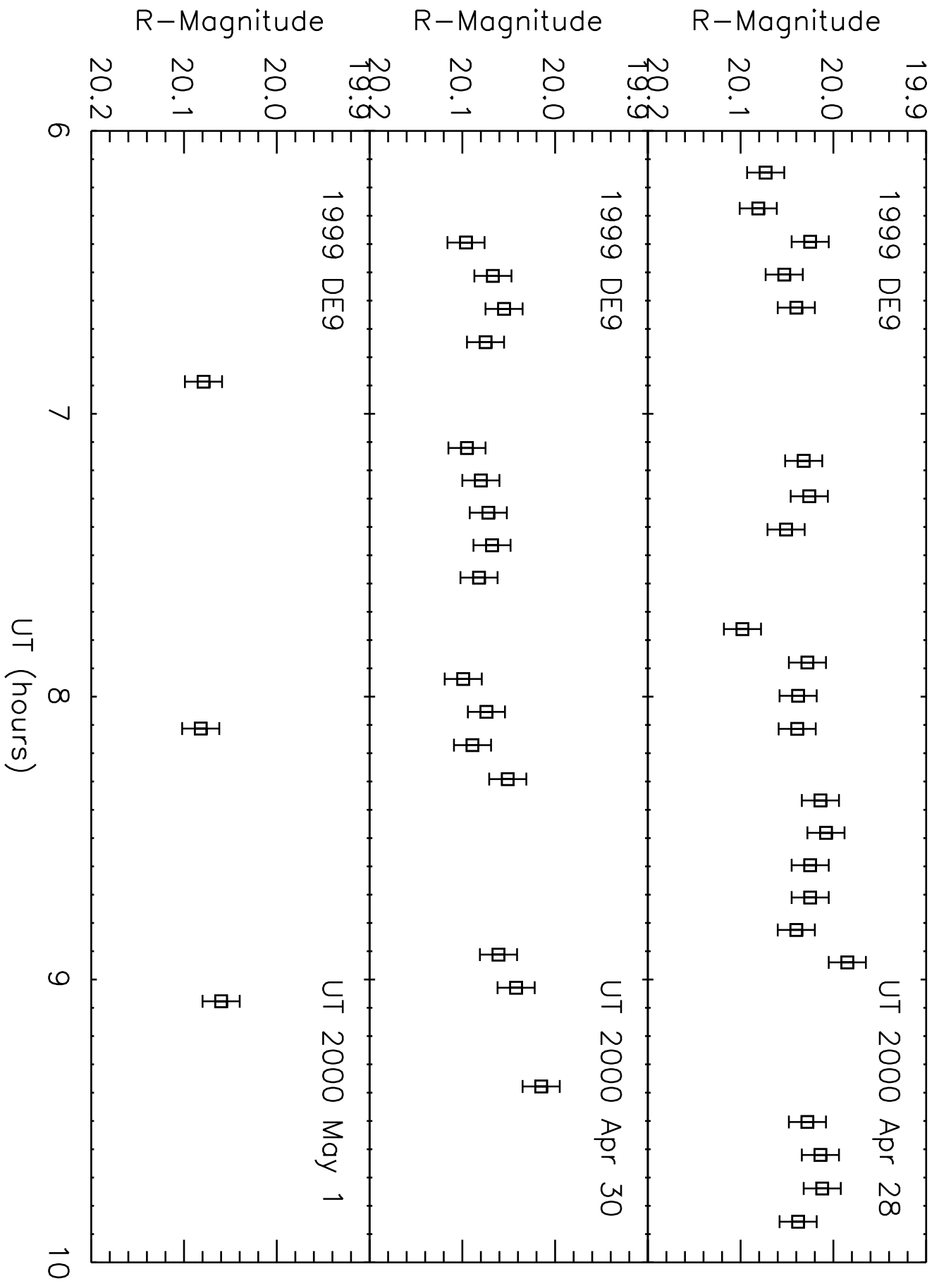


TABLE 10. Shape Models and Densities for KBOs with Lightcurves

Name	H (mag)	D ^a (km)	Albedo		Jacobi		Binary	
			$a : b$	ρ	$a : b : c$	ρ	$a_1 : a_2$	ρ
Varuna ^b	3.7	900	1 : 1	≥ 1090	$\geq 1.5 : 1 : 0.7$	≥ 1050	$\geq 1.4 : 1$	≥ 996
2000 GN ₁₇₁	5.8	400	1 : 1	≥ 157	$\geq 1.75 : 1 : 0.74$	≥ 635	$\geq 1.15 : 1$	≥ 585
1998 BU ₄₈	7.2	240	1 : 1	≥ 109	$\geq 1.87 : 1 : 0.75$	≥ 456	$\geq 1.07 : 1$	≥ 435
1999 KR ₁₆	5.8	400	1 : 1	≥ 77	$\geq 1.18 : 1 : 0.63$	≥ 280	$\geq 2.35 : 1$	≥ 210

^aDiameter computed assuming that the albedo is 0.04.

^bSee Jewitt and Sheppard 2002.

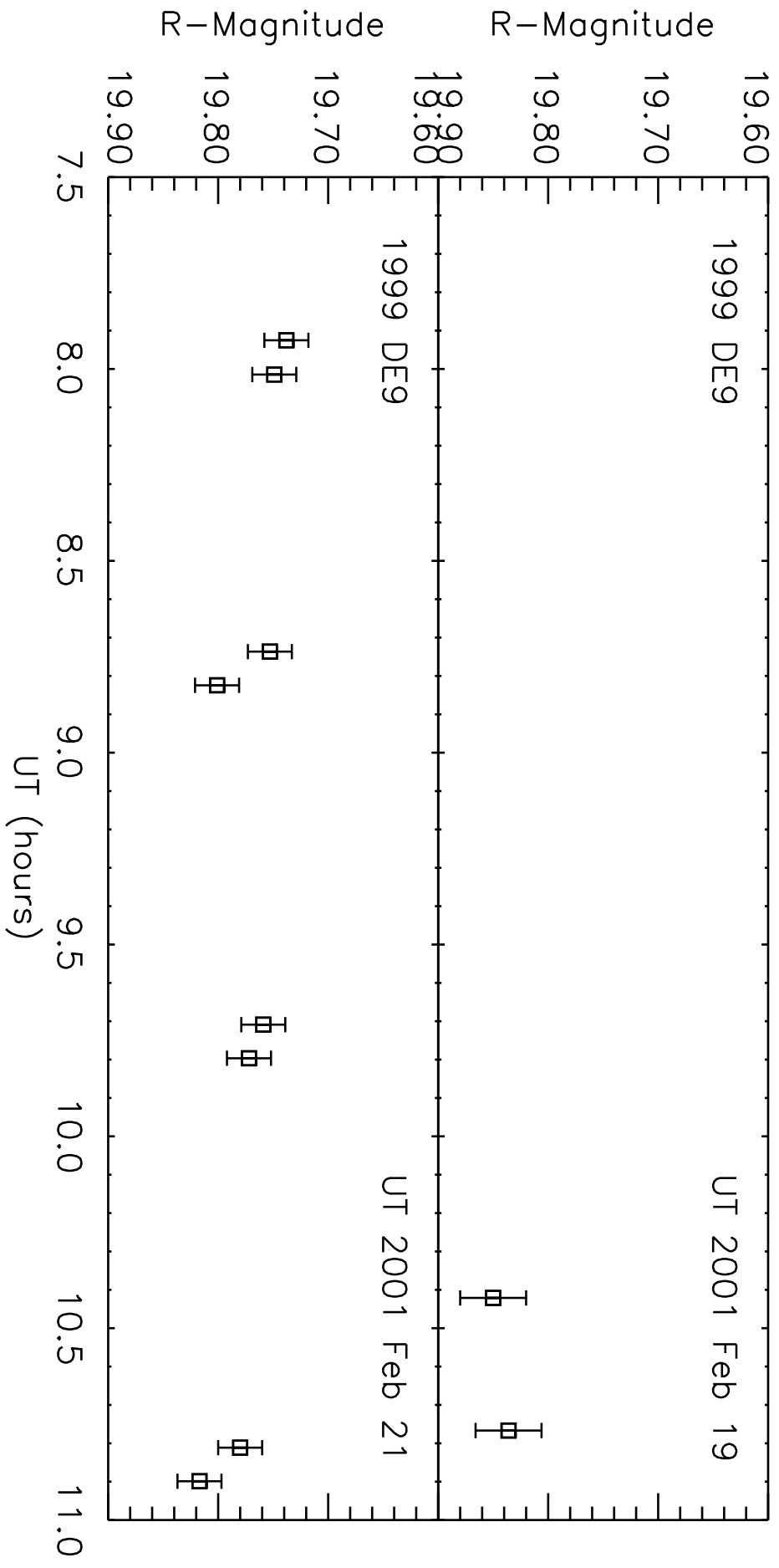
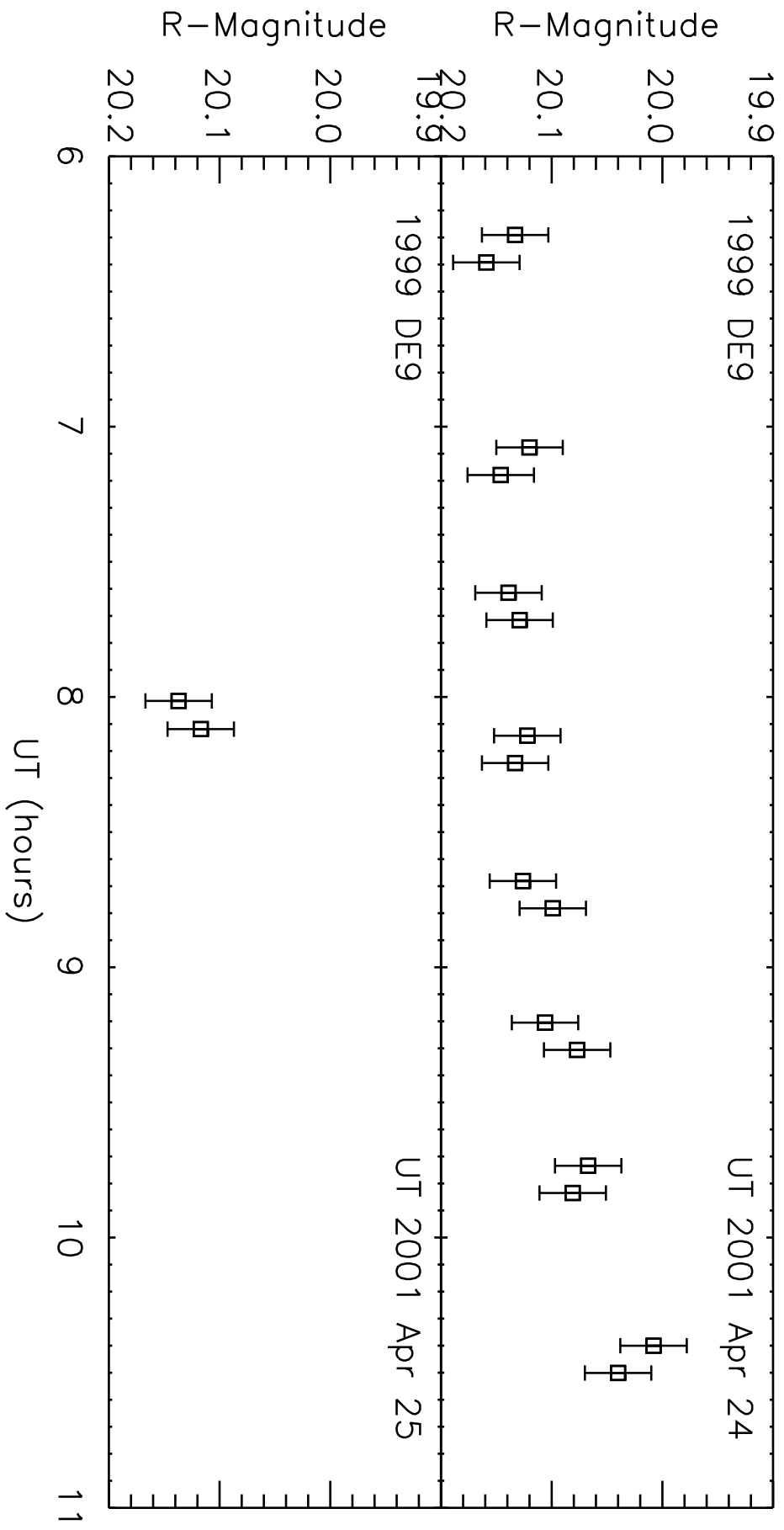


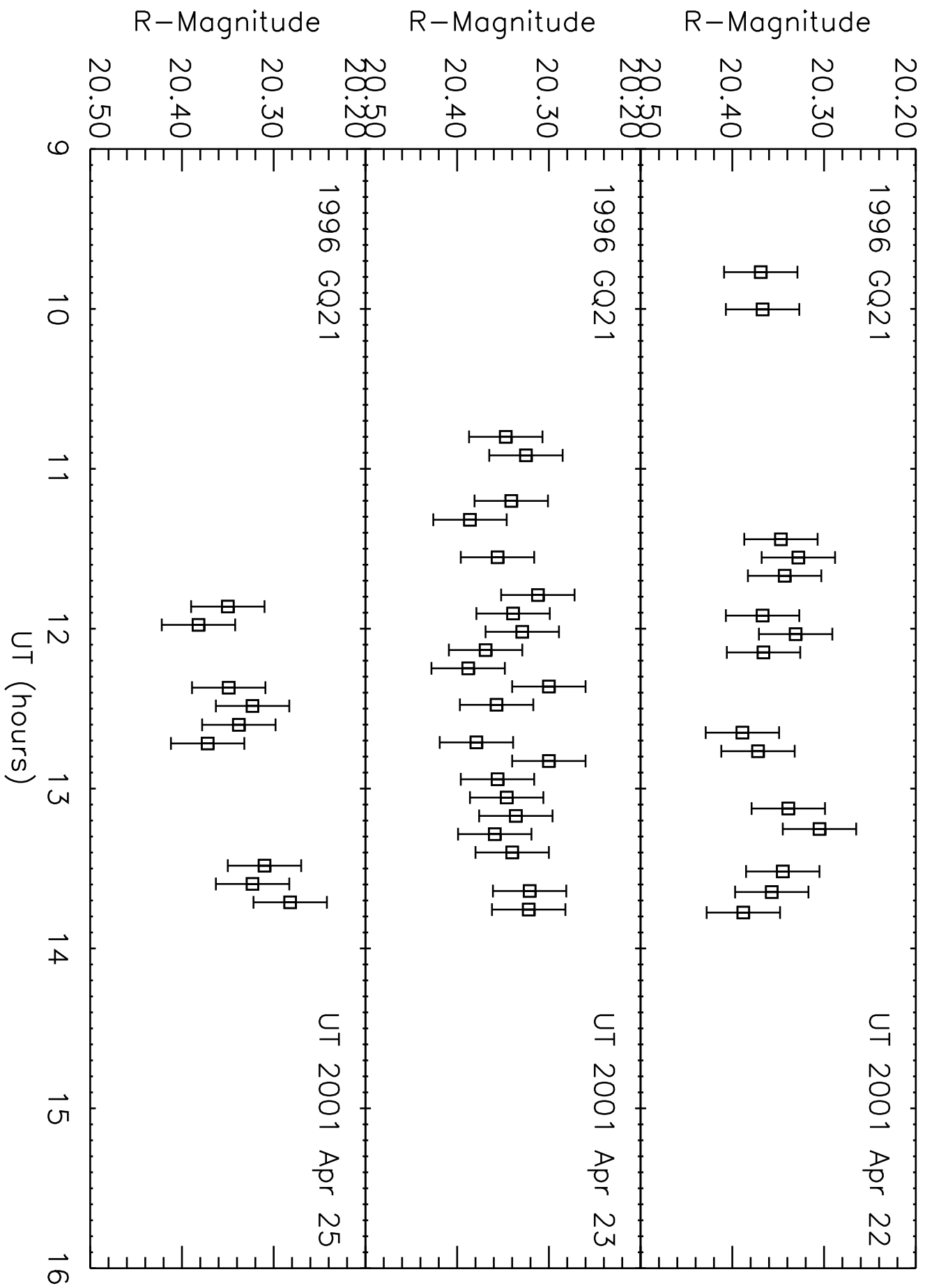
TABLE 11. Other KBOs with Reported Lightcurve Observations

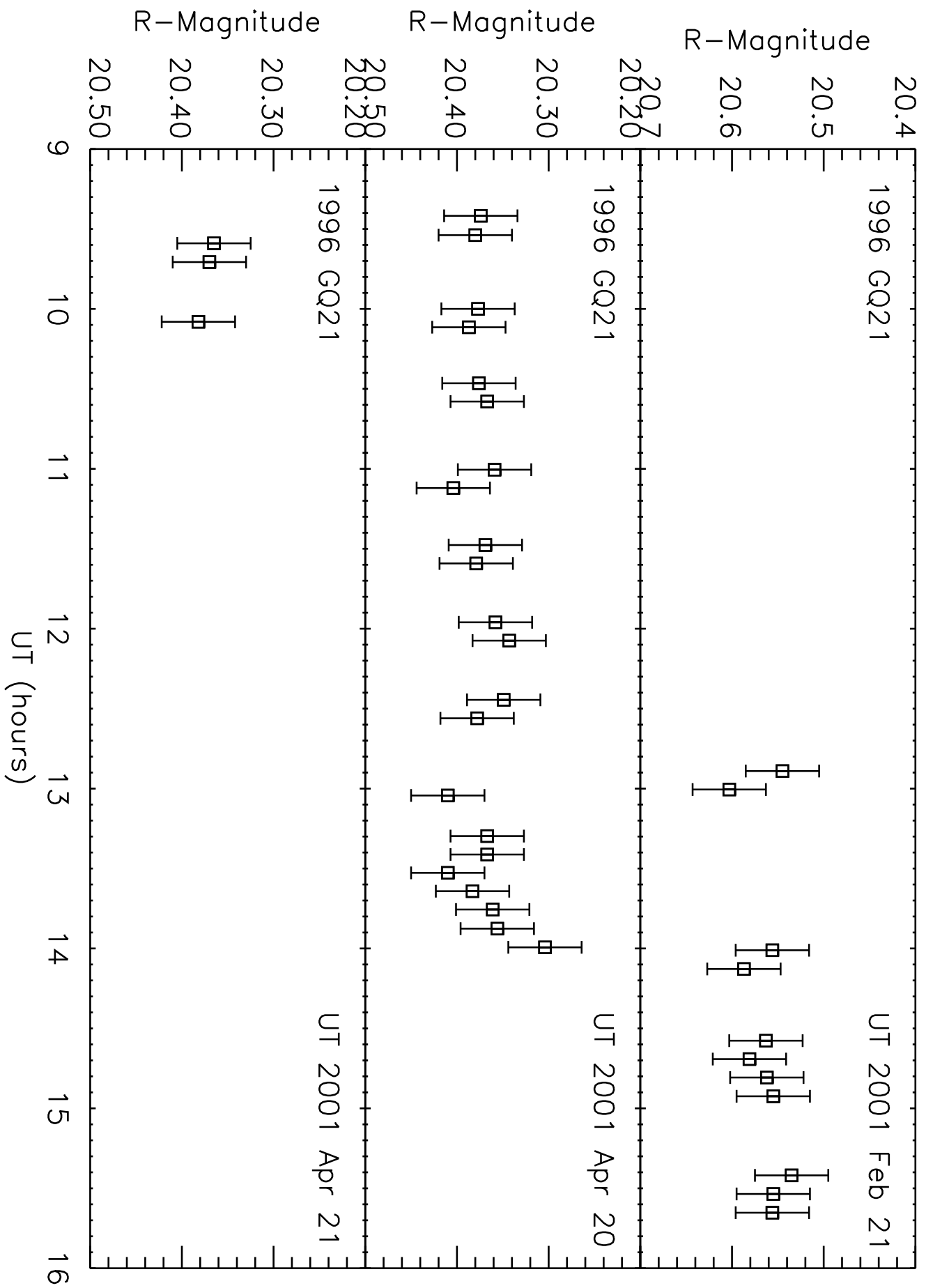
Name	Class ^a	H (mag)	Δ mag (mag)	P (hr)	i ($^{\circ}$)	e	a (AU)	Ref ^b
(28978) Ixion 2001 KX ₇₆	R	3.2	—	—	19.7	0.246	39.3	SS,OR
(19308) 1996 TO ₆₆	C	4.5	0.25	7.9	27.4	0.115	43.4	SS,OH
(24835) 1995 SM ₅₅	C	4.8	—	—	27.0	0.110	42.1	SS
(15874) 1996 TL ₆₆	S	5.4	—	—	23.9	0.587	84.9	RT,LJ
(26308) 1998 SM ₁₆₅	C	5.8	0.45	7.1	13.5	0.371	47.8	SS,R
(15875) 1996 TP ₆₆	R	6.8	—	—	5.7	0.336	39.7	RT,CB
(15789) 1993 SC	R	6.9	—	—	5.2	0.185	39.6	RT,D
(15820) 1994 TB	R	7.1	—	—	12.1	0.321	39.7	SS
(32929) 1995 QY ₉	R	7.5	0.60	7.3	4.8	0.266	39.8	SS,RT

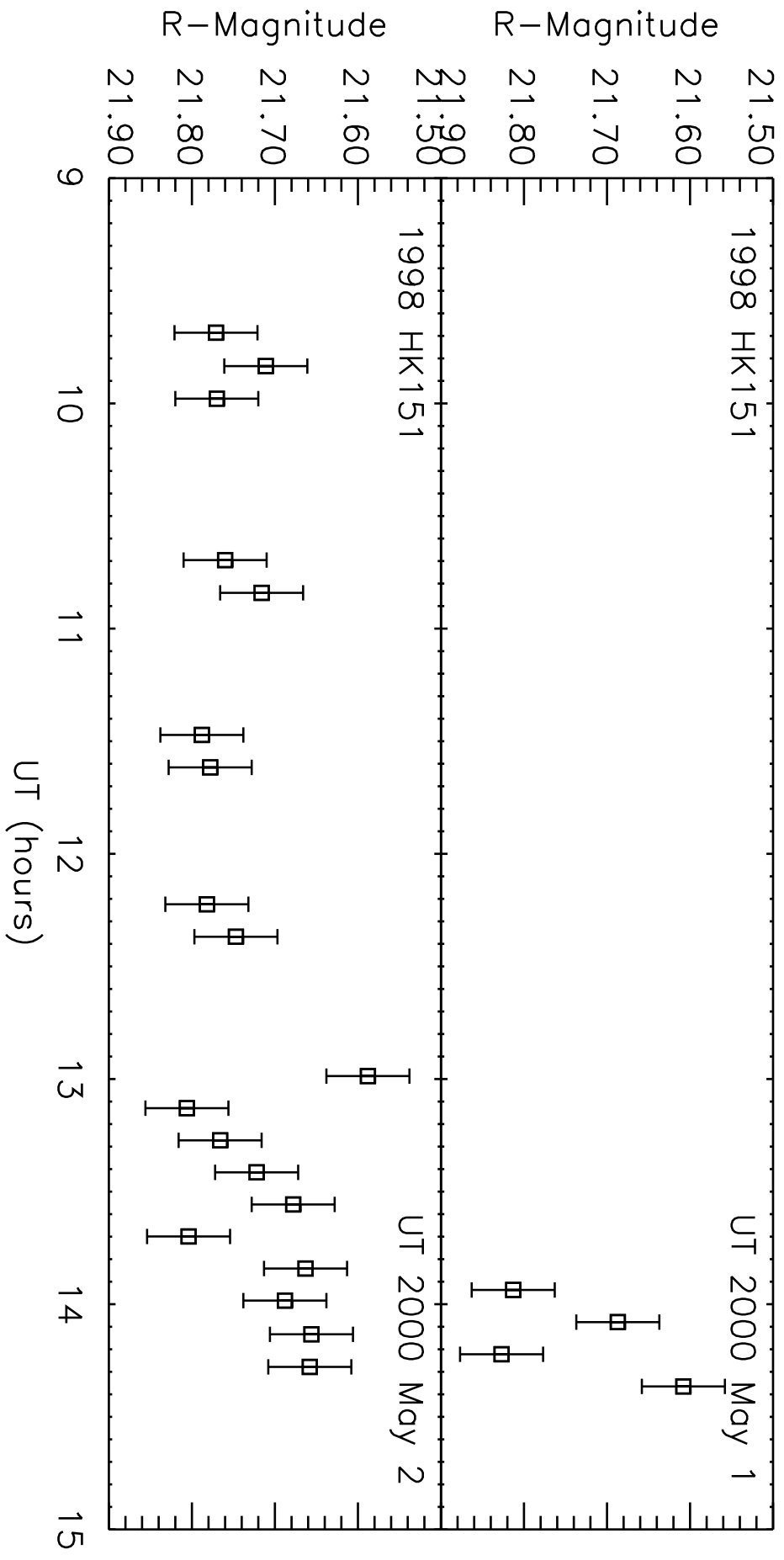
^aS is a Scattered type object, C is a Classical type object, and R is a Resonance type object.

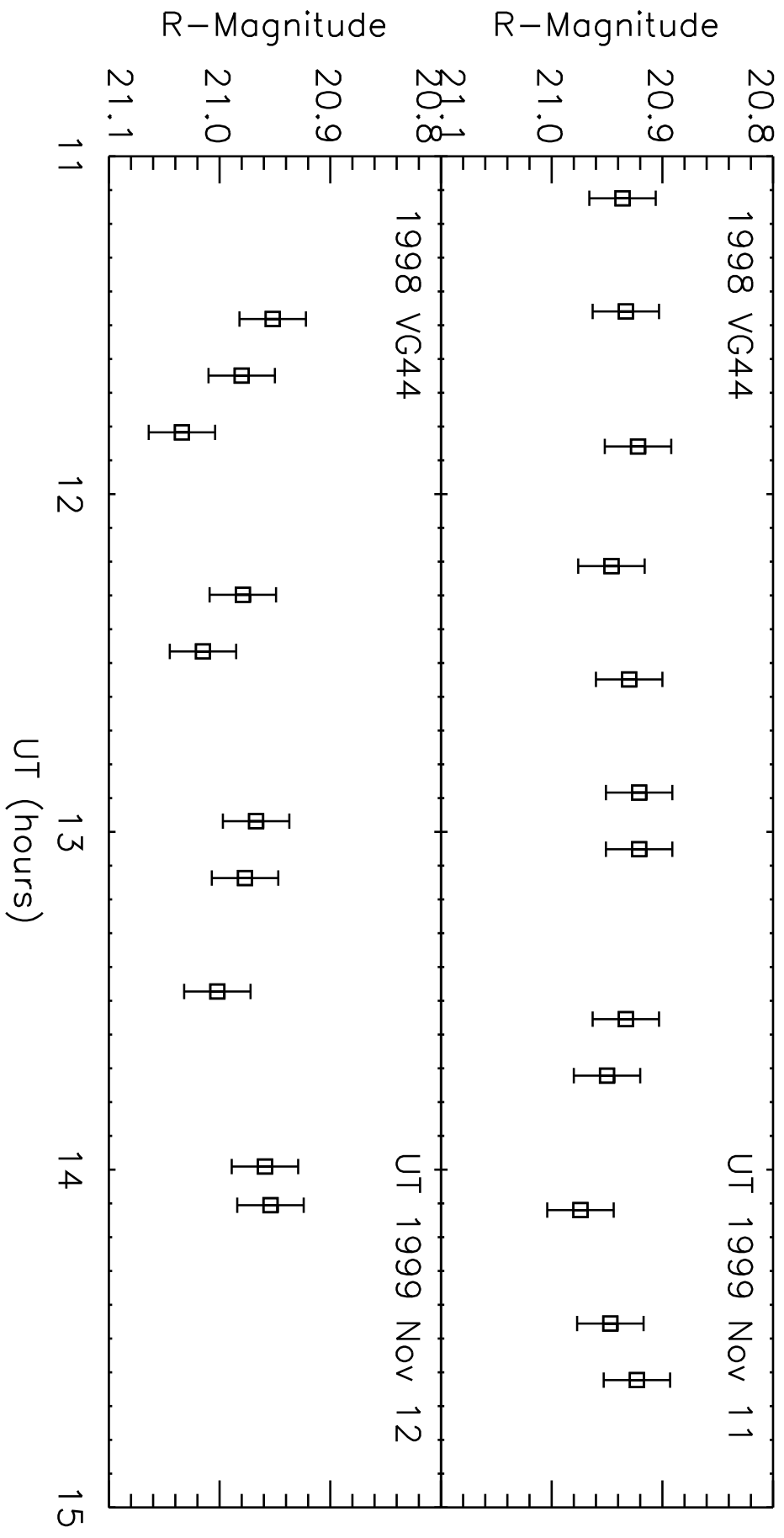
^bReferences where SS is Sheppard 2002; OH is Hainaut et al. 2000; RT is Romanishin & Tegler 1999; OR is Ortiz et al. 2001; R is Romanishin et al. 2001.; CB is Collander-Brown et al. 1999; LJ is Luu and Jewitt 1998; D is Davies et al. 1997

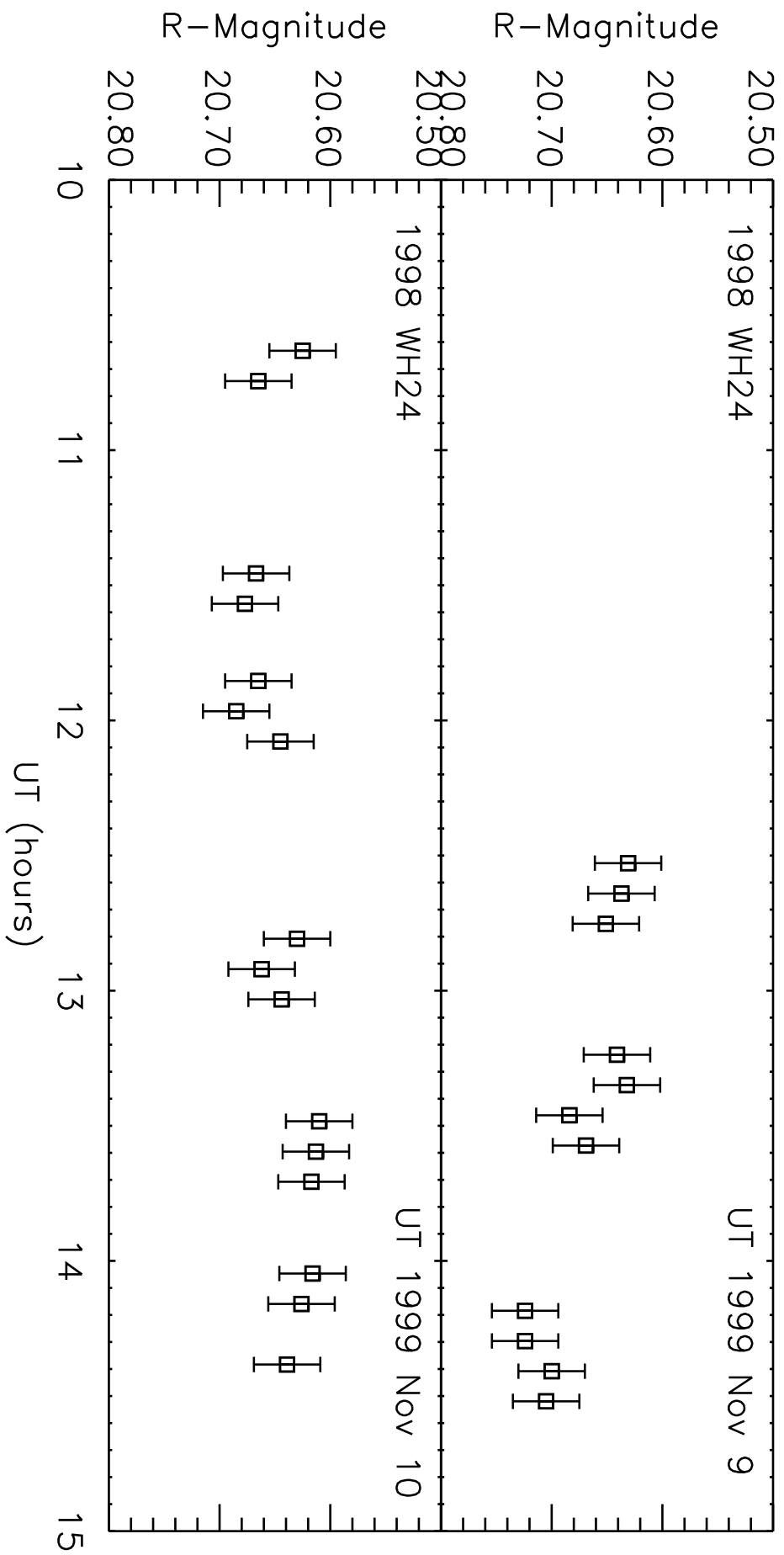












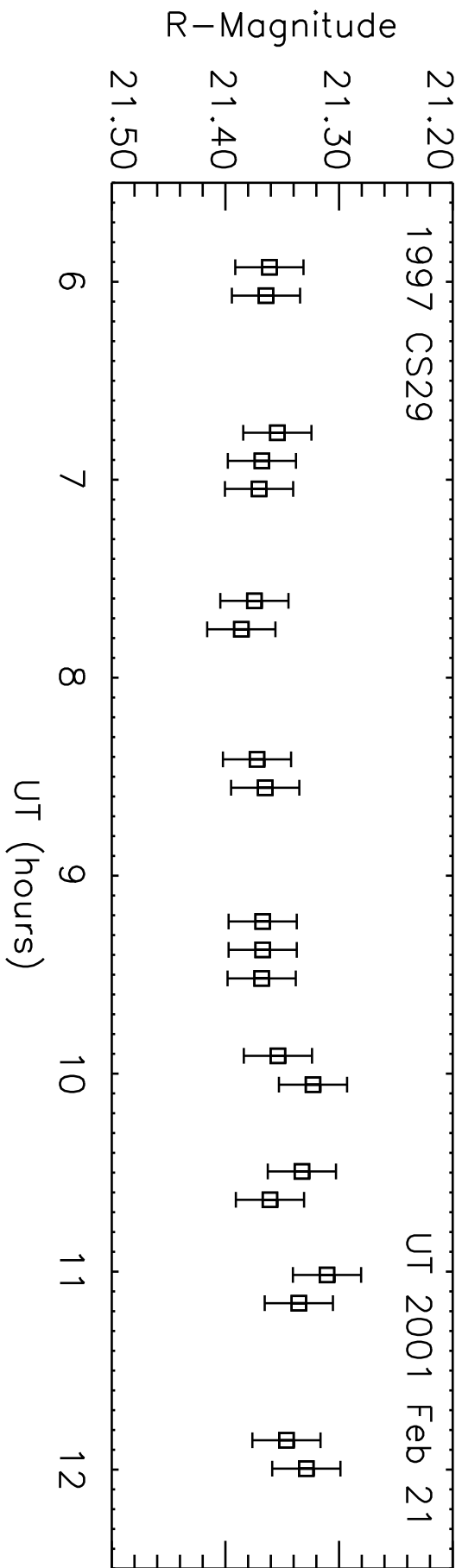


TABLE 12. Phase Function Data for KBOs

Name	H	G	$\beta(\alpha < 2^\circ)^a$
2000 EB ₁₇₃	4.44 ± 0.02	-0.15 ± 0.05	0.14 ± 0.02
Varuna	3.21 ± 0.05	-0.58 ± 0.10	0.19 ± 0.06
1999 DE ₉	4.53 ± 0.03	-0.44 ± 0.07	0.18 ± 0.06
1996 GQ ₂₁	4.47 ± 0.02	-0.04 ± 0.05	0.14 ± 0.03
2000 GN ₁₇₁	5.98 ± 0.02	-0.12 ± 0.05	0.14 ± 0.03
1999 KR ₁₆	5.37 ± 0.02	-0.08 ± 0.05	0.14 ± 0.02
2001 CZ ₃₁	5.53 ± 0.03	-0.05 ± 0.07	0.13 ± 0.04
MEAN	-	-0.21 ± 0.04	0.15 ± 0.01
Pluto ^b	-1.00 ± 0.01	0.88 ± 0.02	0.0372 ± 0.0016

^a $\beta(\alpha < 2^\circ)$ is the phase coefficient at phase angles $< 2^\circ$.

^bData for Pluto from Tholen and Tedesco (1994) while the G value was calculated by us.

